Structure-function studies on two phosphoenolpyruvate carboxylases

Lakshmi Dharmarajan

Dissertation submitted to the faculty of the Virginia Polytechnic Institute and State University in partial fulfillment of the requirements for the degree of

Doctor of Philosophy

in

Genetics, Bioinformatics and Computational Biology

Biswarup Mukhopadhyay, chair

David R. Bevan

Alexey Onufriev

Robert H. White

Paul R. Carlier

October 29, 2010

Blacksburg, Virginia

Keywords: phosphoenolpyruvate, structure-function, active-site lid, anion-quadrupole interaction, PEP-Mn^{2+} distance, inhibition

Structure-function studies on two phosphoenolpyruvate carboxylases

Lakshmi Dharmarajan

ABSTRACT

Phosphoenolpyruvate carboxykinase (PEPCK) and phosphoenolpyruvate carboxylase (Pepc) are two important CO_2-fixation enzymes which share a similar reaction mechanism. Both operate through a lid-gated active site and have a hypothesized enol-pyruvate intermediate in their catalytic pathway. While PEPCK is an important metabolic enzyme in animals and plays a broad role in cataplerosis, gluconeogenesis and glyceroneogenesis, Pepc reaction in plants catalyzes the first committed step in CO_2 fixation in CAM and C4 plants via Rubisco. We are studying the structure-function aspects of both enzymes, with a goal of discovering new elements in these enzymes which can modulate catalysis. We have undertaken an interdisciplinary approach for this work and have shown that a combination of experimental and computational techniques can be complementary and can provide novel information.

We have determined that in human PEPCK, Tyr^{235} forms an anion-quadrupole interaction with the carboxylate of PEP and thus positions the latter with respect to the enzyme-bound Mn^{2+} for optimal phosphoryl transfer and catalysis. We have also identified Pro^{82} as a catalytically influential residue in this enzyme. Using molecular dynamics simulations we have noted that absence of ligands induces active-site lid opening in GTP-PEPCKS and we have made the first observation of the intermediary

structures of the lid opening event, the dynamics of which is an important element that controls GTP-PEPCK catalysis.

We have determined the first three-dimensional crystal structure of an archaeal-type Pepc, i.e. *C. perfringens* PepcA. Our experimental data also provide information about the oligomerization of PepcAs and reveal that aspartate inhibits the *C. perfringens* enzyme competitively compared to the allosteric inhibition in Pepcs. Structure-based modeling has led to the identification of putative aspartate- and bicarbonate-binding residues in *C. perfringens* PepcA, of which Arg^{82}, His^{11}, Ser^{201}, Arg^{390}, Lys^{340}, Arg^{342} and Arg^{344} probably play an important role.

DEDICATION

This work is dedicated to my parents, Saraswathi Dharmarajan and N.S. Dharmarajan.

ACKNOWLEDGEMENTS

I extend my sincere gratitude to my advisor, Dr. Biswarup Mukhopadhyay, for being an excellent mentor throughout my doctoral studies. His passion and commitment towards science have been a great source of inspiration to me. I am extremely thankful for his patience and guidance during my evolution as a researcher.

I also thank my committee members, Dr. David Bevan, Dr. Alexey Onufriev, Dr. Paul Carlier and Dr. Robert White for being approachable and providing valuable insights and suggestions about my research work. I am especially grateful to Dr. Bevan for providing me the resources and helping me learn the basics of molecular dynamics simulations. I am also thankful to Dr. Pete Dunten, SSRL, Stanford, for his collaboration and guidance in the PEPCK and Pepc projects.

Special thanks are due to the members of the Mukhopadhyay laboratory and Virginia Bioinformatics Institute, for making my time spent here a fun-filled, learning experience. I could not have done without the support of Dwi Susanti and Jason Rodriguez, who have not only been colleagues, but more like family to me. I am grateful to Dr. Endang Purwantini, Eric Johnson and Usha Loganathan for their incessant help and kindness. I also appreciate the training I received from Chris Case, a former member of our laboratory, during the first year of my doctoral studies.

I appreciate all the good times shared with fellow GBCBers, and am grateful to Dennie Munson for all her help. I thank all my wonderful friends in Blacksburg who made life here enjoyable, specially Riya Sarker and Tannistha Maiti, who made this “home away from home” a livable place. I also owe it to my best friends, Sayari De and Rummi Roychoudhury, who have always stood by me from across the oceans and were always a phone call away in times of need.

Finally, I thank my family for supporting me at all times. My brother, Mahesh, who has always stood by me and been a protective “big brother”, giving me sane advice when I needed the most. I owe a lot to my husband, Kriti Sen Sharma, who helped me in believing in myself and transformed my life into a beautiful place.

I am thankful to my parents, who have made me the person I am today. My brave mother, who has consistently motivated me and whose love, sincerity and determination have inspired me to push ahead inspite of all obstacles. I cannot even begin to express the role of my father’s unconditional love and belief in my life and work. As he lies back home battling with cancer, I hope I brought him at least a momentary feeling of happiness with the completion of my PhD. studies.

ATTRIBUTION

Chapter 3

Tyr^{235} of human cytosolic phosphoenolpyruvate carboxykinase influencing catalysis through an anion-quadrupole interaction with phosphoenolpyruvate carboxylate

Chapter 3 was published in FEBS Journal 275: 5810-5819 (2008).

Lakshmi Dharmarajan – Graduate student (Genetics, Bioinformatics and Computational Biology doctoral program, Virginia Tech), designed and performed the experiments and prepared the manuscript.

Christopher L. Case – was a researcher in the Mukhopadhyay Laboratory at the Virginia Bioinformatics Institute and currently is a graduate student in Yale University School of Medicine Section of Microbial Pathogenesis. CLC contributed in designing and performing the experiments.

Pete W. Dunten – Crystallographer at the Stanford Linear Accelerator Center, Menlo Park, CA, helped in conceiving the idea for the work and in preparation of the final manuscript.

Biswarup Mukhopadhyay – Associate professor, Virginia Bioinformatics Institute and Adjunct Associate Professor, Departments of Biochemistry and Biological Sciences, Virginia Tech, conceived the idea of the paper, supervised the work, and contributed to the preparation of the final manuscript.

Chapter 4

Dynamics of the active-site lid in GTP-PEPCKs

Lakshmi Dharmarajan – designed and performed experiments and wrote the chapter.

Biswarup Mukhopadhyay – supervised the work.

Chapter 5

Crystallization of *Clostridium perfringens* PepcA

Lakshmi Dharmarajan – designed and performed the experiments and wrote part of the manuscript.

Jessica L. Kraszewski – was a graduate student in the Biochemistry program, Virginia Tech, and is currently working in DuPont, PA. JLK contributed in designing and performing the experiments.

Biswarup Mukhopadhyay – conceived the idea of the project and supervised the work.

Pete W. Dunten – performed experiments, supervised the work and prepared the manuscript.

Chapter 6

Structure of *Clostridium perfringens* phosphoenolpyruvate carboxylase

Lakshmi Dharmarajan – designed and performed the experiments and wrote the chapter.

Jessica L. Kraszewski – contributed in performing the experiments.

Biswarup Mukhopadhyay – conceived the idea of the project and supervised the work.

Pete W. Dunten – performed experiments, supervised the work and prepared the final manuscript.

Chapter 7

Insights into the aspartate and bicarbonate binding sites of *Clostridium perfringens* PepcA

Lakshmi Dharmarajan – designed and performed the experiments and wrote this chapter.

Jessica L. Kraszewski – contributed in performing the experiments and prepared Fig.7.1.

Biswarup Mukhopadhyay – supervised the work.

TABLE OF CONTENTS

LIST OF FIGURES

Chapter 2

Chapter 3

Chapter 4

Chapter 5

Chapter 6

Chapter 7

Chapter 8 – Appendix

LIST OF TABLES

Chapter 3

Chapter 7

Chapter 8 – Appendix

ABBREVIATIONS

ASP	Aspartate
ATP	Adenosine triphosphate
GDP	Guanosine diphosphate
GTP	Guanosine triphosphate
HPLC	High Pressure Liqid Chromatography
NADH	Nicotinamide adenine dinucleotide (reduced)
OAA	Oxaloacetate
PAGE	Polyacrylamide gel electrophoresis
PCR	Polymerase chain reaction
PEP	Phosphoenolpyruvate
PEPC	Phosphoenolpyruvate carboxylase
PEPCK	Phosphoenolpyruvate carboxykinase
RMSD	Root mean square deviation
RMSF	Root mean square fluctuation
SDS	Sodium dodecyl sulfate
TCA	Tricarboxylic acid
Tris	Tris(hydroxymethyl) aminomethane

Chapter 1

Introduction

Phosphoenolpyruvate carboxykinase (PEPCK) and phosphoenolpyruvate carboxylase (Pepc) are two CO_2-fixing enzymes involved in the glucose metabolism pathway. Both enzymes belong to the TIM-barrel family, share a similar reaction mechanism and catalytically operate through a lid-gated active site. A putative enolate has been hypothesized as an intermediary stage in the catalytic pathway of both enzymes.

PEPCK is an important metabolic enzyme in animals and plays a broad role in cataplerosis, the process of removing anions from the citric acid cycle. The enzyme also catalyzes the first committed step in hepatic gluconeogenesis and glyceroneogenesis and has been thought to have an implication in Type 2 diabetes therapeutics development. In bacteria, fungi and plants, PEPCK is involved in the glyoxylate bypass, an alternative to the TCA cycle.

On the other hand, the Pepc reaction in plants catalyzes the first committed step in CO_2 fixation in CAM and C4 plants via Rubisco (*1*). It provides fixed carbon for cell biosynthesis via the complete TCA cycle and its oxidative and reductive branches (*1, 4, 5*). It has implications in energy production, amino acid biosynthesis and cultivation of food crops.

PEPCK

PEPCK catalyzes the reversible GTP or ATP dependent conversion of oxaloacetate (OAA) to phosphoenolpyruvate (PEP) (*3, 6*). The process requires the presence of two

enzyme-bound nucleotide-binding ions, Mg^{2+} and Mn^{2+}.

$$\text{OAA + ATP or GTP (ITP)} \leftrightarrow \text{PEP + } CO_2 \text{ + ADP or GDP (IDP)}$$

The GTP-dependent PEPCK (GTP-PEPCK) is found in mammals, other eukaryotes, some bacteria and archaea (*3, 7-10*). The rate-limiting step in PEPCK catalysis is phosphoryl transfer, which is dependent on the position of Mn^{2+} with respect to PEP or the nucleotide. In our laboratory we focus on residues which can alter the activity of this enzyme by influencing the PEP-Mn^{2+} distance in catalysis. From the crystal structure of human PEPCK it is seen that the aromatic ring of Tyr^{235} moves when PEP binds. We have hypothesized that this residue plays a role in positioning PEP with respect to Mn^{2+}. Pro^{82} is another residue that lies within an activity-modulating element of GTP-PEPCKs that influences PEP-Mn^{2+} distance (*11*). An additional important determinant of GTP-PEPCK catalysis is the active site lid that protects the hypothesized enolate intermediate. Accordingly, this part of the research thesis has the following goals -

1. To determine the role of Tyr^{235} in catalysis (outlined in Chapter 3).
2. To determine whether Pro^{82} is catalytically influential (outlined in Appendix 8.1).
3. To study the conformational dynamics of the active site lid (outlined in Chapter 4).

PEPC

Pepc yields OAA from PEP and bicarbonate (HCO_3^-), liberating P_i in the presence of Mg^{2+} (*1*).

$$PEP + HCO_3^- \rightarrow OAA + P_i$$

Pepc is present in all photosynthetic organisms, like plants, algae, cyanobacteria and photosynthetic bacteria, and also in most non-photosynthetic bacteria and protozoa (*1*). Bacterial and plant enzymes (Pepcs) are homotetrameric with subunit sizes of 100-130 kDa and are highly similar in primary sequence and three-dimensional structure (*1, 12-14*). Plant Pepcs are regulated by both positive and negative regulators (*1, 15, 16*). The archaeal-type Pepc (PepcA), which is ubiquitous in archaea, is however, not significantly regulated by metabolites and shows only 12-16 % sequence similarity to the other two Pepcs (*12, 17-20*). Aspartate is one such metabolite, which inhibits Pepcs strongly and in an allosteric mode. However, PepcAs display differential sensitivity towards aspartate and probably have a different binding mode for the metabolite. Accordingly, the research goals of this portion of the thesis are the following –

1. To determine the crystal structure of *Clostridium perfringens* PepcA and to provide a comparative structural analysis of Pepcs and PepcAs (outlined in Chapters 5 and 6).
2. To comprehend the aspartate and bicarbonate binding modes of *Clostridium perfringens* Pepc (outlined in Chapter 7).

We have undertaken both experimental and computational approaches for these research analyses. Experimental techniques include site-directed mutagenesis, recombinant protein expression, enzyme kinetics, CD spectroscopy and X-ray

crystallography. Computational approaches include bioinformatics analyses, molecular modeling, docking and molecular dynamics simulations.

Chapter 2

Background

2.1. PEPCK

2.1.1. Role of PEPCK

PEPCK has been considered primarily a cataplerotic enzyme and provides substrates to a number of downstream metabolic processes (*21*). The major pathways linked to cataplerosis in which PEPCK plays a major role are shown in Fig. 2.1. Involvement of PEPCK in gluconeogenesis has been widely studied (*3*). However, although the major route of carbon flux in the liver and kidney cortex is gluconeogenesis, it is not the only metabolic pathway PEPCK influences, as was previously thought. PEPCK removes the citric acid cycle anions and links cataplerosis to glucose synthesis and glyceroneogenesis (Fig. 2.1) (*21*). It is involved in energy generation by recycling the TCA cycle anions back into the cycle (*21, 22*). Amino acid carbon enters the cycle and is metabolized to malate in the mitochondria, which exits the latter and is oxidized to oxaloacetate. PEPCK-C plays a role in this process converting OAA to PEP, which is again converted to pyruvate by pyruvate kinase and to acetyl-coA by pyruvate dehydrogenase complex (*22*). The acetyl-coA can re-enter the cycle and get completely oxidized or can be used for fatty acid synthesis in the liver (*21*). Burgess et al. (*23*) have used mice in which the gene for PEPCK-C had been deleted specifically in the liver and have shown the role of PEPCK-C in cataplerosis (*24*). They demonstrate that the loss of hepatic PEPCK-C (the gene is expressed normally in the kidney cortex) results in a

decreased flux through the citric acid cycle, an accumulation of citric acid cycle intermediates, and an almost total block in hepatic gluconeogenesis and fatty acid oxidation. They have used metabolic flux measurements of citric acid cycle function, which employ labeled intermediates. The results clearly demonstrate the important cataplerotic role that PEPCK-C plays in the control of citric acid cycle flux and upstream biosynthetic reactions.

PEPCK-M has been said to be involved in gluconeogenesis from lactate (*25*). Detailed studies have however not been performed to study the metabolic role of PEPCK-M. Despite the equal distribution of the PEPCK isoforms in most mammalian livers, including human liver, it is surprising that the biology of PEPCK-M is poorly studied (*21*). It is not clear whether the factors, which control PEPCK-C gene transcription in the liver, also have a similar effect on hepatic PEPCK-M gene transcription (*21*). This has been mainly due to the fact that the majority of metabolic work has been done in the mice, which is usually the model species for any work related to humans (*21*). However, in this case, 90 % of the PEPCK distribution in mice livers is the cytosolic PEPCK, the mitochondrial being only the remaining. Hence, this system cannot be a model for the human liver, where the distribution of both the isozymes is equal.

2.1.2. ATP and GTP-PEPCKs

GTP-PEPCKs are found in mammals, other higher eukaryotes, archaea and some bacteria. They are so called because they prefer the guanosine nucleotide and use ATP

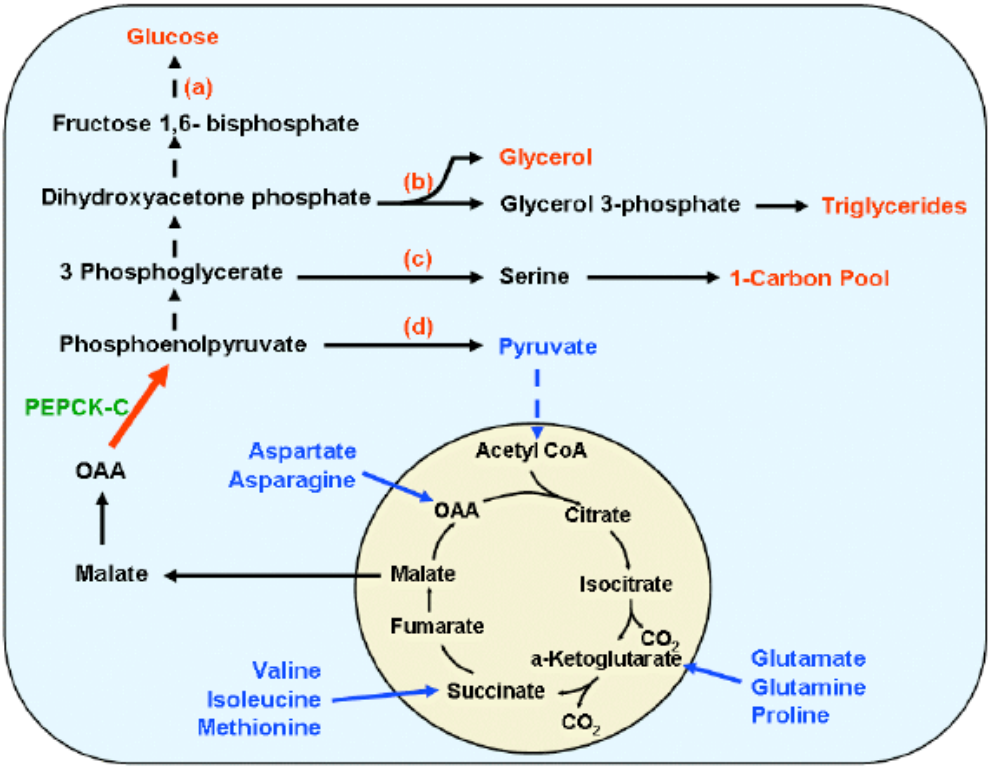

Fig. 2.1. Cataplerosis in action: PEPCK as a feeder reaction for carbon from the citric acid cycle to various biosynthetic and oxidative processes. The entry of selected amino acids into the citric acid cycle and their subsequent disposal via PEPCK-C are shown. The biosynthetic pathways of gluconeogenesis (a), glyceroneogenesis (b), and serine synthesis (c) are outlined, as is the recycling/oxidation of the carbon skeletons of amino acids back into the citric acid cycle (d) as acetyl-CoA for subsequent oxidation or conversion to fatty acids. This research was originally published in Yang, J., Kalhan, S. C., and Hanson, R. W., *J Biol Chem 284*, 27025-27029 (2009) © the American Society for Biochemistry and Molecular Biology (*21*), figure used with permission of ASBMB Journals, 2011.

only at very high non-physiological K_m values. ATP-dependent enzymes are found in plants, most bacteria and fungi. These two classes of enzymes share very little sequence similarity; however, the structures of the active sites of both are highly conserved (Fig. 2.2) (*26*). Hence an evolutionarily conserved mechanism of catalysis has been proposed to exist in the two classes. This includes a direct inline phosphoryl transfer, through an S_N2-like associative mechanism, with an enol-pyruvate intermediate

(*6, 27-32*). GTP-PEPCKs have a unique binding pocket for the nucleotide, formed by the three aromatic residues, Phe^{517}, Phe^{525} and Phe^{530} (according to human PEPCK numbering). In contrast, in ATP-PEPCKs, the adenine-binding pocket is very different. In the *E. coli* enzyme the base is sandwiched between the side-chain of Ile452 and the guanidinium group of Arg^{449} (*E. coli* numbering) (*33*). In this enzyme, upon Mg^{2+}- ATP-binding, the C-terminal domain rotates by 20º by a hinge-like motion with respect to the N-terminal domain (*33*). GTP binding in the GTP-dependent PEPCKs did not demonstrate such a dramatic change in domain conformation (*26*). However, the active sites of both classes of enzyme contain a mobile W-loop lid domain, the closure of which is essential for catalysis (*34*).

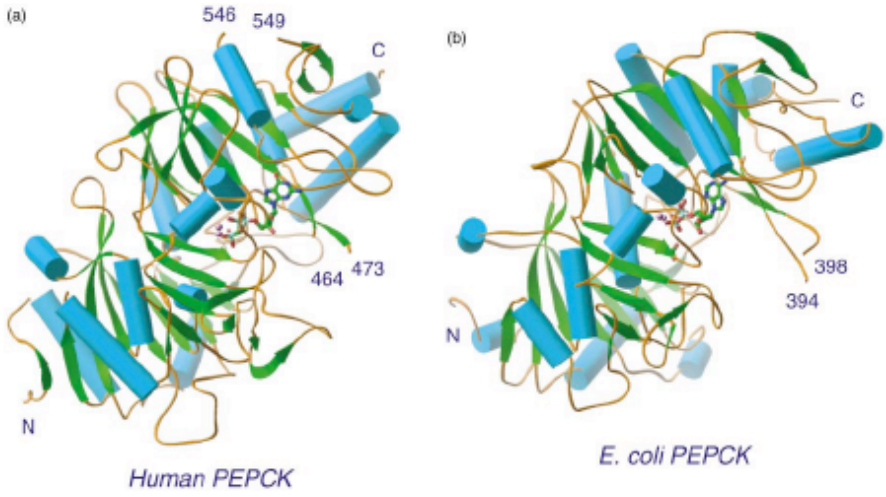

Fig. 2.2. Comparison of the GTP-dependent and ATP-dependent PEPCK structures. (a) Ribbon representation of the human enzyme with metal ions and non-hydrolyzable GTP shown in ball-and-stick form. (b) The *E. coli* enzyme with bound metal ions and ATP shown in the same orientation to highlight the similarity of the fold. This research was originally published in Dunten, P., Belunis, C., Crowther, R., Hollfelder, K., KammLott, U., Levin, W., Michel, H., Ramsey, G. B., Swain, A., Weber, D., and Wertheimer, S. J., *J Mol Biol 316*, 257-264 (2002) (*26*), figure used with permission of Elsevier, 2011.

2.1.3. A stepwise mechanism of PEPCK catalysis

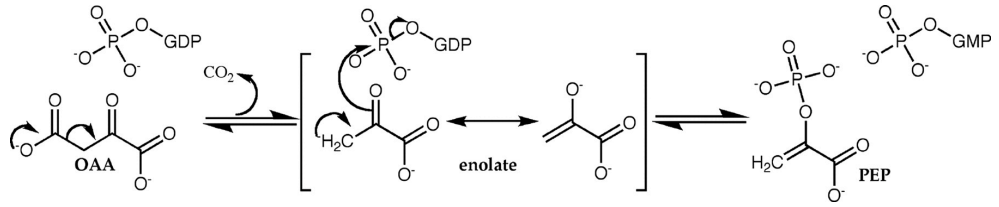

Fig. 2.3. PEPCK-catalyzed interconversion of OAA and PEP. This research was originally published in Carlson, G. M., and Holyoak, T., *J Biol Chem 284*, 27037-27041 (2009) © the American Society for Biochemistry and Molecular Biology (*35*). Figure used with permission of ASBMB Journals, 2011.

PEPCK catalysis i.e. the reversible formation of PEP from OAA and GTP (or ITP), involves two steps – decarboxylation and phosphoryl transfer (Fig. 2.3). Phosphoryl transfer is a key step in the PEPCK reaction. There are many examples of phospho-transfer enzymes using cations like Mg^{2+} and Mn^{2+} selectively in nucleotide binding and catalysis (*36*). Kinetic data on ATP- and GTP-dependent PEPCKs indicate a synergistic dual cation function of Mg^{2+} and Mn^{2+} for activity (*10, 37*). Mg^{2+} facilitates nucleotide binding to the enzyme and appears to activate the γ-phosphate of the nucleotide for nucleophilic attack. It acts as a Lewis acid and polarizes one of the P-O bonds of the γ-phosphate, making the γ-phosphorus atom more electrophilic and reactive to nucleophilic attack by the enolate of pyruvate, a proposed intermediate for the enzymatic reaction (*6*). Enzyme-bound Mn^{2+}, on the other hand, is the preferred cation for enzyme activation and influences phosphoryl transfer from PEP or GTP (*9, 26, 38-42*). Based on known mechanisms of ATP-PEPCKs and from the structures of human,

rat cytosolic and chicken mitochondrial enzymes, an overall stepwise mechanism for the human enzyme has been proposed (*26, 34, 35, 43*).

Michaelis complex formation - OAA binds to the enzyme by direct coordination to the active site Mn^{2+} ion and by interactions with Arg^{87} and Ser^{286} (Fig. 2.4). This ion is further coordinated to the residues Lys^{244}, His^{264} and Asp^{311} and the γ- phosphate of GTP. GTP binds to the enzyme within its unique aromatic binding site, with its β - and γ-phosphoryl groups coordinated with the Mg^{2+} ion. The latter is further coordinated to Thr^{291} and three water molecules, thus satisfying its octahedral configuration. Thus, GTP acts as a bridging ligand between the two metal ions. This coordination of OAA and GTP to the two metal ions places the C-3 carbonyl of OAA and the γ- phosphate of GTP in a perfect orientation for direct inline phosphoryl transfer (*35*).

Active site lid closure - Structural studies have shown that PEPCK operates by a classical induced-fit mechanism, and closure of the active site lid is essential to position the substrates in their correct position for catalysis (*34*). This model also indicates that as ligands bind to the enzyme, it becomes thermodynamically more favorable for the closed state of the lid as compared to the open state (*34*). Closure of the lid, which is correlated with P-loop closure, results in the movement of the nucleotide towards OAA and Mn^{2+} and decreases the phosphoryl transfer distance (Fig. 2.4) (*43, 44*). According to structural data it is seen that the lid-closed state becomes predominant during the catalytic transition, i.e. after the formation of the enolate intermediate (*34*). This leads to

the assumption that the dynamics of the lid play a major role in protecting the enolate from protonation or tautomerization to pyruvate (*34, 35*).

Opening of the lid – In the reverse process, formation and release of products results in a decrease in the thermodynamic favorability of the lid closure and the enzyme again samples the open lid configuration (*34*). PEP shifts away from Mn^{2+} and binds in second-sphere coordination to it, through two water molecules (Fig. 2.4). This lid opening is correlated with the P-loop opening and allow for PEP and GDP release and the transition back to the beginning of the catalytic cycle.

2.1.4. Phosphoryl transfer and PEP-Mn^{2+} distance

Mn^{2+} neutralizes the electrostatic repulsion between the enolate and the nucleotide, moving the enolate oxygen towards the γ-phosphate for nucleophilic attack, promoting catalysis (*9, 26, 38-42*). Therefore the position of Mn^{2+} with respect to PEP or the nucleotide influences phosphoryl transfer. Accordingly, we have hypothesized that the PEP-Mn^{2+} distance is a determining factor in PEPCK catalysis. We have found examples in the case of *M. smegmatis* and human PEPCK, where our kinetic analysis showed that in the case of D81, D84, E89 and Y235 variants, only K_m for PEP and Mn^{2+} changed, but not that for GDP; hence the catalytic effect was due to PEP-Mn^{2+} interaction (*11, 45*).

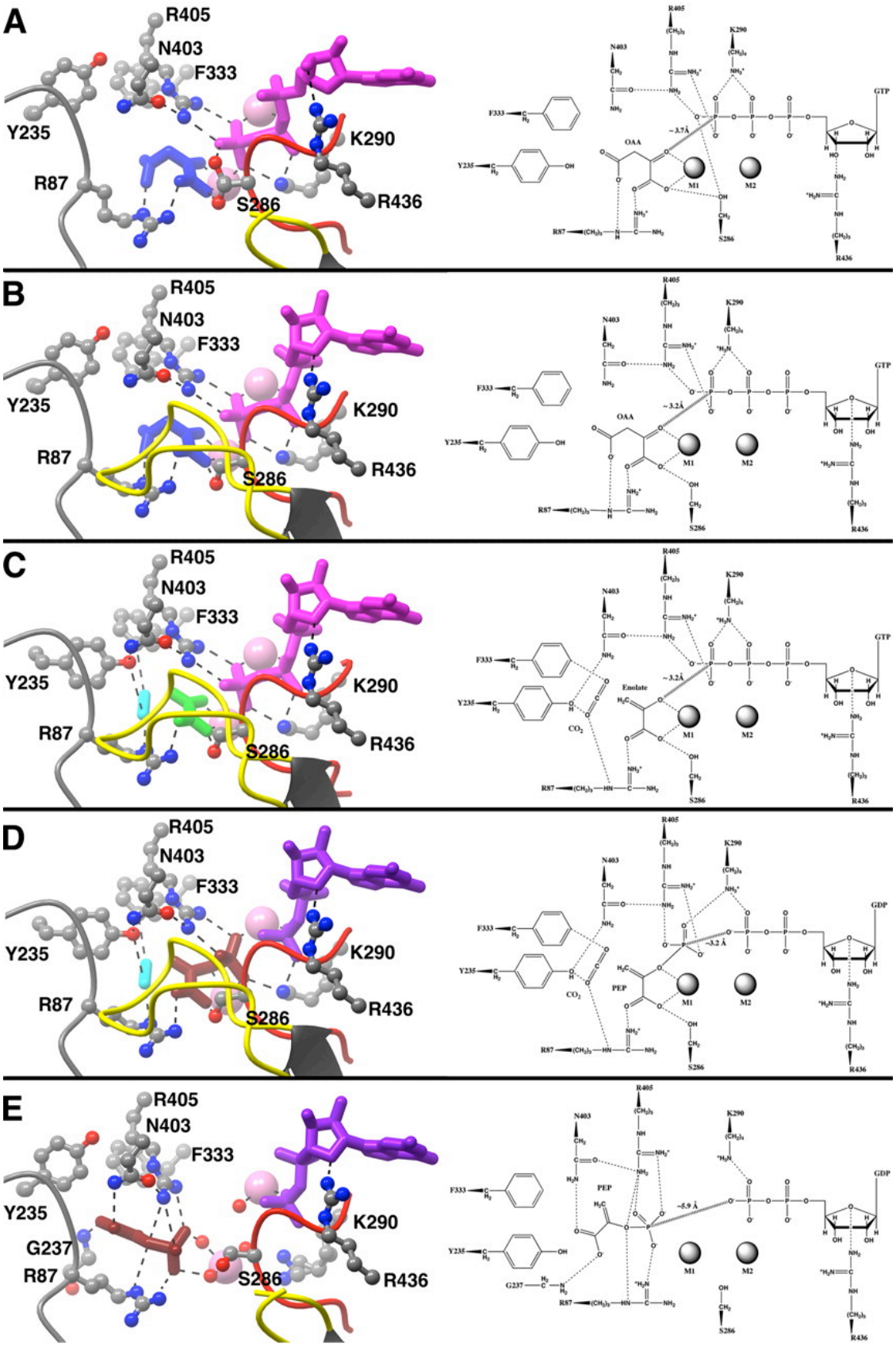
A
R405
N403
F333
Y235
K290
R87
S286
R436
GTP
OAA
M1
M2
B
R405
N403
F333
Y235
K290
R87
S286
R436
GTP
OAA
M1
M2
C
R405
N403
F333
Y235
K290
R87
S286
R436
GTP
Enolate
M1
M2
D
R405
N403
F333
Y235
K290
R87
S286
R436
GDP
PEP
M1
M2
E
R405
N403
F333
Y235
G237
K290
R87
S286
R436
GDP
PEP
M1
M2

Fig. 2.4. Crystallographic images defining the chemical reaction path of PEPCK- mediated conversion of OAA to PEP. A schematic drawing to aid in the interpretation of the structural data is presented on the right-hand side of each panel. In the left-hand images, the substrates/products are rendered as stick models colored by molecule type: GTP (*magenta*), GDP (*purple*), OAA (*blue*), PEP (*burgundy*), CO_2 (*cyan*), and the enolate intermediate (*green*). The active site W-loop lid and P-loop motif are rendered in *yellow* and *red*, respectively. The amino acids involved in important substrate/product interactions are rendered as *gray* ball-and-stick models colored by atom type and labeled adjacent to their respective α-carbon atom. *Dashed lines* illustrate important protein-substrate/product interactions. The positions of the PEP, OAA, enolate, and CO_2 molecules are based upon the authentic binary complexes of the enzyme with those substrates as well as ternary complexes with the substrate analogs 2-phosphoglycolic acid, 3-sulfopyruvate, and oxalate and the corresponding GDP or GTP nucleotide. This research was originally published in Carlson, G. M., and Holyoak, T. *J Biol Chem 284*, 27037-27041 (2009) © the American Society for Biochemistry and Molecular Biology (*35*). Figure and legend used with permission of ASBMB Journals, 2011.

Hence our interest lies in studying how the PEP-Mn^{2+} distance in catalysis in the variant enzymes influences enzyme activity. Since cPEPCK is considered an important marker for hepatic gluconeogenesis and has implications for Type 2 Diabetes therapeutics development, we were interested in this long-term goal for PEPCK study. However, now it is being realized that most studies in this field have been done on mice, which do not represent the human system accurately. 90% of PEPCK in mice is cPEPCK, while only 50% of the total PEPCK activity in humans is cPEPCK. The remaining 50% is mPEPCK, which has not been widely studied. Nevertheless, cPEPCK is an important enzyme, at the junction of many metabolic pathways in the human body; a thorough study in this field will always be of great relevance.

2.1.5. Influencing catalysis from a distance

One approach in any drug discovery is targeting the active site of the enzyme. However,

interference with these catalytically essential residues could fully inactivate the enzyme that might be detrimental to the patient. Drugs targeting the active site could have multiple targets as active sites of similar enzymes are often conserved. Hence we are particularly interested in locating catalytically influential residues that are present at sites far from the active site as viewed in the three-dimensional structure. These would have a long-range yet significant influence on one or more catalytic residues, providing avenues from which enzyme activity could be modulated, instead of causing inactivation. An analogous situation is seen in the case of *E. coli* dihydrofolate reductase, where mutations far from the center of chemical activity affect steps of the catalytic cycle (*7*). Further analysis shows that the distal mutations lead to non-local structural changes and alter the conformational sampling of the enzyme, thereby affecting catalysis (*46*). Approaching distal sites of an enzyme as potential drug targets has been worked on previously, in the case of the HIV-1 protease, where it has been suggested that distal mutations can actually cause drug resistance (*46-48*). Another example comes from the case of membrane proteins (*49*). These have the absolute requirement of a signaling network of long-range interactions, since it is necessary for one end of the protein to communicate with the other end. We are conducting this study on PEPCK, but this approach holds relevance to essentially any enzyme.

Our laboratory has presented a proof of this principle in PEPCK by working on a distal residue Asp^{75} (Asp^{81} in human PEPCK) in the *Mycobacterium smegmatis* enzyme (*11*) (Fig. 2.5 B). It is located on the same loop as Pro^{76}, Asp^{78}, Val^{79}, Arg^{81} and Glu^{83} (Pro^{82}, Asp^{84}, Val^{85}, Arg^{87} and Glu^{89} of human PEPCK) and is highly but not fully conserved.

We hypothesized that it is not catalytically essential but a catalytically influential residue. This was found to be so and our kinetic data suggested that a substitution at Asp^{75} likely changes the positions of the active site residues Asp^{78}, Val^{79}, Arg^{81} and Glu^{83}, and in the process alters the distance between the PEP-phosphate and the enzyme-bound Mn^{2+}. This effect increases the K_m for both PEP and Mn^{2+}. The mycobacterial enzyme is highly similar to the human cytosolic (50% identity) and chicken mitochondrial (46% identity) enzymes (*9*); hence Asp^{81} of human PEPCK would have a similar role as Asp^{75} of *M. smegmatis* PEPCK.

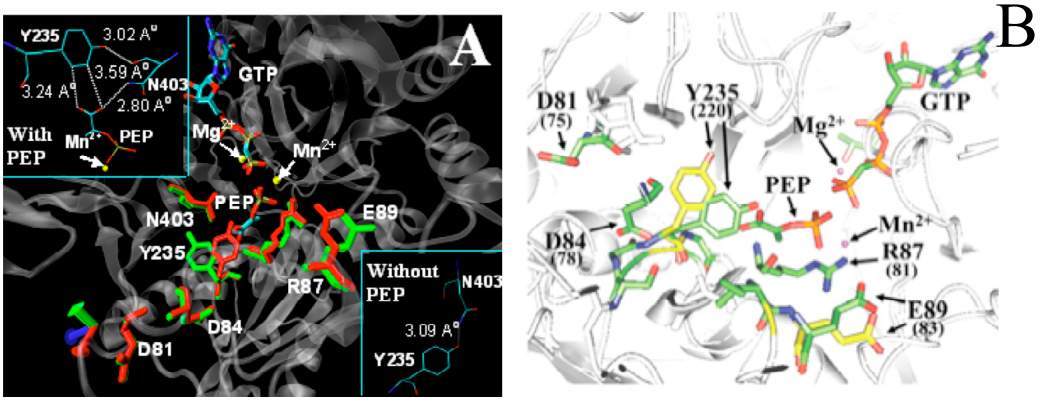

Fig. 2.5. Active site of human PEPCK. *A.* PEP-bound (green) and unbound (red) structures are shown along with interactions of Tyr^{235}; figure taken from Dharmarajan, L., Case, C. L., Dunten, P., and Mukhopadhyay, B. *FEBS J 275*, 5810-5819 (2008) (*45*), used with permission from John Wiley and Sons, 2011. *B.* An activity-modulating element of the human enzyme is shown and equivalent *M. smegmatis* residues are in parentheses. This research was originally published in Case, C. L., Concar, E. M., Boswell, K. L., and Mukhopadhyay, B. *J Biol Chem 281*, 39262-39272 (2006) (*11*) © the American Society for Biochemistry and Molecular Biology. Figure used with permission of ASBMB Journals, 2011.

2.1.6. Anion-quadrupole interaction

The aromatic ring of amino acids has been the subject of extensive study in protein interactions, namely by the cation-pi interactions. However, there have not been many

cases in which the interaction of the edge of the aromatic ring has been considered. The quadrupolar moment of the ring produces a quadrupolar charge distribution, which results in a positive electrostatic potential near the edges of the ring and a negative potential above and below the ring (*50*). *Ab initio* and AM1 calculations for electrostatic potential have depicted surfaces of benzene and phenol rings having a positive potential at the edges (Fig. 2.6) (*51*).

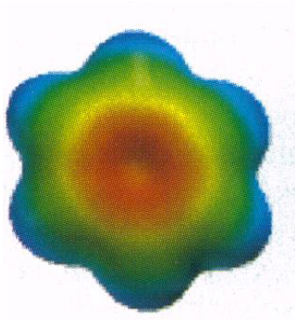

Fig. 2.6. Ab initio electrostatic potential surface of the benzene ring, displaying the positive potential at the edges of the ring. Figure used from Mecozzi, S., West, A. P., Jr., and Dougherty, D. A. *Proc Natl Acad Sci U S A 93*, 10566-10571 (1996) (*51*), fair use determination attached.

Interactions between the edges of phenyl rings and anionic units have been found in protein structures, one such example being in the case of ethacrynic acid and hemoglobin (*52*). Studies conducted from analysis of the environments of 170 phenylalanine residues in 28 protein structures demonstrated a statistical preference for the ∂^- oxygen atoms to the plane of the aromatic ring, near the ∂^+ hydrogen atoms (*52, 53*). These weakly polar interactions, called the anion-quadrupole interactions, are energetically favorable, with an apparent net free energy gain as much as about -1 kcal/mol and varying as a function of $1/r^3$ (*52, 53*). Other investigations have also been conducted, using aromatic - anionic amino acid pairs as models, in one case the net

quantum mechanical interaction energy between a coplanar benzene – formamide pair was calculated to be around -2 kcal/mol (*53*). Dunten *et. al* found such an interaction in human PEPCK, where the aromatic ring of Tyr^{235} forms an edge-on interaction with the carboxylate of PEP (*26*). We further characterized this interaction and are studying the role of this residue in influencing catalysis by affecting the PEP-Mn^{2+} interaction, the details of which are presented in Chapter 3.

2.2. Pepc

2.2.1. Role of Pepc

Pepc primarily fulfils an anaplerotic role in non-photosynthetic tissues by replenishing C_4 dicarboxylic acids for the synthesis of various cellular components and for keeping the citric acid cycle operational (*54-56*). In C_4 and CAM plants, Pepc captures atmospheric CO_2 and catalyzes the first-committed step in CO_2 fixation (*1*). After carboxylation by Pepc, the resulting C_4 compounds are transferred to the chloroplast in the bundle sheath cells. There the compounds are decarboxylated and a high concentration of CO_2 is supplied to Rubisco (*57*). This minimizes the oxygenase activity of Rubisco and consequent loss of fixed carbon through photorespiration, thus maximizing the CO_2-fixing ability of Rubisco(*58*). Pepc also has a high affinity for HCO_3^- , and is not inhibited by O_2 (*12*). On the other hand, in C_3 plants, Rubisco is used at the first CO_2 –fixation stage and as much as 50% of fixed CO_2 is lost to oxygenation (*59*). Some of the C_3 plants, such as rice, wheat, soybean and potato are major crops and trials for introducing C_4 – specific genes into these plants have been carried out using

recombinant DNA techniques, to improve CO_2 –fixation in these systems (*59, 60*). High level of maize Pepc expression in transgenic rice plants showed a reduction of O_2 inhibition of photosynthesis (*61*). However, the major problems in using an engineered C_4 or CAM Pepc include their inhibition and activation by metabolites and regulation by post-translational modifications like phosphorylation (*59*). This necessitates the engineering of a suitable Pepc that will be effective in transgenic plants. In plants, Pepc also has other roles, such as in nitrogen fixation, sucrose loading and the opening of stomata (*62, 63*).

2.2.2. Bacterial and Plant Pepcs

Both the bacterial and plant enzymes are homotetrameric (dimers of dimers) with subunit sizes of 100-130 kDa (*1, 13, 14*). Sequence and structure comparisons of *E. coli* and maize enzymes have shown that plant and bacterial enzymes are similar in their primary, secondary, tertiary and quaternary protein structures, suggesting their reaction mechanism to be similar (Fig. 2.7) (*12*).

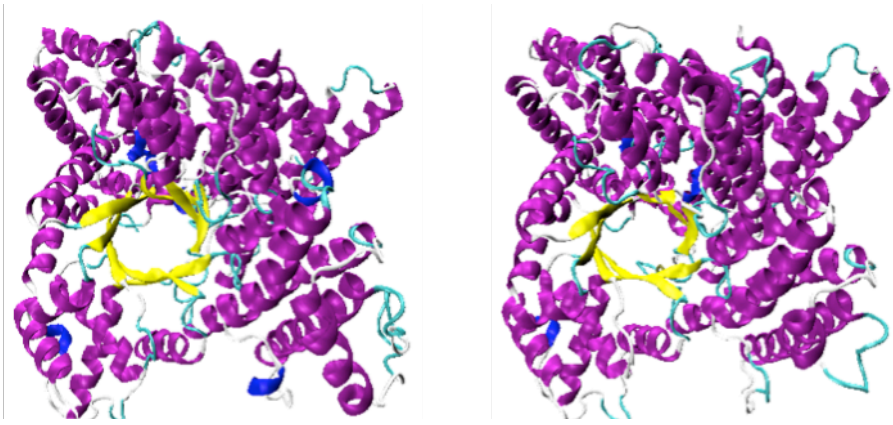

Fig. 2.7. Monomeric structures of Maize (left) and *E. coli* (right) Pepcs. PDB ids. used are 1FIY and 1JQO.

Bacterial Pepc plays an important role in energy production and macromolecular biosynthesis (*64*). It is strongly inhibited by the allosteric inhibitors malate and aspartate (*65*). *E. coli* Pepc is activated by acetyl-coA, fructose 1,6-bisphosphate, long-chain fatty acids and guanosine 3', 5'-bisphosphate (*66*). Plant Pepcs are also inhibited allosterically by aspartate and malate (*65*). Pepcs from dicot plants are activated by glucose-6-phosphate, and those of monocot plants by glycine, alanine and serine (*67*). Plant Pepcs are also controlled by phosphorylation (*1, 15, 16*).

2.2.3. Archaeal Pepc

Pepcs from *Sulforbus acidetifus* and *Methanothermus sociabilis* were the first archaeal enzymes to be characterized but their genes had not been identified (*19, 20*). However, recent studies on archaeal Pepc (PepcA) genes from *Sulforbus solfataricus* and *Methanothermobacter thermautotrophicus* showed that these enzymes are widespread in archaea, rare in bacteria and absent in eukarya (*17, 18*). Sequence comparisons showed that though these enzymes have a low similarity to their bacterial and plant counterparts, the core catalytic residues are conserved (*2, 17, 18*). These 50-60 kDa homo-multimeric enzymes are almost half the size of 100-130 kDa homo-tetrameric bacterial and plant Pepcs (*18-20, 68*). PepcAs are mostly insensitive or mildly regulated by allosteric regulators of Pepcs (*17-20*). The PepcA from *M. sociabilis* is insensitive to aspartate, while *M. thermautotrophicus* is mildly inhibited by this effector

(*18, 20*). In case of *S. solfataricus* and *S. acidocaldarius*, the enzymes are moderately inhibited by aspartate (*17, 19*). PepcAs are not affected by acetyl-coA and glucose-6-phosphate, which activate the plant and bacterial enzymes (*17-20*).

2.2.4. Mechanism of Pepc catalysis

The Pepc reaction is strictly irreversible and an energy-liberating process. Bicarbonate is hypothesized to be the real substrate as opposed to CO_2 in PEPCK. Kinetic analysis and substrate-analog studies have led to the development of a "three-step reaction mechanism" for Pepc catalysis (Fig. 2.8) (*1, 54*). Firstly, through a partial reaction, enol-pyruvate from PEP and carboxyphosphate from bicarbonate are formed. CO_2 is formed in the active site from the carboxyphosphate, and makes an electrophilic attack on the enolate ion, thereby forming oxaloacetate and liberating inorganic phosphate. Bicarbonate-dependent hydrolysis of PEP, which is an abortive side reaction, may occur due to access of water in the active site, loss of CO_2 or stabilization of the enol-pyruvate intermediate. In the active site, PEP makes contact with R773, R456 and R759 (maize Pepc numbering), of which the first and last residues have been shown to be essential for catalysis. These residues and Arg647 partially dissipate the negative charge of the PEP phosphate group. The divalent cation is held tetragonal bipyramidally by D603 and E566 and a water molecule, while making a bidentate coordination with PEP (Fig. 2.9). His177 (maize PEP numbering) stabilizes the carboxyphosphate and helps in transferring the proton from the former to the enolate.

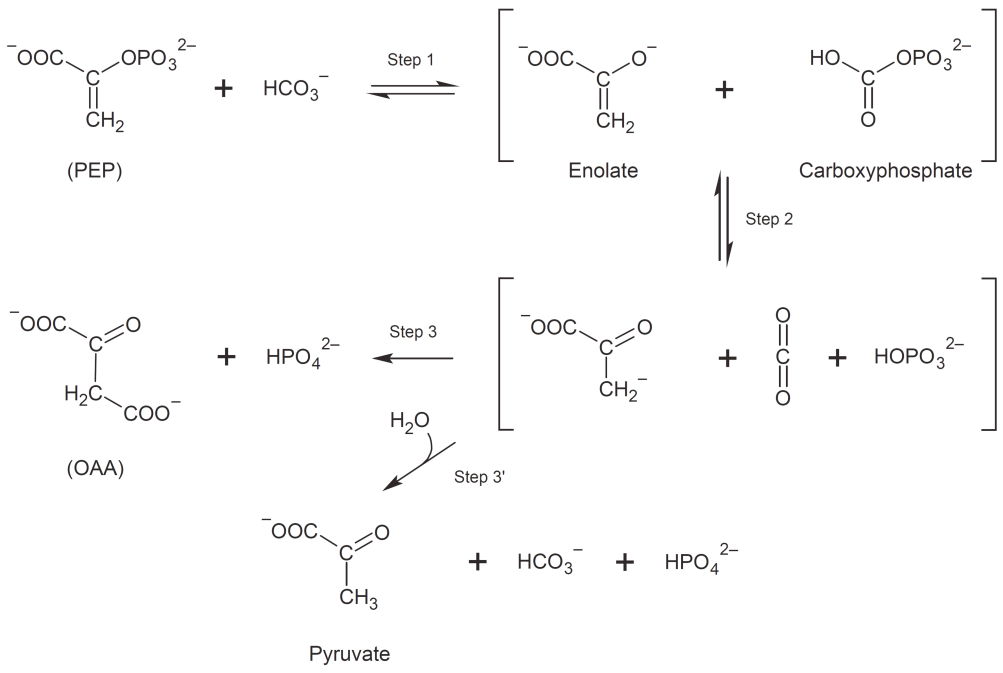

Fig. 2.8. Proposed chemical mechanism of PEP carboxylase reaction. Step 3, PEP carboxylation. Step 3', bicarbonate-dependent PEP hydrolysis. Adapted and modified from (*1*).

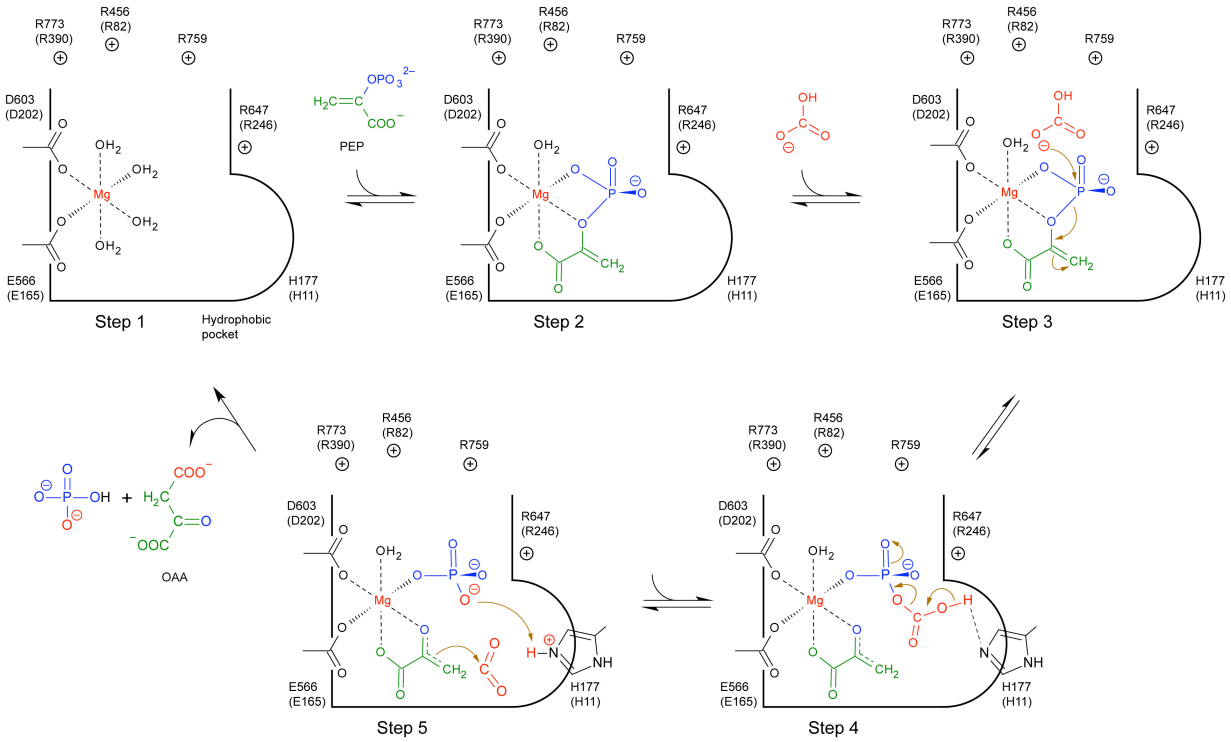

Fig. 2.9. The structural basis for Pepc reaction. Residue numbers shown are for maize Pepc. Numbers within parenthesis are for conjectured homologous residues of *C. perfringens* PepcA. Adapted from (*2*).

Chapter 3

Tyr^{235} of human cytosolic phosphoenolpyruvate carboxykinase influencing catalysis through an anion-quadrupole interaction with phosphoenolpyruvate carboxylate

Published in: FEBS Journal 275: 5810-5819 (2008)

(Used with permission from John Wiley and Sons, 2011)

Lakshmi Dharmarajan[1,2], Christopher L. Case[1,3,4,5] , Pete Dunten[6] and Biswarup Mukhopadhyay[1,2,3,4*]

[1]Virginia Bioinformatics Institute, [2]Genetics, Bioinformatics and Computational Biology PhD Program and Departments of [3]Biochemistry and [4]Biological Sciences, Virginia Polytechnic Institute and State University, Blacksburg, VA, [6]Stanford Linear Accelerator Center, Menlo Park, CA

[5]Current address: Yale University School of Medicine Section of Microbial Pathogenesis, 295 Congress Avenue, BCMM 345 New Haven, CT 06536.

3.1. Abstract

Tyr^{235} of GTP-dependent phosphoenolpyruvate (PEP) carboxykinase is a fully invariant residue. The aromatic ring of this residue establishes an energetically favorable weak anion–quadrupole interaction with PEP carboxylate. The role of Tyr^{235} in catalysis was investigated via kinetic analysis of site-directed mutagenesis-derived variants. The Y235F change lowered the apparent K_m for PEP by about six-fold, raised the apparent K_m for Mn^{2+} by about 70-fold, and decreased oxaloacetate (OAA)-forming activity by about 10-fold. These effects were due to an enhanced anion–quadrupole interaction between the aromatic side chain at position 235, which now lacked a hydroxyl group, and PEP carboxylate, which probably increased the distance between PEP and Mn^{2+} and consequently affected the phosphoryl transfer step and overall catalysis. For the Y235A and Y235S changes, an elimination of the favorable edge-on interaction increased the apparent K_m for PEP by four- and six-fold, respectively, and the apparent K_m for Mn^{2+} by eight- and six-fold, respectively. The pyruvate kinase-like activity, representing the PEP dephosphorylation step of the OAA-forming reaction, was affected by the substitutions in a similar way to the complete reaction. These observations indicate that the aromatic ring of Tyr^{235} helps to position PEP in the active site and the hydroxyl group allows an optimal PEP–Mn^{2+} distance for efficient phosphoryl transfer and overall catalysis. The Y235A and Y235S changes drastically reduced the PEP-forming and OAA decarboxylase activities, probably due to the elimination of the stabilizing interaction between Tyr^{235} and the respective products, PEP and pyruvate.

3.2. Introduction

Phosphoenolpyruvate (PEP) carboxykinase (PEPCK) is an ATP-dependent or GTP-dependent enzyme that catalyzes the formation of PEP from oxaloacetate (OAA).

$$OAA + GTP\ (ITP) \leftrightarrow PEP + CO_2 + GDP\ (IDP)$$

ATP-dependent PEPCK (ATP-PEPCK) is present primarily in bacteria, trypanosomatids, C4 plants and yeast (*6, 44*) whereas GTP-dependent PEPCK (GTP-PEPCK) is found in mammals, other eukaryotes and archaea, and rarely in bacteria (*3, 9*). The PEPCK reaction is considered to be the first-committed step in gluconeogenesis and glycerogenesis (*3, 69*). By virtue of this activity, the GTP-PEPCKs contribute to the overproduction of hepatic glucose in mammals, which is associated with type 2 (noninsulin-dependent) diabetes mellitus (*70*). This correlation has been further established by the observations that overexpression of the liver cytosolic GTP-PEPCK gene causes diabetes mellitus in mice (*70*), and the silencing of hepatic cytosolic PEPCK by RNA interference helps diabetic mice to overcome diabetes-induced hyperglycemia (*43, 71*). For this reason, GTP-PEPCKs have been studied for the development of type 2 diabetes therapeutics (*26, 72*).

One way to alleviate the diabetes-induced hyperglycemia would be to lower the activity of GTP-PEPCK by use of a therapeutic agent; complete inhibition would be undesirable, because it would cause hypoglycemia.

With this rationale, there have been efforts to identify the residues in GTP-PEPCK that have major but not essential roles in catalysis (*11*). The current study deals with the

residue Tyr^{235} in human cytosolic PEPCK, and the following information details the logic for selecting this target.

The overall sequence identity between GTP-PEPCK and ATP-PEPCK is < 20% (*28*). In spite of this apparent dissimilarity, the fold and the active site residues of these enzymes are highly similar (*6, 26*). Also, a common catalytic mechanism is conserved in both classes of PEPCK (*27-32, 44*). A critical component of this conservation is the phosphoryl transfer step. During PEP synthesis by GTP-PEPCK, the phosphoryl transfer task involves the catalytic cleavage of the γ-phosphate bond of GTP, and for the chicken liver mitochondrial enzyme, this event has been argued to be the rate-limiting step (*11, 42*). The cleavage is also dependent on an enzyme-bound divalent cation, which is distinct from the one that complexes the nucleotide substrate (*9, 38, 40, 42, 73-77*). GTP-PEPCKs have been shown to have an absolute requirement for divalent cations. Mn^{2+} is the preferred cation for enzyme activation and phosphoryl transfer from the nucleotide substrate, and Mg^{2+} is a better ligand for the nucleotide (*9, 26, 38-42, 78*). As the enzyme-bound Mn^{2+} would influence phosphoryl transfer from PEP or GTP, we have been interested in learning how the position of Mn^{2+} relative to that of PEP or the nucleotide substrate influences the catalysis (*11*). Consequently, our attention has turned to the residues that play roles in positioning PEP or the nucleotide.

In this study, the focus was on the PEP–Mn^{2+} interaction. On the basis of the available crystal structure data (*26*), we hypothesized that Tyr^{235} helps to position PEP optimally in the catalytic site and therefore influences the PEP–Mn^{2+} distance. We tested this hypothesis via site-directed mutagenesis and kinetic analysis of designed variants, and

found that although Tyr^{235} is not essential for catalysis, it provides fine control of the enzymatic activity through an anion–quadrupole interaction.

3.3. Methods

3.3.1. Site-directed mutagenesis and generation of purified PEPCK proteins

The plasmid pCLC2-19b (*79*) which carries the coding sequence for human cytosolic PEPCK and allows the expression of the protein under the control of a T7 promoter was used as a starting point. The coding sequence was mutagenized using the QuikChange® kit from Stratagene (La Jolla, CA). The details of the mutagenesis method have been described previously (*11*). The mutagenic oligonucleotide pairs used to generate the expression vectors for three PEPCK variants, Y235F, Y235S and Y235A are listed in Table S1. In addition to creating the desired substitutions (Site 1, Table S1), each mutagenic primer introduced an *EcoR*I site at nucleotide position 6096-7001 of the vector (Site 2, Table S1) without changing the corresponding amino acid sequence. The mutated plasmids were initially screened using this restriction site. The wild-type plasmid pCLC2-19b contains two *EcoR*I sites. Upon digestion with *EcoR*I, a mutant plasmid produced three fragments of sizes 1.036, 0.443 and 6.098 kb, whereas the wild-type generated 7.134 and 0.443 kb fragments. For each mutant plasmid DNA sequencing of both strands of the coding region confirmed that the mutagenesis procedure altered only the targeted bases. Recombinant human PEPCK and variant enzymes were expressed and purified as described previously (*79*). The His-tag was removed from homogenous rHumcPCK-His_{10} through treatment with enterokinase

(Novagen, Inc.), leaving behind one non-native His residue at the N-terminus. All data in this study were collected using this enzyme.

3.3.2. Enzyme and protein assays and data analysis

Protein was assayed according to Bradford (*80*) using the dye reagent from Bio-Rad Laboratories (Richmond, CA). PEPCK activity was determined in both the OAA-forming and PEP-forming directions using modifications of previously described procedures (*69, 74, 81, 82*). In the direction of OAA formation the progress was followed by coupling the PEPCK reaction to the malate dehydrogenase (MDH) reaction and by monitoring NADH oxidation spectro-photometrically at 340 nm (*82*). The thermophilic MDH from *Thermus flavus* (Sigma, St. Louis, MO), which is sufficiently active at 37 °C, was used for this purpose. The PEP-forming or gluconeogenic activity was measured via a coupled assay with lactate dehydrogenase (LDH) (Roche, Indianapolis, IN) and pyruvate kinase (PK) (Roche) where the consequent consumption of NADH was monitored (*81*). The standard reaction mixture for measuring the OAA-forming activity contained 100 mM HEPES-NaOH, pH 7.2, 100 mM $KHCO_3$, 3 mM PEP, 2 mM GDP, 2 mM $MgCl_2$, 1.5 mM $MnCl_2$, 10 mM DTT, 0.2 mM NADH and 2 units of MDH per mL. For assaying the PEP-forming activity, a standard reaction mixture contained 100 mM HEPES-NaOH, pH 7.2, 0.3 mM OAA, 0.2 mM GTP, 2 mM $MgCl_2$, 0.2 mM $MnCl_2$, 10 mM DTT, 0.2 mM NADH, 11 units of LDH per mL, 3 units of PK per mL and 1 mM ADP. To measure the pyruvate kinase-like (PK-like) activity the standard reaction mixture contained the same ingredients that were used for the OAA-forming activity assay, except that the former lacked bicarbonate and MDH and contained 20 units of LDH per mL. The OAA

decarboxylase (OAD) activity was determined both in the presence and absence of 0.5 mM GDP using the same reaction mixture prepared for the PEP-forming assay, except that the mixture lacked PK, ADP and GTP. The spontaneous decarboxylation of OAA was measured, and then PEPCK was added to start the reaction. All assays were performed at 37^{o}C.

The initial rate data were analyzed according to Cleland (*83*) using the KinDist, a PC-graphics program obtained from Bryce V. Plapp, University of Iowa (Iowa City, IA). The Henri-Michaelis-Menten relationship ($v=V_m*S/(K_m+S)$) was used for analyzing the initial velocity data. The symbols used are as follows: *v,* initial velocity, μmol min^{-1} mg^{-1}; *S,* substrate concentration, mM; V_m, maximum initial velocity, μmol min^{-1} mg^{-1}; K_m, Michaelis' constant, mM.

3.3.3. Circular Dichroism (CD) spectroscopy

The CD spectra of purified PEPCK proteins were collected between 190 and 260 nm and analyzed as described previously (*11, 84-86*), except the molar ellipticity was calculated based on the value of 623 for the number of residues per PEPCK subunit, including the extra histidine residue which remained after the His_{10} tag was removed.

3.4 Results

3.4.1. Substrate kinetics for the OAA-forming activity of human cytosolic PEPCK and variants

The Y235F variant exhibited low OAA-forming activities at 0.2 mM $Mn^{2+,}$ and the concentration of Mn^{2+} required for optimal activity was 1.5 mM (data not shown). For the

Y235A and Y235S variants, the optimal Mn^{2+} concentration was 0.8 mM (data not shown). A kinetic study of the wild-type enzyme with varying concentrations of PEP conducted at two different Mn^{2+} concentrations, 0.2 mM and 1.5 mM, yielded similar values of apparent K_m and V_{max} for PEP (Fig. S1). The kinetic parameters for the Y235A and Y235S variants did not change significantly when the Mn^{2+} concentration was raised from 0.8 to 1.5 mM (data not shown). Hence, all further kinetic assays in the OAA-forming direction were performed at 1.5 mM Mn^{2+} and 2 mM Mg^{2+}.

The apparent V_{max} values of the Y235A and Y235S variants were about 34% and 50% lower, respectively, than that of the wild-type enzyme (Table 3.1). The Y235F variant had substantially lower OAA-forming activity, the apparent V_{max} of this enzyme being about 10% of that of the wild-type enzyme (Table 3.1). As compared to the wild-type enzyme, the Y235F variant displayed an approximately six-fold lower apparent K_m for PEP (Fig. S1, Table 3.1). Apparent K_m values for PEP of the Y235A and Y235S variants were approximately four- and six-fold higher, respectively, than that of the wild-type enzyme (Fig. S1, Table 3.1). The Y235S and Y235A changes affected the catalytic efficiency values for PEP or kcat/K_m (PEP) more severely than the Y235F substitution (Table 3.1). This is because the former two substitutions increased the K_m for PEP, whereas with the latter, this value dropped; in both cases, the specific activity decreased.

Table 3.1. Apparent values of kinetic constants in the OAA-forming direction for human cytosolic PEPCK and its variants[a]

Variable substrate (concentration range tested, mM)	Metal ion (concentration, mM)	Enzyme	K_m	V_{max}	$k_{cat}{}^{b}/K_m$	Fig. for the plot
			μM	$\mu mol\ min^{-1}\ mg^{-1}$	x 10^5 M^{-1} S^{-1}	
PEP (0.005-4)	Mn^{2+}(1.5), Mg^{2+}(2)	Y235	217 ± 15	31 ± 0.5	1.6	S1
		Y235F	36 ± 1	3 ± 0.2	0.9	S1
		Y235A	919 ± 13	20 ± 1.1	0.3	S1
		Y235S	1256 ± 11	15 ± 0.6	0.1	S1
Mn^{2+} (0.005-1.5)	Mg^{2+} (2)	Y235	9 ± 1	31 ± 0.6	39.3	S6
		Y235F	607 ± 11	4 ± 0.3	0.1	S6
		Y235A	73 ± 9	19 ± 0.5	2.9	S6
		Y235S	58 ± 2	13 ± 0.8	2.6	S6

[a] From the fits shown in corresponding figures.
[b] Based on a subunit molecular mass of 68.5 kDa for the monomeric PEPCK.

Replacement of Tyr^{235} by Phe, Ala and Ser did not bring about any notable change in the apparent K_m value for GDP (Fig. S2, Table 3.2). The substantially low k_{cat}/K_m(GDP) value for the Y235F variant was due to a low specific activity of this variant. For the bicarbonate, apparent K_m values of the Y235F, Y235A and Y235S variants were 2.8-, 3- and 2.7-fold lower than that of the wild-type enzyme (Fig. S3, Table 3.2). Owing to parallel drops in specific activities and K_m values, the values for the variants were about the same as those of the wild-type enzyme. The CD data showed that the engineered changes in the PEPCK primary structure did not cause any substantial alterations in the enzyme's secondary structure (data not shown).

Table 3.2. Apparent kinetic constants in the OAA-forming direction of human cytosolic PEPCK and its variants[a]

Variable substrate (concentration range tested, mM)	Metal ion (concentration, mM)	Enzyme	K_m	V_{max}	K_{cat} [c]/K_m	Fig. for the plot
			μM	$\mu mol\ min^{-1}\ mg^{-1}$	x 10^5 M^{-1} S^{-1}	
GDP (0.005-2)	Mg^{2+}(2)	Y235	45 ± 4	33 ± 0.6	8.4	S2
		Y235F	47 ± 8	3 ± 0.1	0.7	S2
		Y235A	34 ± 5	15 ± 0.4	5.0	S2
		Y235S	44 ± 4	11 ± 0.2	2.9	S2
GDP (0.005-2)	Mg^{2+}(5)	Y235	44 ± 3	35 ± 0.5	9.1	S2
		Y235F	60 ± 1	3 ± 0.1	0.6	S2
		Y235A	35 ± 4	15 ± 0.3	4.9	S2
		Y235S	40 ± 3	10 ± 0.1	2.9	S2
GDP (0.005-2)	Mg^{2+}(7.5)	Y235	41 ± 3	35 ± 0.6	9.7	S2
		Y235F	67 ± 2	3 ± 0.2	0.5	S2
		Y235A	34 ± 3	15 ± 0.2	5.0	S2
		Y235S	53 ± 2	11 ± 0.8	2.4	S2
HCO_3^- (5-300)[b]	Mg^{2+}(2)	Y235	20,700 ± 2,500	44 ± 1.9	0.02	S3
		Y235F	7,200 ± 220	5 ± 0.1	0.01	S3
		Y235A	6,800 ± 670	21 ± 0.5	0.03	S3
		Y235S	7,500 ± 200	14 ± 1.0	0.02	S3

[a] From the fits shown in corresponding figures.
[b] The kinetic values recorded were from the fits obtained of data from 5 to 100 mM concentrations of bicarbonate.
[c] Based on a subunit molecular mass of 68.5 kDa for the monomeric PEPCK.

3.4.2. Substrate kinetics for the PEP-forming activity of human cytosolic PEPCK and variants

In the PEP-forming direction, there was no significant variation in the apparent K_m values for OAA or GTP among the wild-type, Y235F, Y235A and Y235S enzymes (Figs S4 and S5, Table 3.3). The apparent V_{max} values of the Y235A and Y235S variants were approximately 13-fold lower than that of the wild-type enzyme, whereas the Y235F variant was as active as the wild-type enzyme (Table 3.3). The changes in the

k_{cat}/K_m(OAA) and k_{cat}/K_m(GTP) values also confirmed the negative effects of the Y235S and Y235A substitutions on catalysis in the PEP-forming direction.

Table 3.3. Apparent kinetic constants in the PEP-forming direction of human cytosolic PEPCK and its variants[a]

Variable substrate (concentration range tested, mM)	Enzyme	K_m	V_{max}	$K_{cat}{}^{b}/K_m$	Fig. for the plot
		μM	$\mu mol\ min^{-1}\ mg^{-1}$	x 10^5 M^{-1} S^{-1}	
OAA (0.001-0.3)	Y235	33 ± 2	35 ± 0.5	12.1	S4
	Y235F	38 ± 4	39 ± 0.9	11.7	S4
	Y235A	47 ± 6	3 ± 0.9	0.7	S4
	Y235S	61 ± 6	3 ± 0.9	0.6	S4
Mn^{2+} (0.0005-0.2)	Y235	0.8 ± 0.06	29 ± 0.3	413.9	S7
	Y235F	0.7 ± 0.03	31 ± 0.2	505.6	S7
	Y235A	0.4 ± 0.05	2 ± 0.7	57.1	S7
	Y235S	0.7 ± 0.01	2 ± 0.2	32.6	S7
GTP (0.001-0.2)	Y235	64 ± 6	39 ± 1.2	6.9	S5
	Y235F	26 ± 3	41 ± 0.9	18.0	S5
	Y235A	59 ± 2	3 ± 0.2	0.6	S5
	Y235S	43 ± 6	3 ± 0.1	0.8	S5

[a] From the fits shown in corresponding figures.
[b] Based on a subunit molecular mass of 68.5 kDa for the monomeric PEPCK.

3.4.3. Mn^{2+} kinetics of human cytosolic PEPCK and variants

In the OAA-forming direction, the apparent K_m values for Mn^{2+} of the Y235F, Y235A and Y235S variants were approximately 70-, eight- and six-fold higher, respectively, than that of the wild-type enzyme (Fig. S6, Table 3.1). The drastic drop in the value due to the Y235F change highlighted the deleterious effect of this substitution in terms of the utilization of Mn^{2+} by the enzyme in the OAA formation reaction. Raising the $MgCl_2$ concentration from the standard 2 to 5 mm and 7.5 mm did not significantly change the apparent K_m and of the wild-type and variant enzymes for Mn^{2+} (Fig. S6, Table 3.4).

In the PEP-forming direction, there was no significant variation in the apparent K_m values for Mn^{2+} among the wild-type and variant enzymes (Fig. S7, Table 3.3); the observed reduction in the value due to the Y235A and Y235S substitutions was primarily due to a decrease in the specific activity.

3.4.4. Pyruvate kinase (PK)-like activity of human cytosolic PEPCK and variants

The apparent K_m for PEP of the Y235F variant measured via the PK-like activity was approximately six-fold lower than that of the wild-type enzyme, whereas apparent K_m values of the Y235A and Y235S variants were not significantly different from that of the wild-type enzyme (Fig. S8, Table 3.5). The apparent V_{max} values of the Y235F, Y235S and Y235A variants were approximately six-, three- and three-fold lower, respectively, than that of the wild-type enzyme (Table 3.5). The observed drop in the k_{cat}/K_m(PEP) value resulting from the Y235S and Y235A substitutions was solely due to the poorer specific activities of the variants; parallel drops in K_m and V_{max} values allowed k_{cat}/K_m(PEP) to remain unchanged for the Y235F variant.

Table 3.4. Apparent kinetic constants for Mn^{2+} of human cytosolic PEPCK and its variants[a] in the OAA-forming direction

Variable substrate (concentration range tested, mM)	Metal ion (concentration, mM)	Enzyme	K_m	V_{max}	$K_{cat}{}^{b}/K_m$	Fig. for the plot
			μM	$\mu mol\ min^{-1}\ mg^{-1}$	x 10^5 M^{-1} S^{-1}	
Mn^{2+} (0.005-1.5)	Mg^{2+}(5)	Y235	9 ± 1	31 ± 0.6	39.3	S6
		Y235F	562 ± 14	4 ± 0.3	0.1	S6
		Y235A	64 ± 8	18 ± 0.5	3.2	S6
		Y235S	48 ± 1	13 ± 0.7	3.1	S6
Mn^{2+} (0.005-1.5)	Mg^{2+}(7.5)	Y235	9 ± 1	31 ± 0.4	39.3	S6
		Y235F	521 ± 10	4 ± 0.2	0.1	S6
		Y235A	57 ± 7	18 ± 0.5	3.6	S6
		Y235S	43 ± 1	13 ± 0.6	3.5	S6

[a] From the fits shown in corresponding figures.
[b] Based on a subunit molecular mass of 68.5 kDa for the monomeric PEPCK.

Table 3.5. Apparent oxaloacetate decarboxylase and pyruvate kinase-like activities of human cytosolic PEPCK and its variants[a]

Activity	Variable substrate (concentration range tested, mM)	Enzyme	K_m	V_{max}	$K_{cat}{}^{d}/K_m$	Fig. for the plot
			μM	$\mu mol\ min^{-1}\ mg^{-1}$	x 10^5 $M^{-1}S^{-1}$	
PK-like	PEP (0.05-4)	Y235	1.9 ± 0.66	3.8 ± 0.6	0.02	S8
		Y235F	0.3 ± 0.11	0.6 ± 0.04	0.02	S8
		Y235A	1.8 ± 0.54	1.1 ± 0.1	0.01	S8
		Y235S	1.8 ± 0.64	1.2 ± 0.2	0.01	S8
OAD	OAA (0.025-1)	Y235	0.3 ± 0.02,0.4 ± 0.04[c]	4 ± 0.1, 3 ± 0.2[c]	0.15, 0.1	S9,S10[c]
		Y235F	0.3 ± 0.05,0.4 ± 0.02[c]	2 ± 0.2, 3 ± 0.1[c]	0.08, 0.1	S9,S10[c]
		Y235A	ND[b], 0.3 ± 0.07[c]	ND[b], 0.2 ± 0.01[c]	ND[b], 0.01	S9,S10[c]
		Y235S	ND[b], 0.3 ± 0.04[c]	ND[b], 0.1 ± 0.01[c]	ND[b], 0.004	S9,S10[c]

[a] From the fits shown in corresponding figures.
[b] Due to very low activity reliable values of kinetic constants could not be obtained.
[c] In presence of GDP.
[d] Based on a subunit molecular mass of 68.5 kDa for the monomeric PEPCK.

3.4.5. Oxaloacetate decarboxylase (OAD) activity of human cytosolic PEPCK and variants

OAD activities were measured both in the presence and in the absence of the nucleotide, GDP. In both cases, the values of each kinetic constant were similar (Figs S9 and S10, Table 3.5). In the case of the Y235A and Y235S variants, activities in the absence of GDP could not be analyzed reliably in kinetic terms (Fig. S9). In the presence of GDP, apparent K_m values for OAA of the wild-type, Y235F, Y235A and Y235S enzymes were about the same (Fig. S10, Table 3.5). Apparent V_{max} values of the Y235 and Y235F variants were similar, whereas the Y235A and Y235S variants showed very low OAD activities; the k_{cat}/K_m values for OAA had a similar pattern.

3.5. Discussion

The results presented above, combined with the available structural data (*26, 43, 44*), provide an insight into the role of the fully invariant Tyr^{235} of human cytosolic PEPCK in catalysis. In the absence of PEP, the hydroxyl of Tyr^{235} forms a hydrogen bond with the side chain amide of the fully conserved Asn^{403} (Fig. 3.1A) (*26*). When PEP binds, Tyr^{235} moves; the oxygen of the hydroxyl group is displaced by 4.7 Å. At this new location, the aromatic ring undergoes an edge-on interaction with the carboxylate of PEP (Fig. 3.1A). The hydroxyl of Tyr^{235} forms a hydrogen bond with the main chain carbonyl group of Asn^{403}; PEP forms a hydrogen bond with the latter's side chain amide. Both PEP and Tyr^{235} are stabilized by these interactions. The binding of the nucleotide and the closure of the active site lid facilitate movement of PEP towards Mn^{2+} (*44*). Tyr^{235} moves back to

re-form a hydrogen bond with the side chain amide of Asn^{403}. These processes facilitate the inner sphere coordination of the phosphate of PEP to enzyme-bound Mn^{2+} by pushing PEP further towards this divalent cation, which has been proposed to facilitate phosphate transfer between PEP and GDP (*41*). In fact, in this state, PEP is more susceptible to nucleophilic attack by the β-phosphate of GDP (*44*).

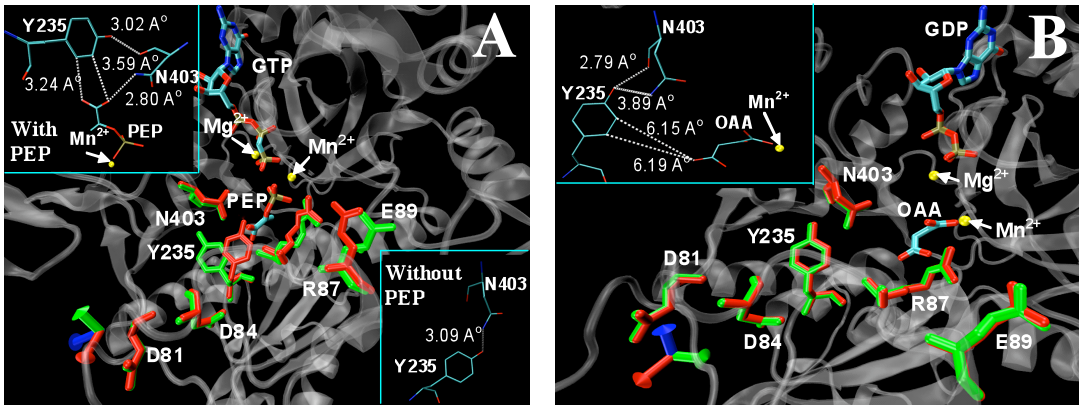

Fig. 3.1. Active sites of human and rat cytosolic PEPCKs. In each case, the structural data were manipulated using VMD (*87*) to generate the image shown here. (A) Structures with and without bound PEP and GTP analog have been superimposed. Positions of the relevant residues when PEP is not bound are shown in red, and their positions in the enzyme with bound PEP are shown in green. The insets with PEP and without PEP show the interactions of Tyr^{235} and Asn^{403}. The Protein Data Bank IDs are 1KHG, 1KHF and 1KHB. (B) Structures with and without bound OAA and GDP have been superimposed. Positions of the relevant residues when OAA is not bound are shown in red, and their positions in the enzyme with bound OAA are shown in green. The inset shows the distances between Tyr^{235}, Asn^{403} and OAA. The Protein Data Bank IDs are 2QEW and 2QF2.

Examples of interactions analogous to that of Tyr^{235} with PEP are found in studies involving oxygen atoms and phenyl rings in a set of small molecules, where the oxygen atoms are coplanar with the aromatic rings (*50, 52, 88*); aromatic amino acid–anionic amino acid pairs have been used as models in some of these investigations (*50*). Similar cases involving substrates or inhibitors that carry phenyl rings and the anionic

units of the protein have also been found; in one such example, the partners are ethacrynic acid and hemoglobin (*89*). These edge-on interactions occurring between anions and the positively charged edges of aromatic rings have been termed anion–quadrupole interactions (*50*). The positive charge is a result of the quadrupole moment of the ring, which produces a quadrupolar charge distribution (*50*). The results are a positive electrostatic potential near the edges and a negative potential above and below the ring (*50*). Ab initio and AM1 calculations for electrostatic potential also depict the surfaces of benzene and phenol rings as having a positive potential at the edges (*51*). As a result, the edge-on interaction is energetically favorable, with an energy gain as much as –1 kcal·mol^{-1}, which varies as a function of 1/r3 (*52*).

In the Y235F variant, the absence of the hydroxyl group increases the positive potential on the aromatic ring and enhances the stabilizing edge-on interaction between PEP and the residue. The observed lowering of apparent K_m for PEP by about six-fold in the Y235F variant is consistent with this deduction (Table 3.1). As Phe does not have a hydroxyl group, it cannot form a hydrogen bond with the side chain of Asn^{403}, and might not facilitate the eventual inner sphere coordination of PEP to Mn^{2+}, like the wild-type enzyme. Perhaps these effects led to an increased distance between enzyme-bound Mn^{2+} and PEP phosphate, and consequently raised the apparent K_m for Mn^{2+} substantially (Table 3.1), affected phosphoryl transfer, and resulted in lower activity of the Y235F variant (Table 3.1). The increased requirement for Mn^{2+} was not due to a change in the need for a divalent cation to complex the nucleotide substrate, because

an increase in the concentration of Mg^{2+} from 2 to 5 mm and 7.5 mm did not lower the apparent K_m for Mn^{2+} (Table 3.4).

The Y235A and Y235S changes abolished the edge-on interaction that existed between Tyr and PEP, and in turn affected the apparent K_m for PEP, albeit only slightly (Table 3.1). These substitutions did not lead to increased binding of PEP, as seen in the Y235F variant, and hence catalysis was not perturbed substantially. On the other hand, a simultaneous rise in the apparent K_m value and lowering of the specific activity in each of these cases decreased the catalytic efficiency (Table 3.1).

PK-like activity represents the dephosphorylation step of the complete PEP to OAA conversion of the PEPCK reaction. Hence, to analyze whether the mutations caused any changes in the dephosphorylating activity of the enzyme, the PK-like activities of the wild-type enzyme and the variants were measured. The resulting data provided finer elucidation of the role of Tyr^{235}. A change from Tyr to Phe caused an approximately six-fold drop in the apparent K_m for PEP and V_{max} of the PK-like activity, whereas replacement with Ala or Ser did not have a significant effect on this kinetic parameter (Table 3.5). These observations support the hypothesis that Tyr^{235}, with its phenyl ring and hydroxyl group, positions PEP optimally and thereby maintains an effective PEP–Mn^{2+} distance. Loss of Tyr^{235} lessens this effectiveness and affects phosphoryl transfer.

In the Escherichia coli ATP-PEPCK, the residues equivalent to Tyr^{235} and Arg^{87} of the human enzyme are part of the binding pocket for CO2 (*90*). In our studies, replacement

of Tyr^{235} slightly affected the apparent K_m value for bicarbonate (Fig. S3, Table 3.2). This observation is consistent with a minor role of Tyr^{235} in binding CO_2.

As seen from the crystal structure of the rat cytosolic PEPCK, which is very similar to the human enzyme, no change in the position of Tyr^{235} occurs when OAA binds the enzyme (Fig. 3.1B) (*43*). The distance between Tyr^{235} and OAA, which is approximately 6–7 Å, is also not conducive to a significant interaction between them. The PEP-forming activities of the Y235A and Y235S variants were extremely low, and this is the first time that a change in the primary structure has been found to reduce the gluconeogenic activity of a GTP-PEPCK (Table 3.3). However, no significant changes were noted in the apparent K_m values for OAA, Mn^{2+} or GTP in these variants, in comparison with the wild-type enzyme, which implies that the interactions of these substrates with the active site were not affected appreciably. An analysis of the OAD activity, which represents the decarboxylation step of the PEP-forming reaction, provided a rationale for the above-mentioned observations. This activity was measured both in the presence and in the absence of GDP, as previous studies suggest a requirement for NDP in the decarboxylation of OAA by GTP-PEPCKs (*38, 43, 81*). However, the OAD activity of the human enzyme was not influenced by GDP (Figs S9 and S10; Table 3.5). In terms of this activity the Y235F variant was not significantly different from the wild-type enzyme, whereas the Y235A and Y235S variants were severely impaired. The low activities of the Y235A and Y235S variants could not be attributed to a change in the apparent K_m for OAA, as the values of this parameter for the two variants were similar to that of the wild-type enzyme. These effects most likely originated from the perturbed interaction

between PEP (or pyruvate) and Tyr^{235}. When OAA is converted to PEP, Tyr^{235} probably helps to release this product from the Mn^{2+} by an edge-on interaction with the carboxylate. In the Y235A and Y235S variants, an absence of the aromatic ring slows this release, and the activity of the variant enzymes is reduced severely.

In summary, Tyr^{235} is not an essential residue for GTP-PEPCKs, but it is critical for maintaining an appropriate PEP–Mn^{2+} distance for optimal phosphoryl transfer and catalysis in the OAA-forming direction. It also allows efficient progress of the PEP-forming reaction by aiding in the release of the product.

Author contributions : Lakshmi Dharmarajan designed and performed experiments and prepared the manuscript, Christopher L. Case designed and performed experiments, Pete Dunten and Biswarup Mukhopadhyay conceived the idea of the manuscript and supervised the work, and all authors contributed to the preparation of the final manuscript.

3.6. Supplementary Tables and Figures

Table S1. Oligonucleotides for site-directed mutagenesis

Template for PCR[a]	Variant PEPCK enzyme generated	Oligonucleotide sequence[b]	
		Site 1	Site 2
pCLC2-19b	Y235F	5' CCTTTGGCAGTGGG***TTC***GGCGG**GAATTC**GCTGCTCGGG 3'	
	Y235A	5' CCTTTGGCAGTGGG***GCC***GGCGG**GAATTC**GCTGCTCGGG 3'	
	Y235S	5' CCTTTGGCAGTGGG***TCC***GGCGG**GAATTC**GCTGCTCGGG 3'	

[a]Wild-type nucleotide sequence of the targeted area :
5' CCTTTGGCAGTGGGTACGGCGGGAACTCGCTGCTCGGG 3'
[b]Only forward primers listed. Site 1, for altering the amino acid sequence; Site 2, for introducing an *EcoR*I site without changing the amino acid sequence

Supplementary Figures

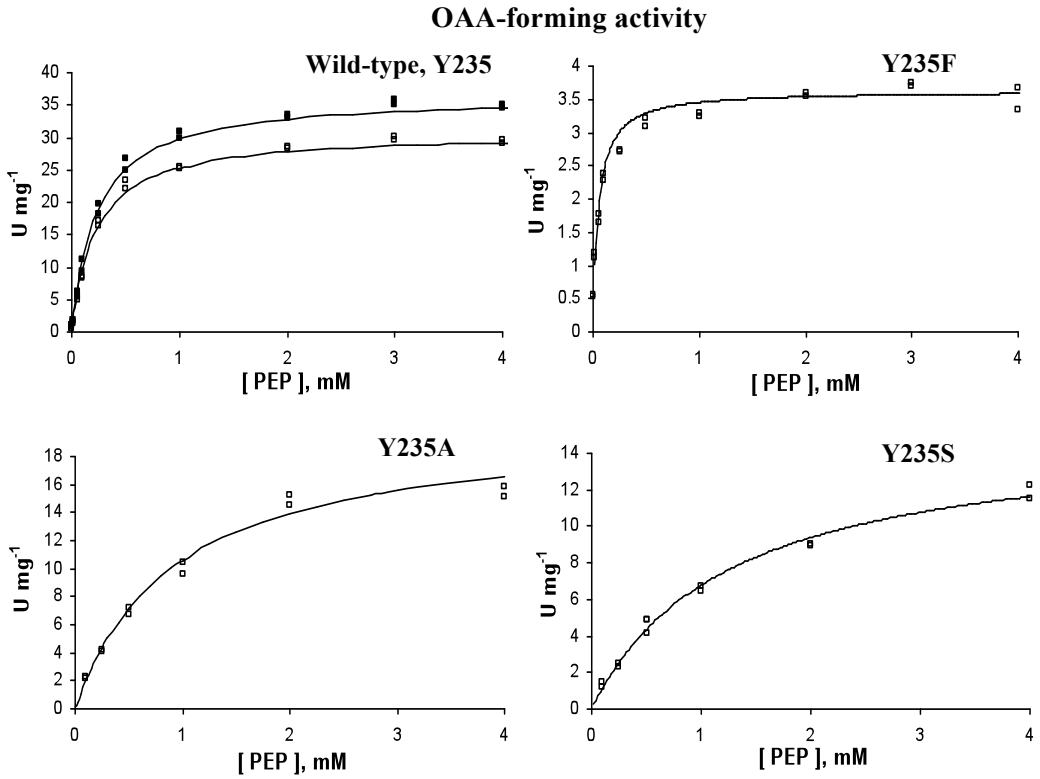

Figure S1. PEP kinetics of the wild-type and Y235 variants for the OAA synthesis activity. The assay mixture was standard as described in the Experimental Methods section except PEP concentration was varied. For the wild-type, assays were performed at two different Mn^{2+} concentrations, 0.2 mM (filled squares) and 1.5 mM (open squares). The variants were assayed with 1.5 mM Mn^{2+} (open squares). The line drawn through the points for each data set is the best fit to the hyperbola $v = V_{max} * S/(K_m + S)$.

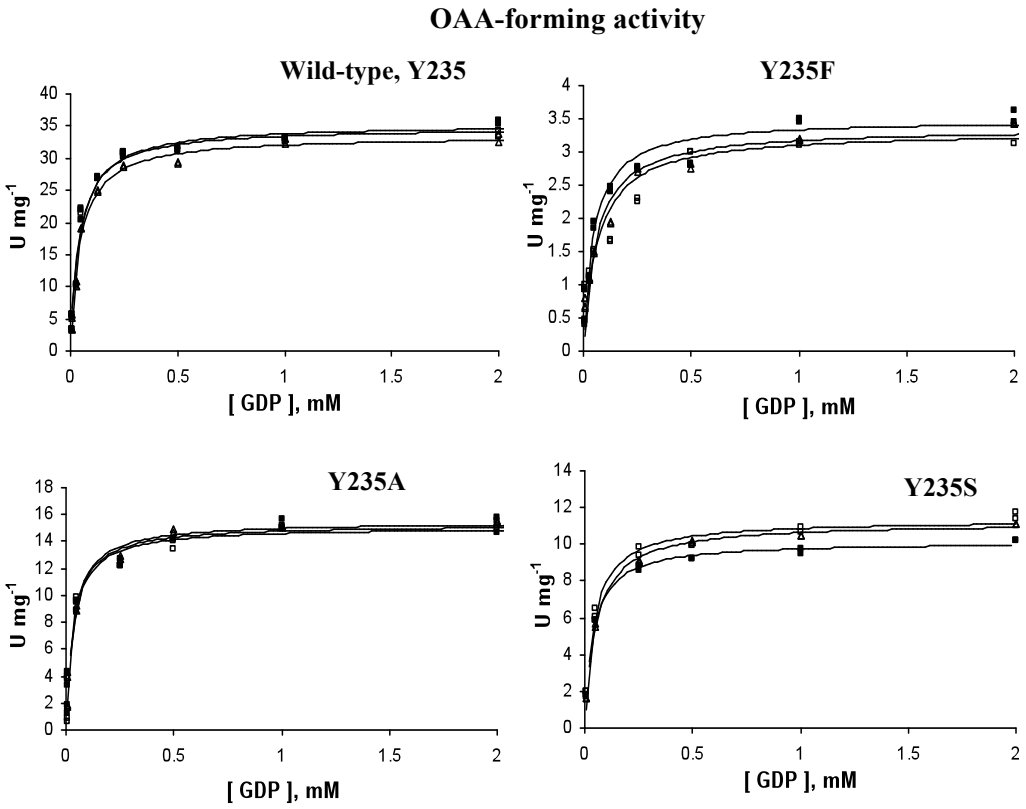

Figure S2. GDP kinetics of the wild-type and Y235 variants for the OAA synthesis activity. The assay mixture was standard as described in the Experimental Methods section except GDP concentration was varied. Assays were performed at three different Mg^{2+} concentrations, 2 mM (filled squares), 5 mM (open squares) and 7.5 mM (open triangles). The line drawn through the points for each data set is the best fit to the hyperbola $v = V_{max} * S/(K_m + S)$.

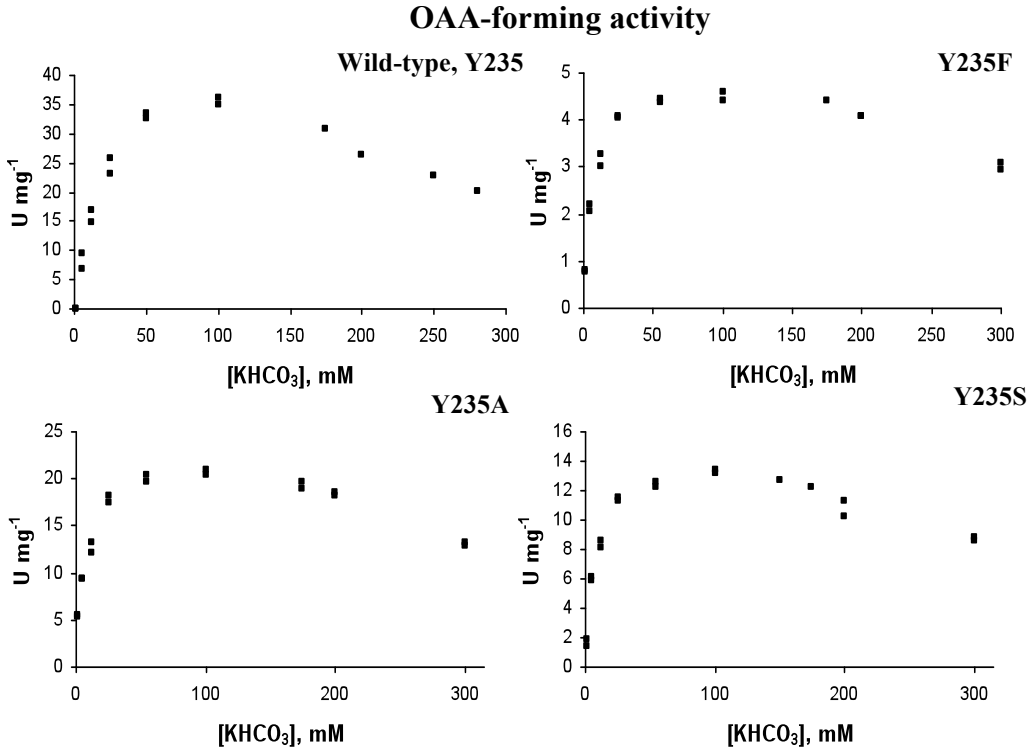

Figure S3. Bicarbonate kinetics of the wild-type and Y235 variants for the OAA synthesis activity. The assay mixture was standard as described in the Experimental Methods section except bicarbonate concentration was varied. The data did not fit the standard substrate inhibition relationship; the apparent K_m and V_{max} values for bicarbonate reported were determined by fitting the data at 5 to 100 mM bicarbonate concentrations to the standard Henri–Michaelis–Menten equation $v = V_{max} * S/(K_m + S)$.

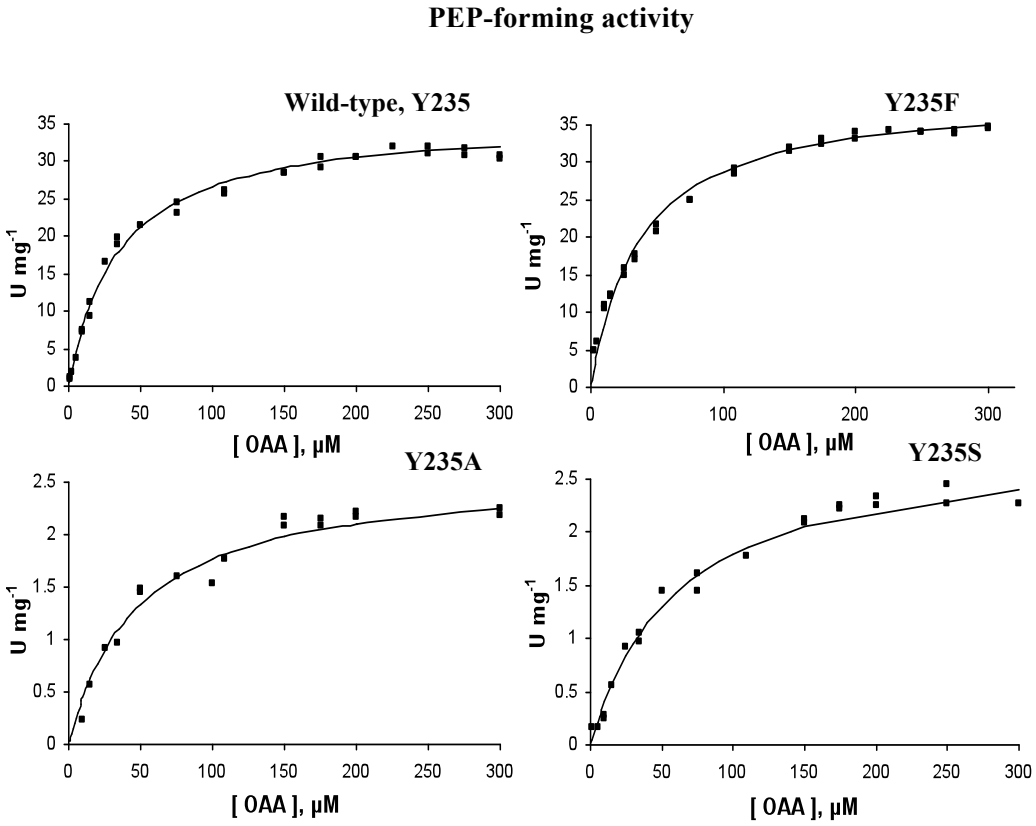

Figure S4. OAA kinetics of the wild-type and Y235 variants of cytosolic human PEPCK for the PEP synthesis activity. The assay mixture was standard as described in the Experimental Methods section except OAA concentration was varied. The line drawn through the points for each data set is the best fit to the hyperbola $v = V_{max} * S/(K_m + S)$.

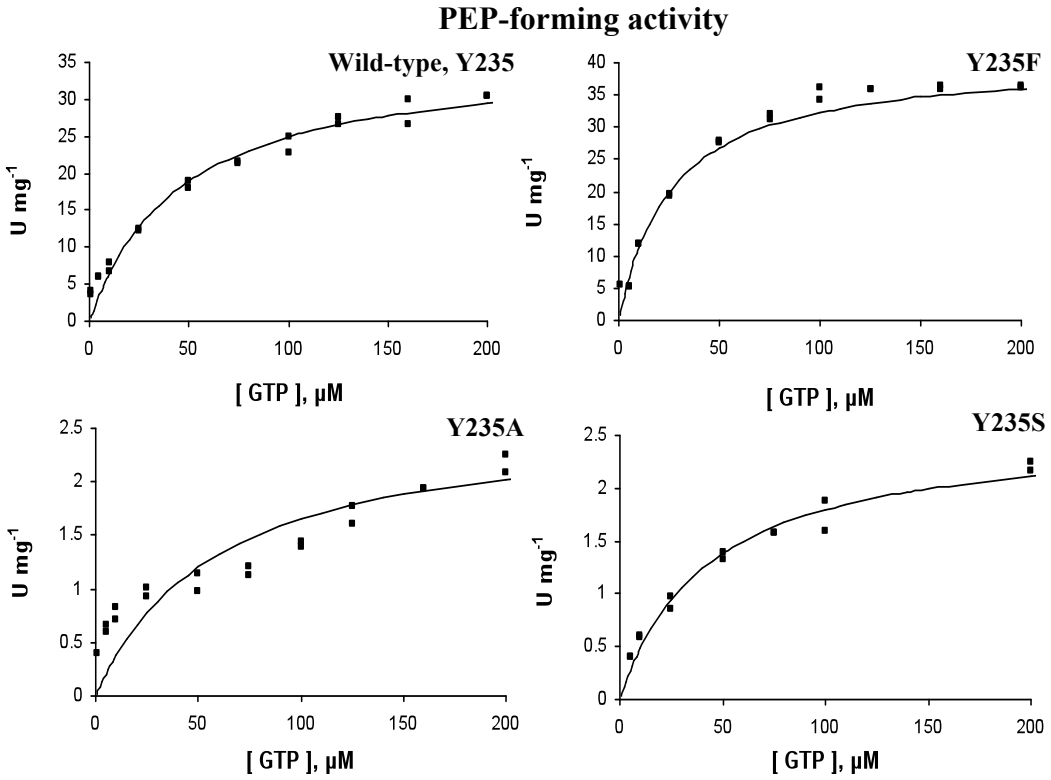

Figure S5. GTP kinetics of the wild-type and Y235 variants for the PEP synthesis activity. The assay mixture was standard as described in the Experimental Methods section except GTP concentration was varied. The line drawn through the points for each data set is the best fit to the hyperbola $v = V_{max} * S/(K_m + S)$.

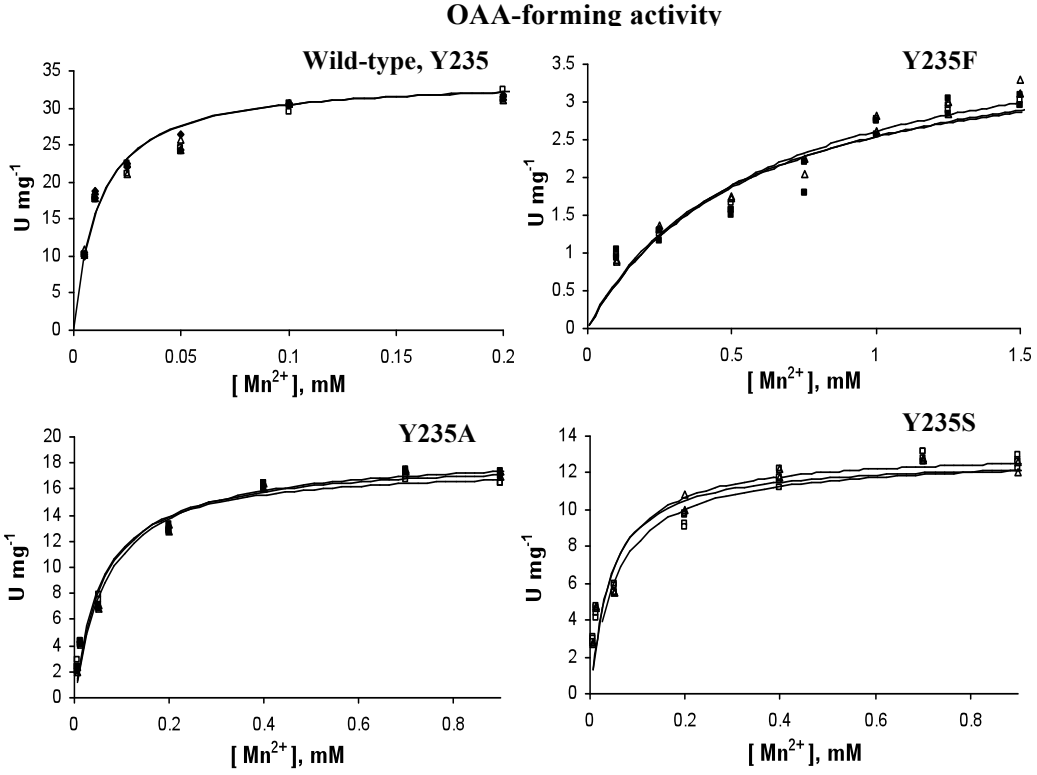

Figure S6. Mn^{2+} kinetics of the wild-type and Y235 variants for the OAA synthesis activity. Assays were performed at three different Mg^{2+} concentrations, 2 mM (filled squares), 5 mM (open squares) and 7.5 mM (open triangles). The assay mixture was standard as described in the Experimental Methods section except Mn^{2+} concentration was varied. Apparent K_m and V_{max} values for Mn^{2+} reported were determined by fitting the data from 0.005 to 0.2, 0.8 and 0.8 mM Mn^{2+} concentrations for Y235, Y235A and Y235S, respectively. The line drawn through the points for each data set is the best fit to the hyperbola $v = V_{max} * S/(K_m + S)$.

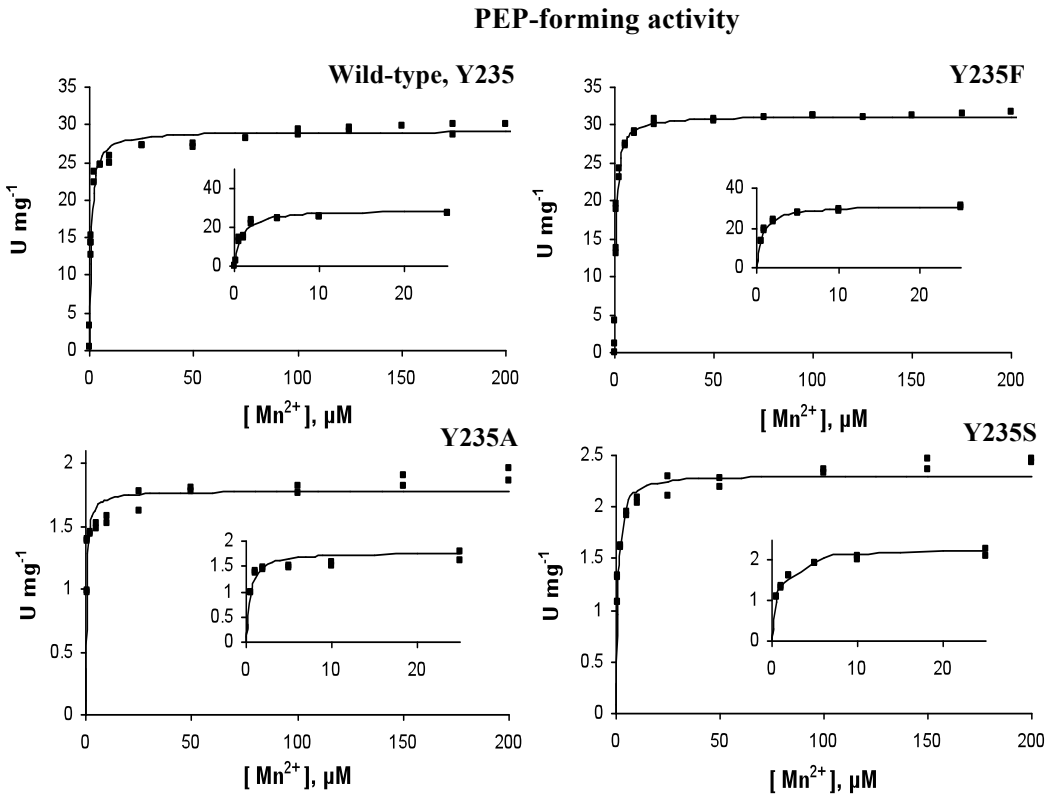

Figure S7. Mn^{2+} kinetics of the wild-type and Y235 variants for the PEP synthesis activity. The assay mixture was standard as described in the Experimental Methods section except Mn^{2+} concentration was varied. The line drawn through the points for each data set is the best fit to the hyperbola $v = V_{max} * S/(K_m + S)$. The insets show the plots for 0-20 mM Mn^{2+}.

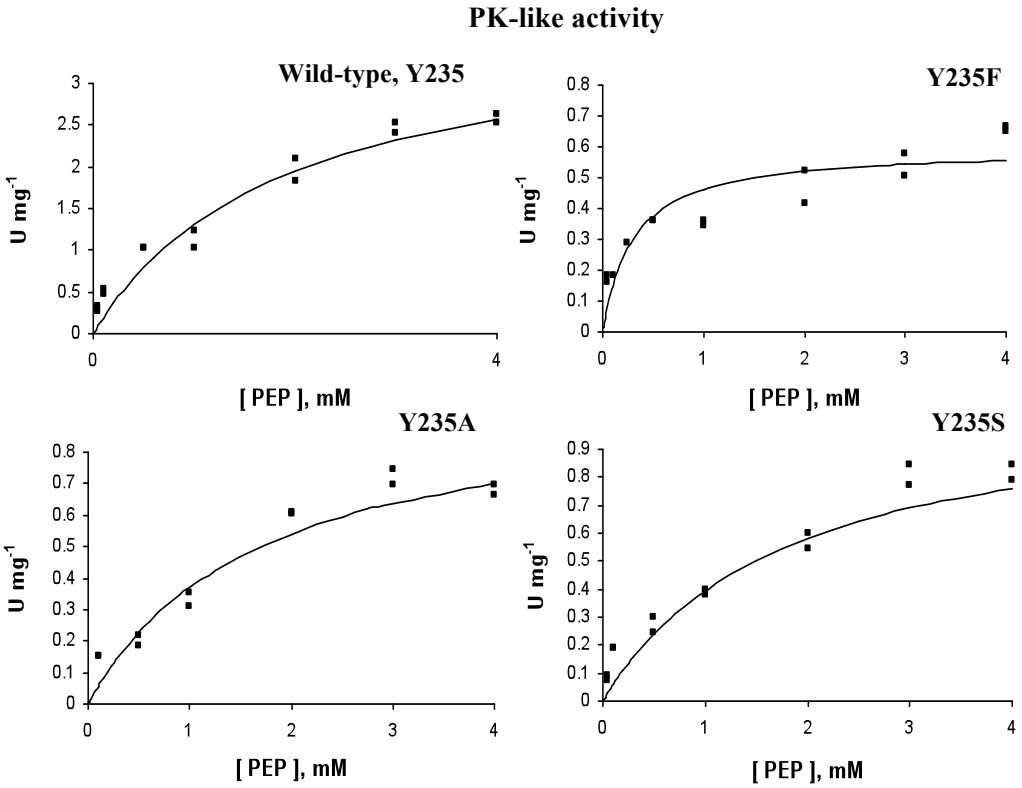

Figure S8. Kinetics of pyruvate kinase-like activity of the wild-type and Y235 variants of cytosolic human PEPCK. The assay mixture was standard as described in the Experimental Methods section except PEP concentration was varied. The line drawn through the points for each data set is the best fit to the hyperbola $v = V_{max} * S/(K_m + S)$.

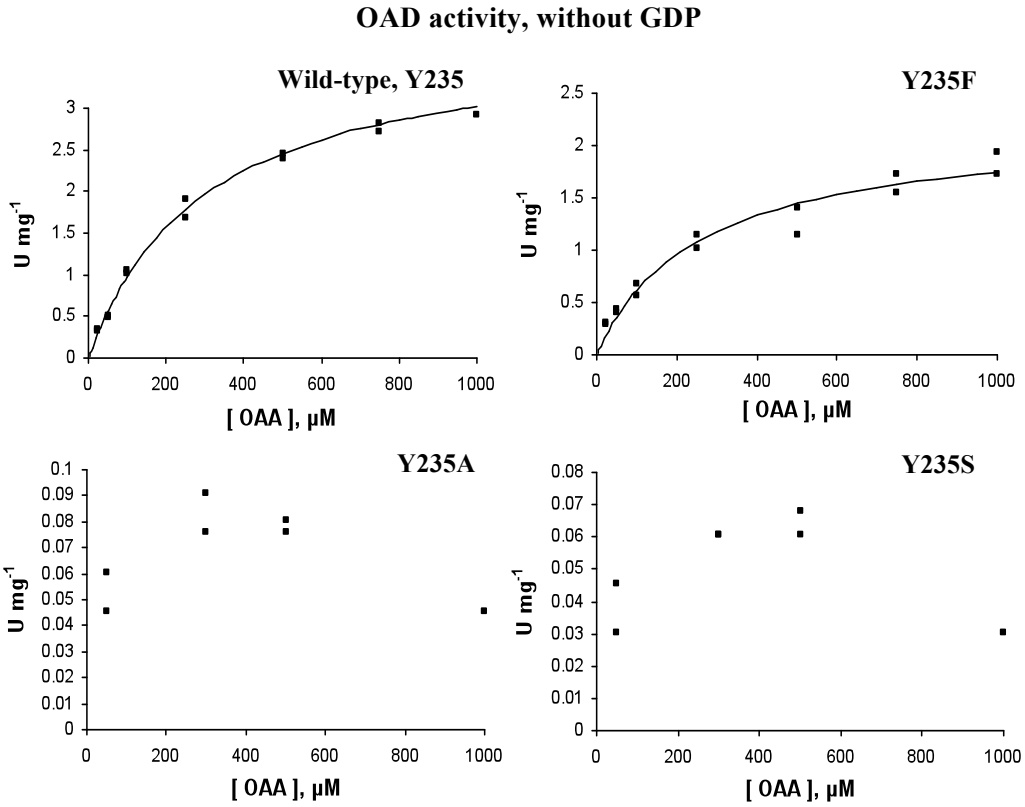

Figure S9. Kinetics of oxaloacetate decarboxylase activity of the wild-type and Y235 variants in the absence of GDP. The assay mixture was standard as described in the Experimental Methods section except OAA concentration was varied. The line drawn through the points for each data set is the best fit to the hyperbola $v = V_{max} * S/(K_m + S)$. For Y235A and Y235S, due to very low activities, a reliable kinetic analysis could not be performed.

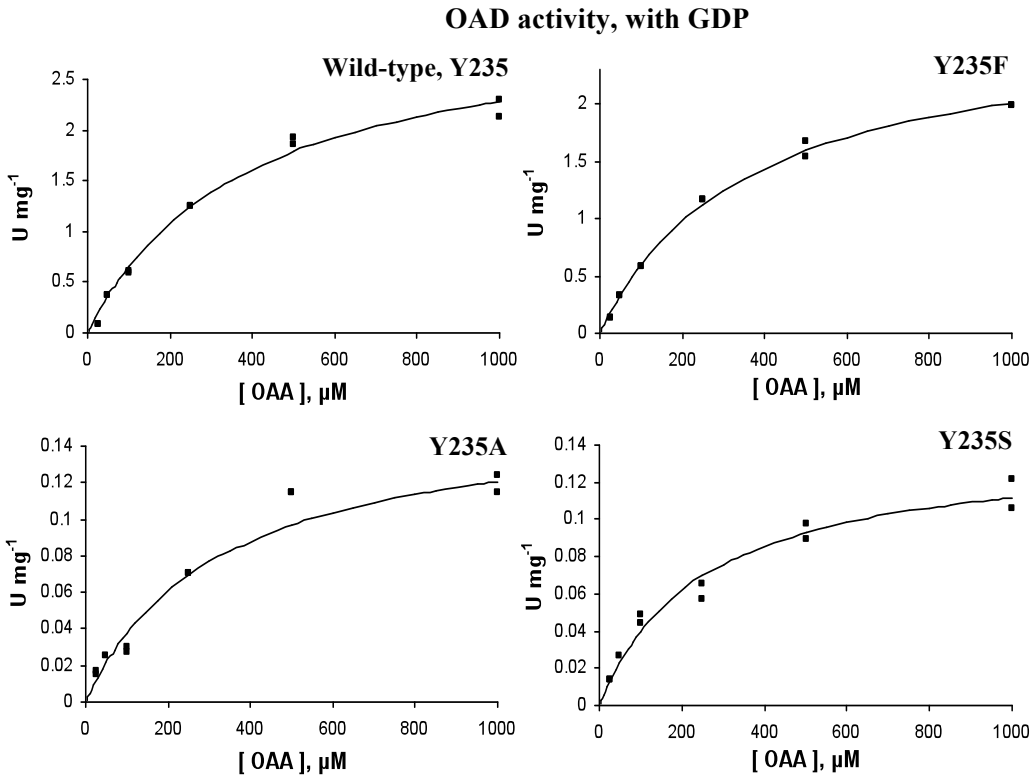

Figure S10. Kinetics of oxaloacetate decarboxylase activity of the wild-type and Y235 variants in the presence of GDP. The assay mixture was standard as described in the Experimental Methods section except OAA concentration was varied. The line drawn through the points for each data set is the best fit to the hyperbola $v = V_{max} * S/(K_m + S)$.

Chapter 4

Dynamics of the active site lid in GTP-PEPCKs

This chapter outlines the preliminary results of MD simulations conducted to study the conformational changes of the active site lid of GTP-PEPCKs. A detailed study is in progress.

Authors : Lakshmi Dharmarajan and Biswarup Mukhopadhyay

4.1. Abstract

Recent crystallographic studies have elucidated that GTP-PEPCKs operate through a lid-gated mechanism (*34*). This active site lid is supposed to protect the hypothesized enolate intermediate from hydrolysis (*3, 34, 91*). The available crystal structures of GTP-PEPCKs all depict the closed conformation of this lid (*3, 34, 43, 44, 91*). Since the loop becomes disordered in the open state, there is no structure available for the lid region. This limits our understanding of the dynamics of this element, an important modulatory site for GTP-PEPCKs (*34, 44, 91*). This motivated us to use molecular dynamics to study the conformation of the open lid and identify the interactions, which would stabilize an open state as compared to the closed state. It is hypothesized that lid closure is induced by the binding of the ligands, PEP and GDP, as shown from existing crystallography data (*34, 43, 91*). In our simulations we have removed these ligands from a lid-closed structure to determine whether absence of ligand binding induces opening of the lid element. Our analysis indicates so, making this the first observation of a lid-open configuration and intermediates of the lid opening process for GTP-PEPCKs. This work is in progress and in this chapter I have presented preliminary data from the analysis.

4.2. Introduction

PEPCKs catalyze the nucleotide-dependent reversible conversion of oxaloacetate (OAA) to phosphoenolpyruvate (PEP) and the enzyme can be divided into two groups, ATP-PEPCKs and GTP-PEPCKs, depending on nucleotide specificity (*3*). The ATP-dependent enzymes are mainly found in bacteria and trypanosomatids, C4 plants and

yeast (*3*). GTP-PEPCKs, on the other hand are present in mammals, eukarya, archaea and some bacteria (*3*). These classes of enzymes do not share much sequence similarity, however their active site residues are conserved and their catalytic mechanisms are similar (*3, 26*). ATP-PEPCKs undergo a large domain movement, around 20^{o} upon ATP-binding, leading to a more compact structure of the enzyme, as observed in *E. coli* PEPCK structure (*3, 26*). GTP-PEPCKs show no such domain movement upon nucleotide binding; however, ligand binding does seem to induce closure of a 10-residue long omega-loop element over the active site (*34, 43*). No dynamic studies have however, been conducted to show this phenomenon. For this study, we reasoned that if ligand binding could lead to loop closure, then the reverse could also occur, i.e. removing the ligands could cause the lid to eventually open. Using this hypothesis, we proceeded with the simulations. We also wanted to identify the stabilizing forces in the protein that guide the opening and closing of the lid. It has also been hypothesized from crystal structure data that the movements of the active-site lid, P-loop and nucleotide-binding domain are correlated. We also wanted to observe the basis of this hypothesis in the course of our simulations.

4.3. Methods

GROMACS 4.0.7 was used for the entire simulation, in conjunction with the ffAmber ’03 force field (*92, 93*). The starting structure was that of rat PEPCK complexed with ions, GDP and phosphoglycolic acid (PGA), which is a structural analog of PEP (PDB i.d. 3DTB) (*34*). The parameters for PGA and GDP were derived from Antechamber from the Amber10 molecular dynamics suite (*94*) and manually corrected to adhere to

GROMACS file formats. In case of constructing the second system, the ligands were removed from the crystal structure. The systems were solvated using a TIP3P water model (*95*) and the charge of the system was neutralized by adding requisite sodium or chloride ions. Each system was then minimized by the steepest descent integrator (*96*) until the maximum force was less than 1000 kJ mol^{-1} nm^{-1} on any atom. A 200 ps NVT equilibration was performed at 310 K with position restraints applied to all of the backbone atoms. A Berendsen thermostat (*97*) was used with a temperature coupling time constant (τ_T) of 0.1 ps. Bond lengths were constrained using the linear constraint solver (LINCS) algorithm, (*98*) and this allowed for a 2 fs time step. Long-range electrostatic interactions were approximated using the particle-mesh Ewald (PME) method (*99, 100*) with a fourth-order spline interpolation and a 0.12 nm Fourier grid spacing. This was followed by a 200 ps NPT simulation, using an isotropic Parrinello–Rahman barostat (*101, 102*) set to 1.0 bar of pressure in all directions and a pressure coupling time constant (τ_P) of 1.0 ps. Production MD runs of 17 ns each were conducted using Berendsen's modified thermostat and Parrinello-Rahman barostat, as well as LINCS and PME. The simulations were performed on Virginia Tech's System X Supercomputer, a 12.25 Teraflop computer comprising 1100 Apple PowerMac G5 computers with dual 2.3 GHz PowerPC 970FX processors (*103*). Simulation data were analyzed using the GROMACS suite of tools; all two-dimensional data were plotted by the program Grace (*104*). VMD was used to visualize the protein structures and to generate figures (*87*).

4.4. Results and discussions

Opening of the loop region and structural changes

In case of the system with the ligands bound, there was no observable conformational change in the active site lid and P-loop regions after a 17 ns simulation (Fig. 4.1A).

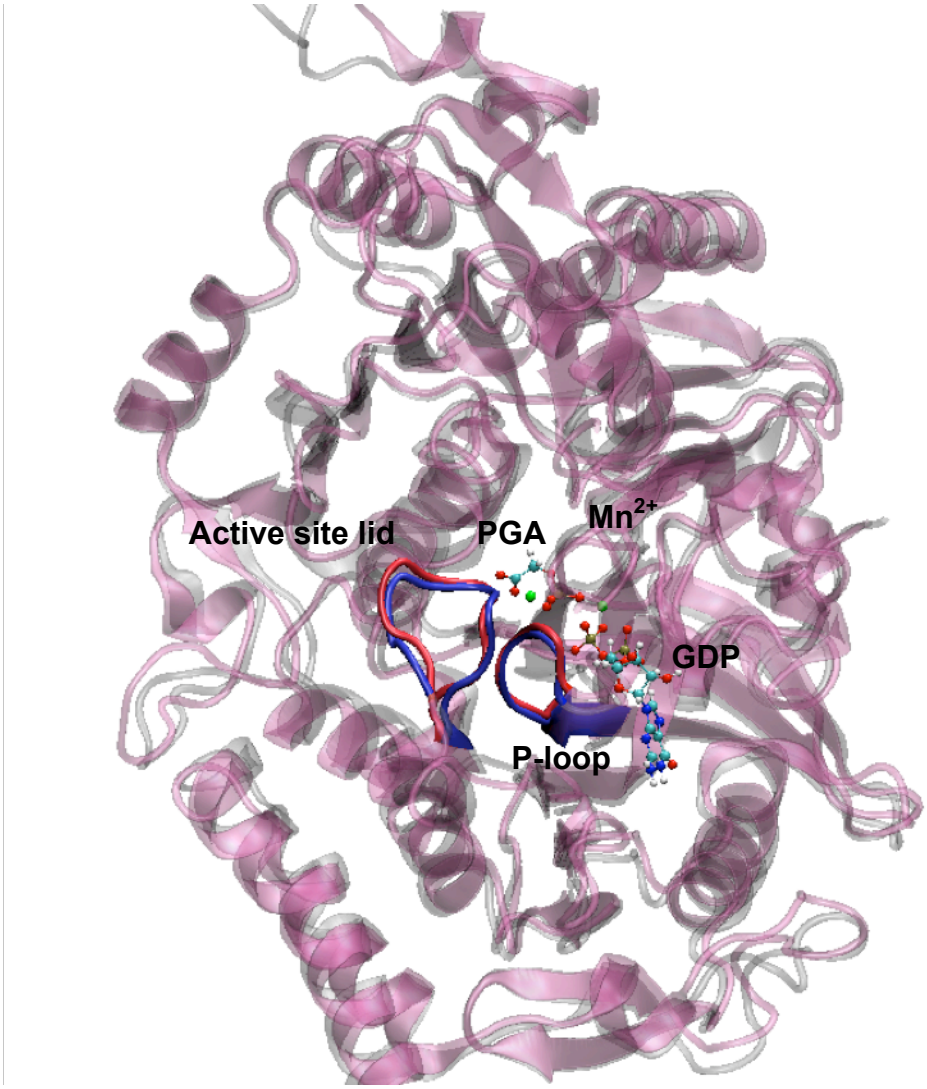

Fig. 4.1A. Superposition of structures of wild-type PEPCK with ligands. Structure at 0 ns (in silver) and after 17 ns simulation (in pink). Loop regions at 0 ns are depicted in blue, that after 17 ns simulation are in red. Mn^{2+} ions are also indicated.

In case of the system without the ligands, however, we could observe a more open state of both the active-site lid and P-loop after the same simulation time (Fig. 4.1B).

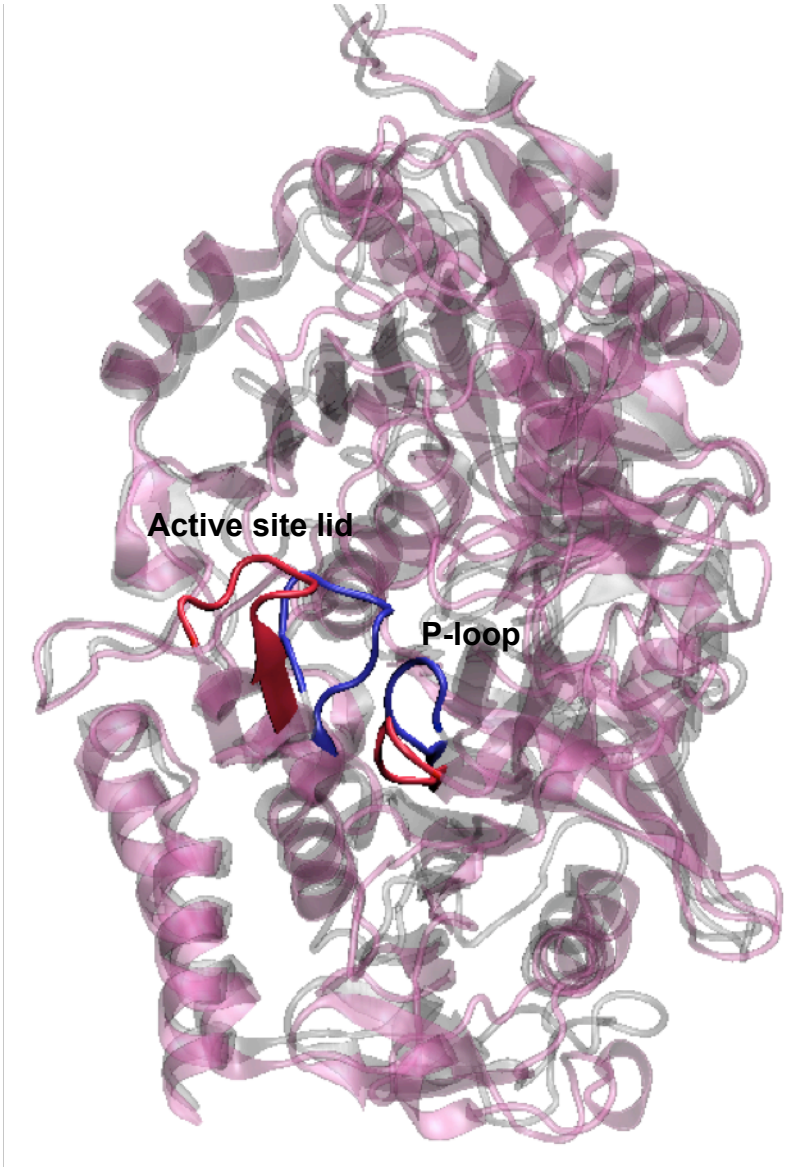

Fig. 4.1B. Superposition of structures of wild-type PEPCK without ligands. Structure at 0 ns (in silver) and after 17 ns simulation (in pink). Loop regions at 0 ns are depicted in blue, and that after 17 ns simulation are in red.

RMSD and RMSF analysis of the overall structure

Comparisons between the average backbone root mean square deviations (RMSDs) of

the closed (with ligands) and open (without ligands) structures are shown in Fig. 4.2. The closed structure appears to be more stable with a lower average RMSD. The open structure, in the absence of ligands, appears to deviate stronger from the starting point.

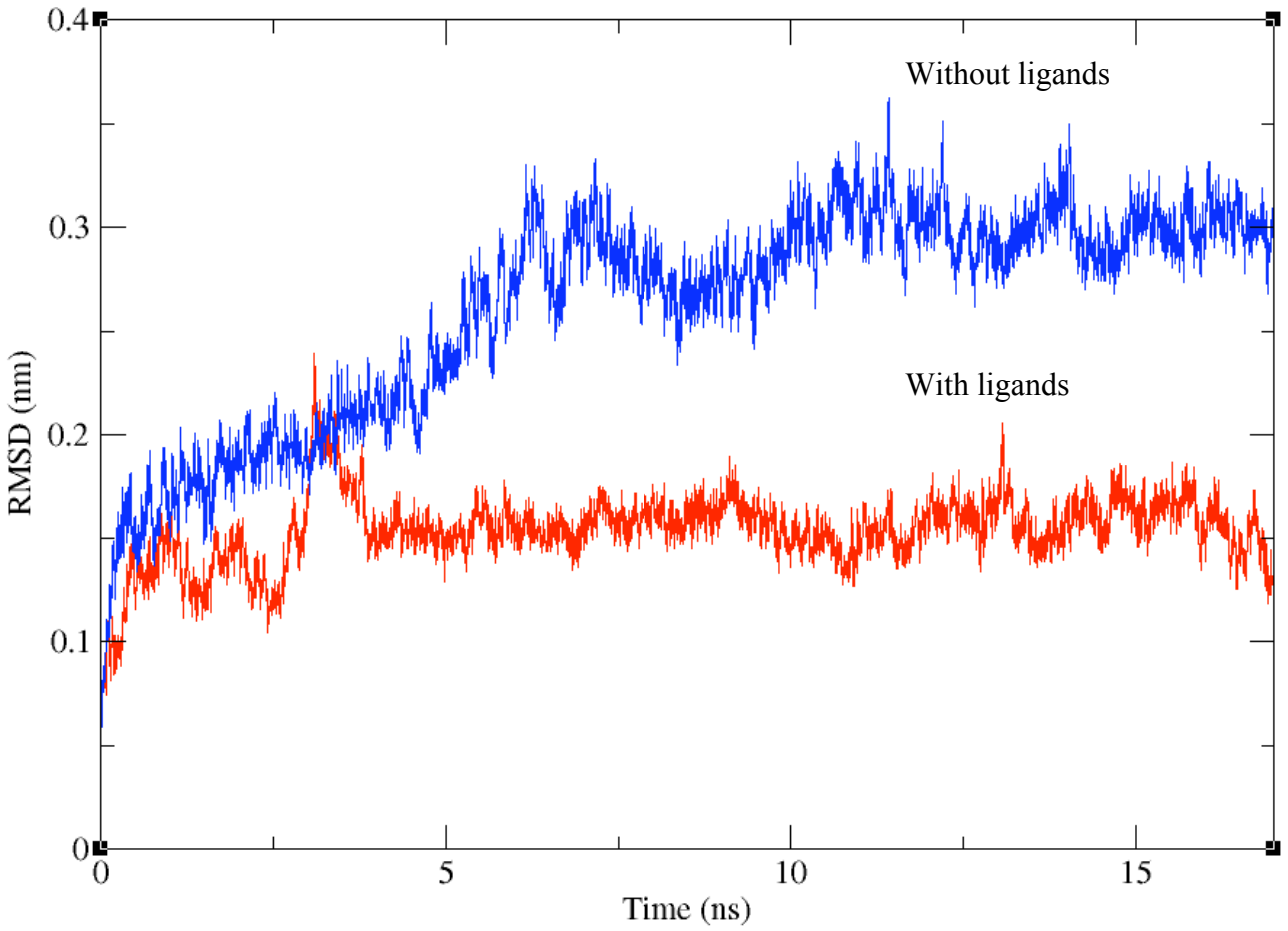

Fig. 4.2. Average backbone RMSDs of wild-type PEPCK. RMSD without ligands - in blue and with ligands - in red.

Root mean square fluctuation (RMSF) analysis per residue revealed more new fluctuations for the open structure than the closed one (Fig. 4.3). The regions near the active site residues (near residues 87, 235, 405, 417, 311, 244, 264, 436, 530, 533), near the active-site lid (near residues 463-470) and near the P-loop (residues 284-288)

all show more fluctuations in the open structure.

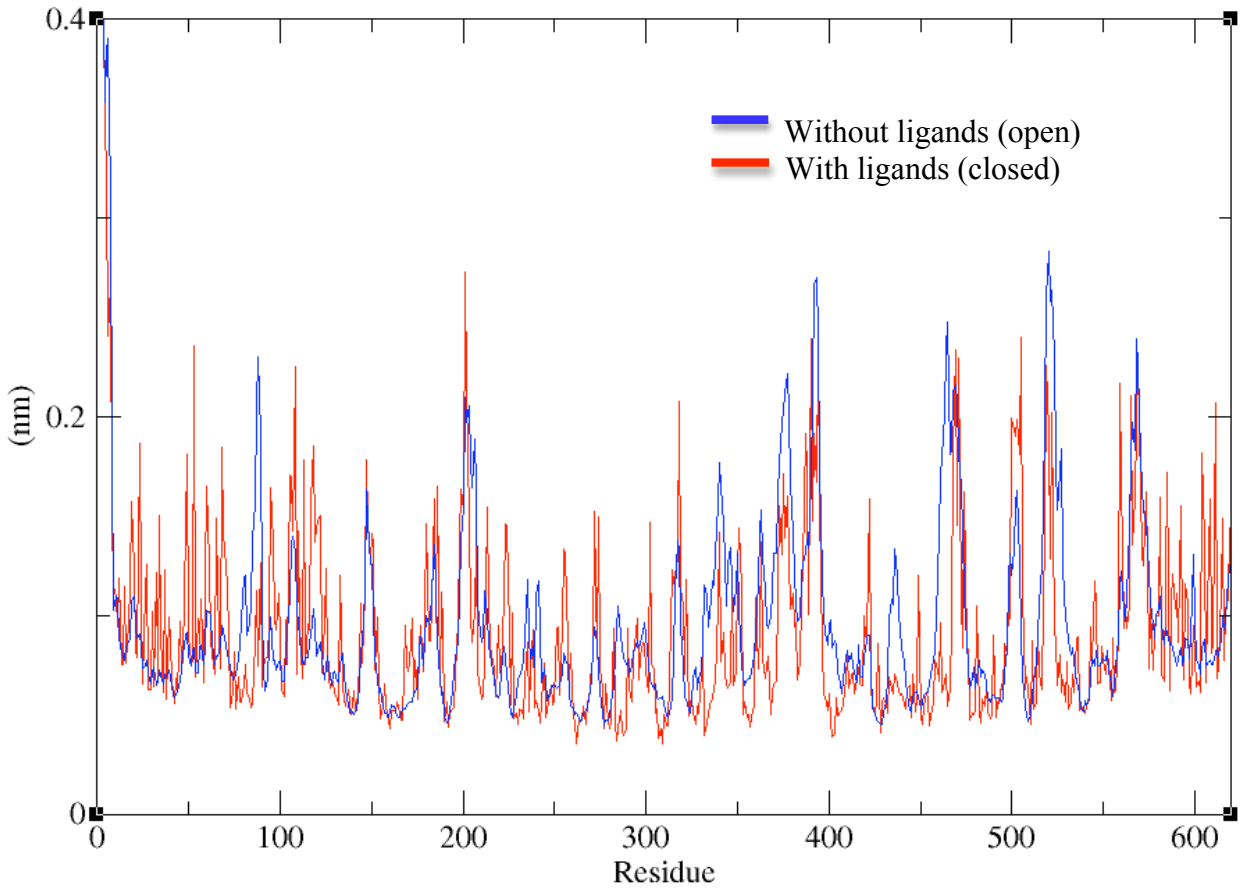

Fig. 4.3. RMSF of wild-type PEPCK. RMSF without ligands (in blue) and in the presence of ligands (in red).

RMSD analysis of the active-site lid region

RMSD analysis of the lid region (residues 463 to 470) also indicated that this region is stabilized in presence of ligands (Fig. 4.4). This is in agreement with the structural snapshots in Fig. 1B, which show the opening of the loop in the absence of ligands.

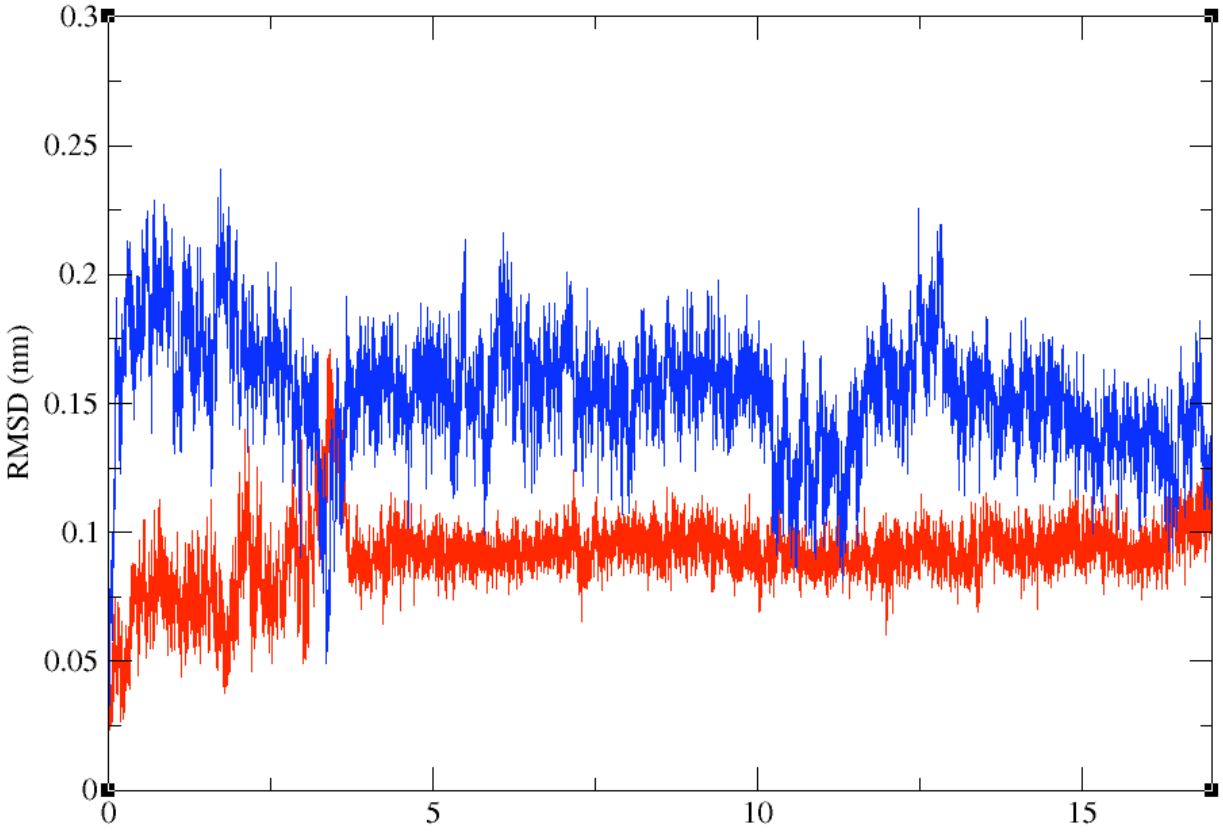

Fig. 4.4. RMSD of the loop region of wild-type PEPCK. RMSD without ligands (in blue) and in the presence of ligands (red).

In addition, the protein adopts a slightly more compact structure when all the ligands are bound, as observed in some crystal structures (*34*). This is observed in Fig. 4.5, where in the ligand-bound structure (in yellow), the loop region around the active site seems to be in a closed state making the active site more compact. In the ligand-free structure (in blue), these loops seem to open outwards more and the region around the active site seems less compact.

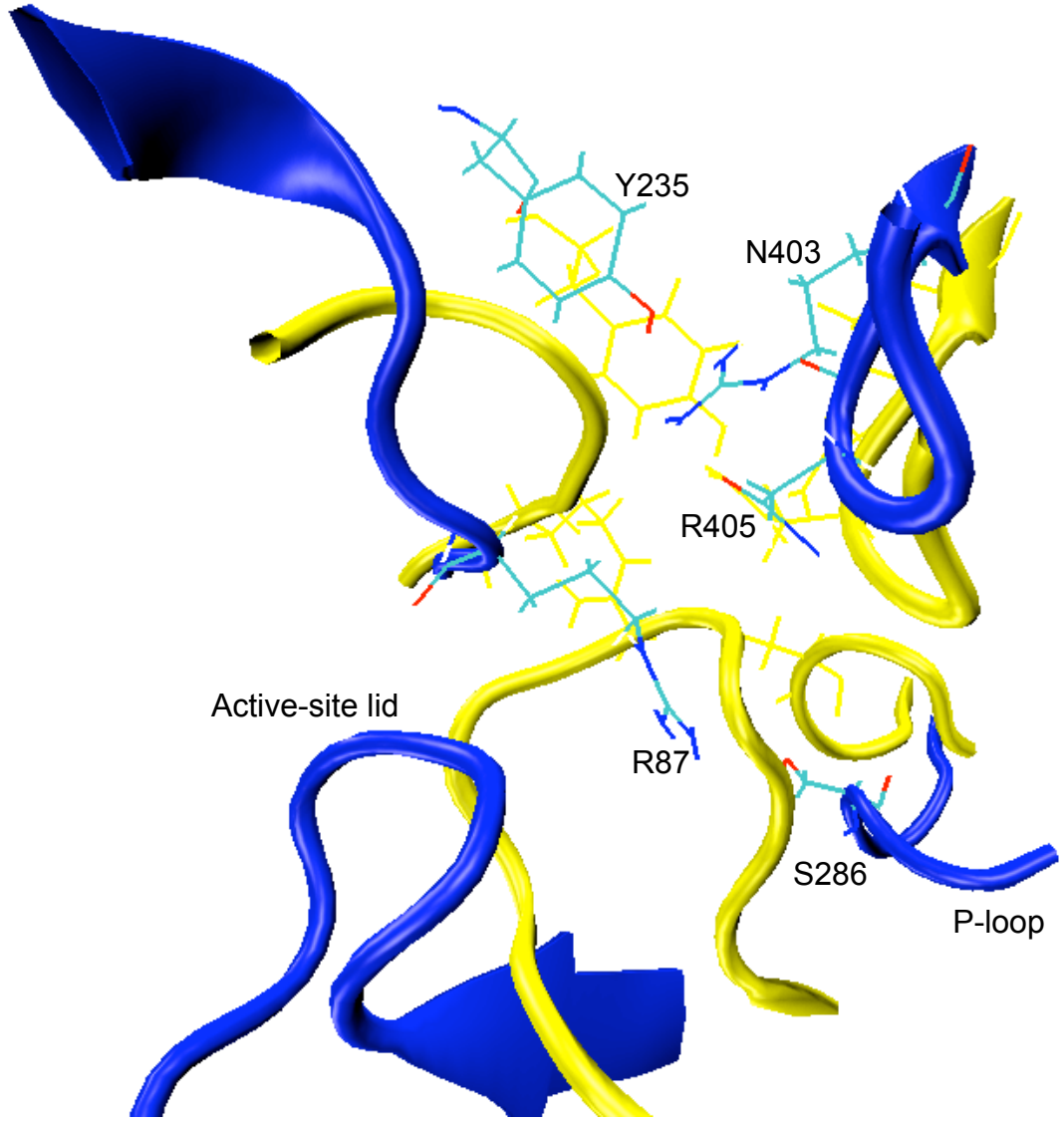

Fig. 4.5. Conformations of the loop region around the active site of wild-type PEPCK. Structure in presence (in yellow) and in absence (blue) of ligands. Active site residues (R87 and R405) and other catalytically important residues on this loop region have been shown.

Correlation between movements of active site lid, P-loop and nucleotide binding region

As hypothesized by Holyoak et al. (*43*) we observed from our simulations the correlation

between movements of active site lid, P-loop and nucleotide binding regions (Fig. 4.6). This further emphasizes that concerted motions are an aspect of this enzyme function.

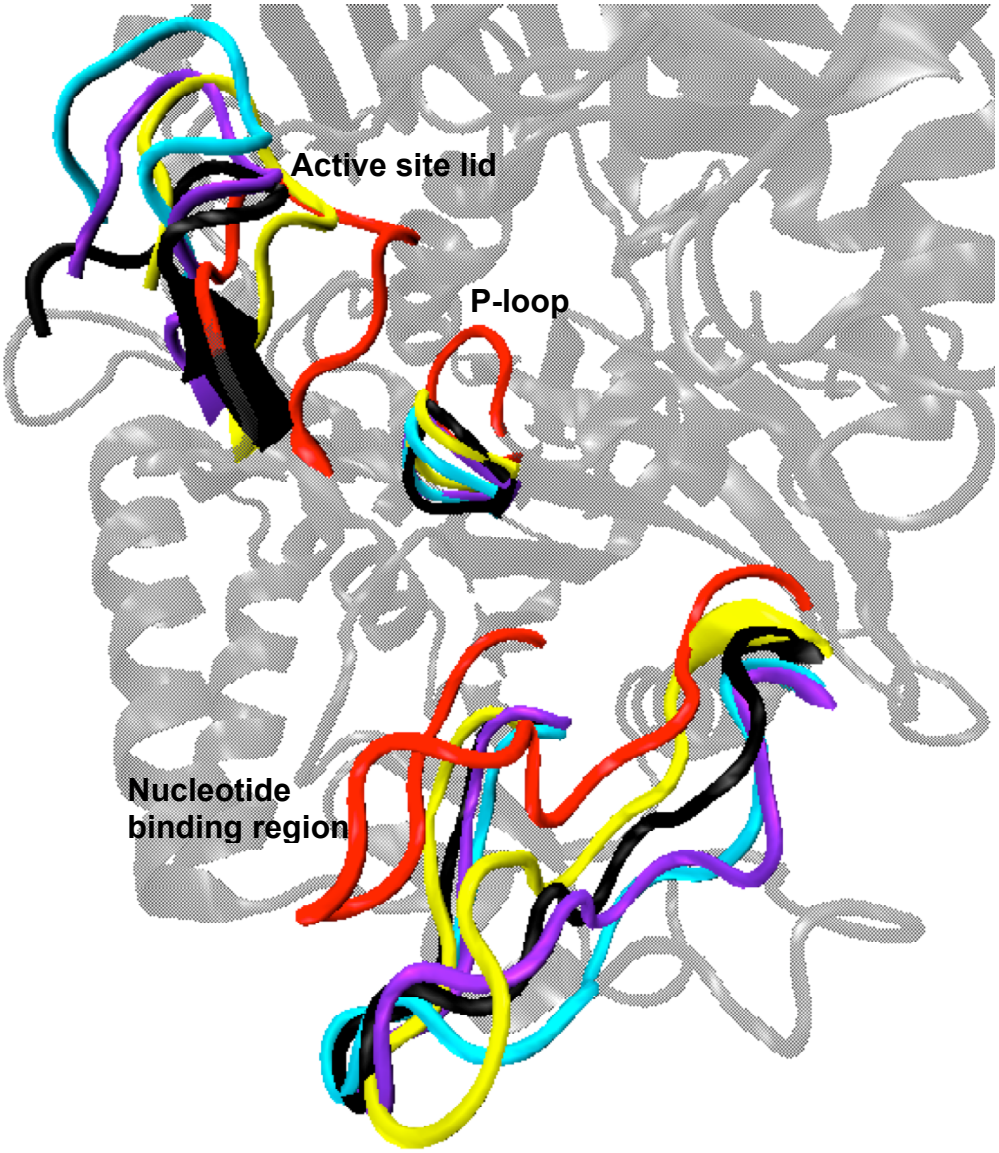

Fig. 4.6. Correlation between movements of active-site lid, P-loop and nucleotide binding region. Loops are colored according to simulation time: 0 ns - red, 5 ns – yellow, 10 ns - cyan, 15 ns - violet, 17 ns – black.

An examination of the intermediates of the lid opening process led to the interesting observation that the position of the lid after 10 ns simulation (Fig. 4.6 in cyan) appeared

to be more open than that seen after 17 ns simulation (Fig. 4.6 in black). It is possible that the position of the lid at 10 ns is an intermediary state in the lid opening process and that the open structure finally stabilizes after 17 ns of simulation. A correlated phenomenon is observed in the P-loop and the nucleotide binding regions (Fig. 4.6).

4.5. Summary

The conformation of the active-site lid in GTP-PEPCKs is important for catalysis, as indicated by previous studies (*34, 91*). Using molecular dynamics simulations we show that the loop opening process is induced by the absence of ligands. Our studies also point towards a correlation between the movements of active site lid, P-loop binding and nucleotide-binding regions, as hypothesized previously. Further detailed studies focusing on the roles of the relevant amino acid residues of the lid on catalysis are in progress.

Author contributions : Lakshmi Dharmarajan designed and performed the experiments and Biswarup Mukhopadhyay supervised the work.

Chapter 5

Crystallization of *Clostridium perfringens* PepcA

This chapter is a modified version of the manuscript –

Dharmarajan L, Kraszewski JL, Mukhopadhyay B, Dunten PW. Expression, purification and crystallization of an archaeal-type phosphoenolpyruvate carboxylase. Acta crystallographica. Section F, Structural biology and crystallization communications. 2009 Nov;65(Pt 11):1193-6. Reproduced with permission of the International Union of Crystallography, 2011 (http://journals.iucr.org).

5.1. Abstract

An archaeal-type phosphoenolpyruvate carboxylase (PepcA) from *Clostridium perfringens* has been expressed in *E. coli* in a soluble form with an amino-terminal His-tag. The recombinant protein is enzymatically active and two crystal forms have been obtained. Complete diffraction data extending to 3.13 Å have been measured from a crystal soaked in $KAu(CN)_2$, using radiation at a wavelength just above the Au-L3 edge. The asymmetric unit contains two tetramers of PepcA.

5.2. Introduction

Phosphoenolpyruvate carboxylase (Pepc) catalyzes the formation of oxaloacetate (OAA) from phosphoenolpyruvate (PEP) and bicarbonate. The enzyme from C4 plants has been intensively studied, as it plays a vital role in CO_2 fixation (*1, 54*). The C4 compounds produced after carboxylation of PEP are transported into chloroplasts, where subsequent decarboxylation supplies ribulose 1,5-bisphosphate carboxylase/oxygenase (Rubisco) with a high local concentration of CO_2 (*58*). C4 plants are thus able to suppress oxygenation, a competing reaction catalyzed by Rubisco that lowers the efficiency of CO_2 fixation (*58*). C3 plants lack a mechanism to concentrate CO_2 and fix CO_2 with only ~50% efficiency (*105*). Attempts to express C4-type Pepc in C3 plants have not improved the efficiency of carbon fixation (*105*). The high K_M of the introduced C4-type Pepc for PEP and its sensitivity to inhibition by malate are thought to be responsible (*106, 107*). The activity of Pepc in plants is modulated by both positive

and negative allosteric regulation, via binding of small molecule effectors and by phosphorylation (*1*). The *E. coli* enzyme has also been studied in detail (*1*). The bacterial enzyme is highly homologous to the plant enzyme and subject to allosteric regulation, though not via phosphorylation (*1*). The archaeal-type Pepc (PepcA), in contrast, shows a simpler pattern of regulation (*17-20*). No inhibitors or activators are known for PepcA from *Methanothermus sociabilis* or *Methanothermobacter thermautotrophicus* (*2*). PepcA is therefore an interesting candidate for expression in C3 plants, with the goal of improving the efficiency of carbon fixation. PepcA and Pepc share only 12-16% sequence identity, and the only X-ray structures available are those of Pepc from *E. coli* and maize (*12, 65*). The enzymes from *E. coli* and maize are homotetramers of 4 x 883 and 4 x 970 residues, respectively. In solution, both dimers and tetramers of the *E. coli* Pepc are present, with a shift towards the tetrameric form in the presence of the allosteric inhibitor aspartate (*108*). PepcA from *Methanothermus sociabilis*, *Sulfolobus acidocaldarius*, and *Methanothermobacter thermautotrophicus* have all been reported to be tetramers in solution, based on gel filtration (*18-20*). Attempts have been made to model the structure of PepcA based on the known X-ray structures of the *E. coli* and maize Pepcs (*2*). The PepcA structure has also been targeted by the structural genomics consortia, given the difficulty of modeling the fold. The PepcA sequence family includes many representatives from the archaea and three bacterial homologs that are found in *Clostridium perfringens*, *Oenococcus oeni* and *Leuconostoc mesenteroides* (*18*). The sequence most closely related to that of the PepcA from *C. perfringens* is from an archaeal methanogen, *Methanopyrus kandleri*; the

sequences are 537 and 532 residues in length, respectively, and share 35% sequence identity. Production of the archaeal enzymes in *E. coli* has been difficult (*17, 109*). The 537 residue PepcA homolog from the bacterium *C. perfringens* expressed well in *E. coli* when fused to an N-terminal His_{10}-tag. Crystals of the recombinant, tagged protein diffract to ~3 Å and complete X-ray data have been collected.

5.3. Methods

5.3.1. Cloning and protein expression

The ORF CPE1094 was PCR amplified from *C. perfringens* strain 13 chromosomal DNA using the oligonucleotides - CpePpc/1F, 5'-GAAAAGGGGGACTTCATATGAAGATACCTTGTTCCATGATGAC-3' and CpePpc/2R, 5'-CAAGGATCCTTTAGCCTATACTTCCTCTTACTTTACCCATTC-3'. The amplified DNA was digested with NdeI and BamHI and cloned into similarly digested pET19b (Novagen, San Diego, CA). In the resulting construct, the full-length PepcA protein is preceded by the affinity tag MGHHHHHHHHHHSSGHIDDDDKH. The PepcA expression plasmid, designated pJLK15-19b, was introduced into *E. coli* strain BL21(DE3)(RIL).

Cultures were grown at 310 K in LB medium containing ampicillin (100 μg/mL) and chloramphenicol (25 μg/mL) to an optical density of 0.5 before adding IPTG (1 mM) to induce expression of PepcA. Cells were harvested 4 hours post-induction by centrifugation for 10 min at 9600 xg and the cell pellets were stored at 253 K.

5.3.2. Protein purification

5 g of cell pellet was thawed on ice with 10 mL of 100 mM potassium phosphate buffer, pH 7.0. Cells were broken by passage through a French pressure cell. 0.02 g of DNase was added, and the mixture incubated on ice for 20 min. The extract was centrifuged at 18,000xg for 1 hour at 277 K. All further purification steps were carried out at 293 K. The soluble portion of the extract was equilibrated with 50 mM potassium phosphate buffer, pH 7.0, 300 mM NaCl and 10 mM imidazole (equilibration buffer). The extract was filtered through a 0.2 μm filter and loaded on a 10 mL Superflow Ni^{2+} - NTA (Qiagen, Inc., Valencia, CA) column at a flow rate of 1 mL/min. The column was washed with 4 column volumes of equilibration buffer, then with 2 volumes of a solution containing 50 mM potassium phosphate buffer, pH 7, 10 mM imidazole, 400 mM NaCl. Washing was continued with equilibration buffer until the absorption at 280 nm was stable. PepcA was eluted using an imidazole gradient over 6 column volumes (50 mM to 600 mM imidazole in equilibration buffer). Column fractions were analyzed using SDS-PAGE. The 400-500 mM imidazole fractions contained homogenous PepcA. The buffer was exchanged via ultrafiltration to 50 mM sodium phosphate, pH 7, 150 mM NaCl (SEC buffer), and the protein was concentrated to a volume of 2 mL. The Ni^{2+} - NTA pool was loaded onto a HiPrepTM 16/60 Sephacryl S-300 HR column pre-equilibrated with SEC buffer. PepcA was eluted using the same buffer. The protein was concentrated to 5 mg/mL (determined using the Bradford Coomassie-binding assay (Bio-Rad, Hercules, CA) and the buffer changed to 20 mM Hepes, pH 7 via ultrafiltration prior to crystallization.

Enzyme activity was assayed as described previously (*18*) but with a modified assay mixture containing 50 mM Hepes pH 7.2, 0.2 mM NADH, 30 mM KHCO3, 1.5 mM sodium PEP, 2 mM $MgCl_2$, and 1 unit per mL of thermophilic malate dehydrogenase from *Thermus flavus* (Sigma, St. Louis, MO).

5.3.3. Crystallization screens

Crystals were set up in 24-well plates by hanging-drop vapor diffusion method using 2 μL protein and 2 μL reservoir solution at 295 K and 273 K. The Crystal Screen kit from Hampton Research was used to set up the experiments. The plates were monitored under the microscope everyday.

5.3.4. Crystallization for data collection at SSRL facility

Crystals were grown via hanging-drop vapor diffusion at 295 K, in drops formed from 2 μL of protein plus 2 μL of reservoir solution. Hexagonal rods appeared within 1-3 days using 0.2-0.3 M magnesium formate, 0.1 M bis-tris pH 5.5 or 0.1 M tris pH 8.5 as precipitant. These crystals diffracted to only 8 Å after cryo-protection with either 20% PEG200 or ethylene glycol. Blocks appeared after 6 days using 1.25-1.5 M sodium malonate, pH 7, as precipitant. These crystals could be cryo-protected with 1.5 M sodium malonate, pH 7, and diffracted to 3 Å. A native data set was collected at 100 K using a Rayonix MX-325 detector at SSRL BL9-2 from a crystal of approximate dimensions 0.15 x 0.2 x 0.4 mm. Data collection was based on a strategy suggested by *Web-Ice* (*110*). 450 images were collected, with a $\Delta\phi$ of 0.4°, for a total of 180° of data. The *a** axis was closest to the rotation axis. Data integration and scaling were done

with *Mosflm* (*111*) and *Scala* (*112*). A derivative was prepared by soaking a crystal in 1.5 M sodium malonate, pH 7, 2 mM $KAu(CN)_2$ for 16 hours. A SAD data set was collected at 100 K using a Rayonix MX-325 detector at SSRL BL11-1 from a soaked crystal of approximate dimensions 0.1 x 0.1 x 0.2 mm. 480 images were collected, with a $\Delta\phi$ of 0.75°, for a total of 360° of data. The *c** axis was closest to the rotation axis, minimizing the problem of overlapped reflections. Data integration and scaling were performed with *HKL2000* (*113*), keeping I+ and I- separate during scaling and calculation of Rmerge. For both data sets, the total X-ray dose was estimated before choosing the exposure time per image, to avoid radiation damage to the crystals. The dose estimated by *RADDOSE* (*114*) was 2.4 MGy for the native data set and 2.5 MGy for the KAu(CN)2 derivative data set.

5.4. Results and discussions

The purified protein was judged homogenous by using 12 % denaturing SDS-PAGE (Fig. 5.1). The yield was 1.5 mg of pure PepcA from each gram of cell paste. The gel filtration data suggested that the enzyme was a dimer, with an apparent molecular weight of 62.3 kDa, which was agreeable with the SDS-PAGE data. The specific activity of the purified enzyme was typically in the 38 – 65 μmol min^{-1} mg^{-1} range.

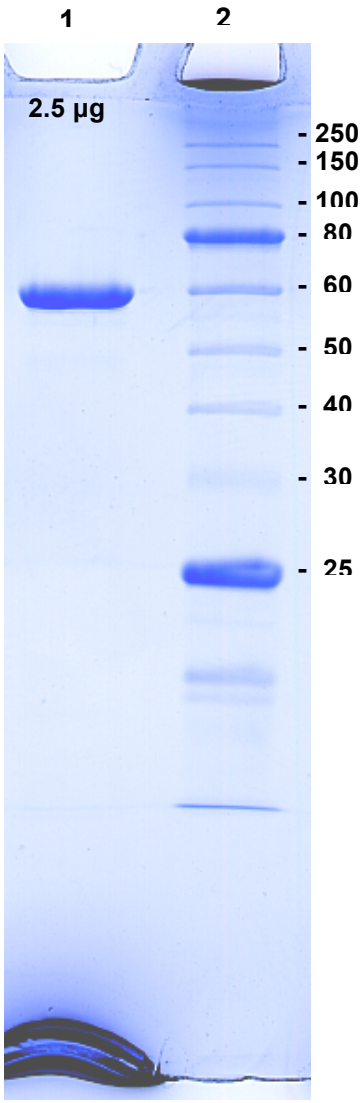

Fig. 5.1. Purified over-expressed PepcA after gel filtration. Lane (1) purified PepcA (2.5 µg), (2) molecular weight markers.

Small needle-like and rod-shaped crystals were observed in the plates set up for screening after 4-5 days (Fig. 5.2 and Fig. 5.3). The former appeared in the well containing 0.1 M Tris-HCl, pH 8.5 and 2 M ammonium sulfate. The rods appeared in the well containing 0.2 M magnesium formate dihydrate as precipitant.

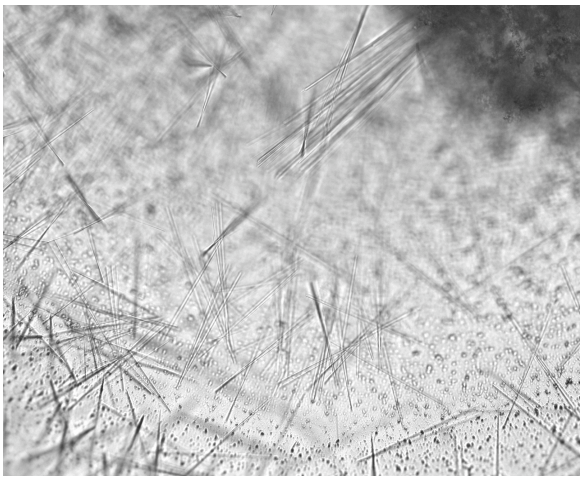

Fig. 5.2. Needle-like clusters of *Clostridium perfringens* PepcA

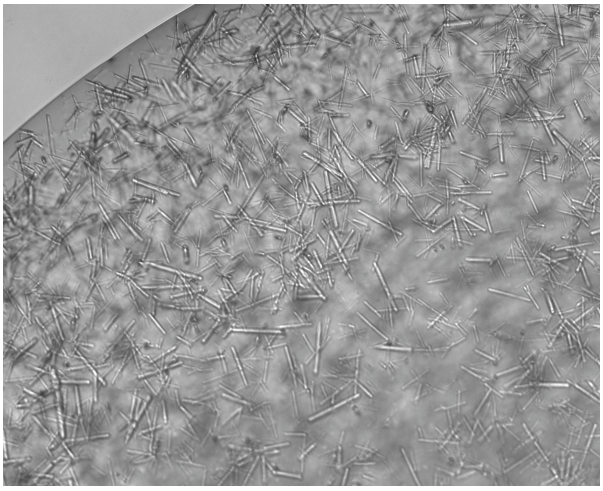

Fig. 5.3. Rod-like crystals of *Clostridium perfringens* PepcA

Crystals grown in the SSRL facility were obtained as blocks after 6 days using 1.5 M sodium malonate, pH 7 as precipitant (Fig. 5.4). The unit cell dimensions of these were : a = 123.3, b = 164.1, c = 283.3 Å suggest eight copies of PepcA per asymmetric unit, with a solvent content of 57% and Matthews coefficient of 2.9 Å3/Da. A slightly smaller unit cell was obtained for a crystal soaked in $KAu(CN)_2$, with a = 121.4, b = 161.7, c = 280.1 Å.

Fig. 5.4. Crystals of PepcA grown in 1.5 M sodium malonate, pH 7. Shown together with 'haystacks' of needles and precipitate.

Data with a useful anomalous signal were collected from the Au-containing crystal at a wavelength just above the Au L3 edge.

Two factors contributing to the higher quality of the data from the Au-soaked crystal are the greater redundancy and the favorable orientation of the crystal (the longest axis was closest to the rotation axis). An additional feature unique to the native diffraction pattern was the variation in spot shape. In the native diffraction pattern, the spot shape varied markedly across the face of the detector (Figure 5.5A), whereas in the diffraction pattern of the $KAu(CN)_2$ soaked crystal, the spot shape was uniform across the detector (Figure 5.5B). Molecular replacement with models including the conserved Pepc β-barrel was not successful. A SAD solution of the structure is underway. Sixteen gold sites were located with *SHELXD* and after density- modification *SHELXE* reported a mean figure-of-merit of 0.459 (*115*). The local symmetry of the gold sites indicates the asymmetric unit contains two tetramers of PepcA, and the tetramers possess 222 point-group

symmetry.

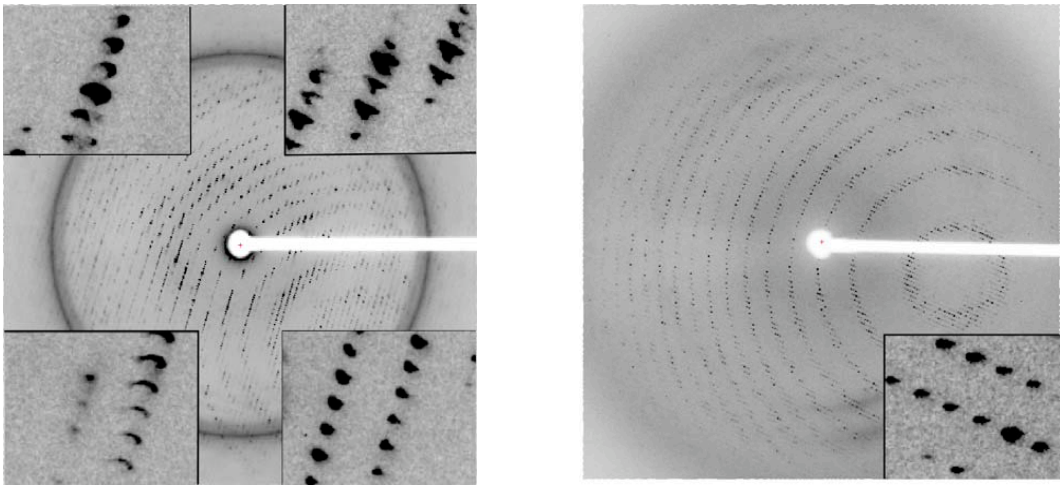

Fig. 5.5. Diffraction patterns taken from PepcA crystals. (A) An 0.4° oscillation from the native data set, with insets in the image showing the variation of spot shape across the detector. The resolution at the detector edge (inscribed circle) was 3 Å. (B) An 0.75° oscillation from the KAu(CN)2 soaked crystal. Resolution at the detector edge (inscribed circle) was 3.13 Å.

The regulation of PepcA from *C. perfringens* has not been studied, and it is not known what factors influence the quaternary structure of the enzyme. The precipitant, malonate, may have favored crystallization of tetramers. Malonate is an inhibitor of the *E. coli* Pepc, and the quaternary structure of the *E. coli* Pepc is known to be sensitive to inhibitor binding (*108, 116*). Whether or not the PepcA quaternary structure is also influenced by inhibitor binding is an open question.

Author contributions : Lakshmi Dharmarajan performed experiments and wrote part of the manuscript, Jessica L. Kraszewski performed experiments, Pete W. Dunten performed experiments and wrote the manuscript, Biswarup Mukhopadhyay and Pete W. Dunten supervised the work, and all authors contributed to the preparation of the final manuscript.

Chapter 6

Structure of *Clostridium perfringens* phosphoenolpyruvate carboxylase

This chapter consists of unpublished data, a portion of which has been accepted as a manuscript to PROTEINS: Structure, Function, and Bioinformatics (*117*) and will be published soon.

Authors : Lakshmi Dharmarajan, Jessica L. Kraszewski, Biswarup Mukhopadhyay and Pete W. Dunten

6.1. Abstract

We have determined a 3 A^{o} crystal structure of *Clostridium perfringens* PepcA, which is the first archaeal-type Pepc structure to be solved. The quaternary structure of the enzyme comprises an octameric unit formed by the dimerization of two individual tetramers (each a dimer-of-dimers). The 65 kDa PepcA is almost half the size of plant and bacterial Pepcs and lacks the allosteric binding sites of aspartate and glucose-6-phosphate, which are observed in the *E. coli* and maize Pepc structures, respectively. This structure is highly similar to the active R-state configuration of *Z. mays* Pepc. A molecule of the precipitant, malonate, which is also weak inhibitor of Pepcs is observed at the active site of the enzyme.

6.2. Introduction

Pepc yields OAA from PEP and bicarbonate (HCO_3^-), liberating Pi in the presence of Mg^{2+} (*1*). It is present in all photosynthetic organisms, like plants, algae, cyanobacteria and photosynthetic bacteria, and also in most non-photosynthetic bacteria and protozoa (*1*). The X-ray crystallographic structures of the *E. coli* and maize Pepcs reveal identical structures of the two, consistent with their highly similar primary structures (*12, 65*). The plant and bacterial enzymes are homotetrameric with subunit sizes of 100-130 kDa (*1, 12, 14, 65*). A new type of Pepc was discovered in archaea, which had subunit sizes of ~ 60 kDa (*19, 20*). Further studies revealed that these archaeal-type Pepcs (called PepcAs) are widespread in the archaea, rare in the bacteria, and absent in the eukaryotes (*17, 18*). Plant Pepcs are regulated by both positive and negative regulators

(*1, 15, 16*). The PepcAs are not significantly regulated by metabolites and show only 12-16 % sequence similarity to the other two Pepcs (*12, 17-20*). In spite of the low sequence similarities between Pepcs and PepcAs, several catalytically important sequence elements of maize and *E. coli* Pepcs were identified in PepcAs (*17, 18*).

Matsumara et al. have generated a structure-based alignment of Pepcs and PepcAs and have further identified more elements of similarity between the two classes of enzymes (*2*). They have also attempted to explain the basis of the differing sensitivities of different PepcAs to aspartate using in-silico models of PepcAs and have suggested an allosteric binding site for this metabolite, similar to the *E. coli* enzyme. Our crystal structure confirms most of the general characteristics of Matsumara *et al*'s models, however, it also highlights the difficulty in modeling specific interactions and subunit assembly. Our structure also suggests a distinct mode of inhibition for aspartate in *C. perfringens* PepcA, than that suggested by Matsumara's studies. This will be discussed in more detail in Chapter 7 of this thesis.

Our structure also indicates the interplay of four loop regions all around the active site, which are probably required to be in the closed conformation for catalysis. The closed structure would protect the active site from entry of water and thus could stabilize the enol-pyuvate intermediate similar to PEPCK (*34*). Loop II probably is similar to the active site lid in PEPCK and a fully ligated active site is essential for closed-lid conformation (*34*). This suggests that Pepcs and PepcAs could also operate by the induced-fit mechanism proposed by Koshland (*118*).

6.3. Methods

The details of the crystallization and X-ray diffraction analysis have been published in (*68*) and described in Chapter 5 of this thesis. Residues 349-354 were not observed in the electron density. The main-chain for residues 355-359 following the missing residues was found in either of two slightly different conformations in the eight independent molecules of the asymmetric unit as a consequence of different crystal packing environments. The N-terminal His-tag was not observed in the electron density. Density present in the active-site was interpreted as bound malonate, with occupancy of ~70%. Wiring diagrams were generated using PDBSum (*119*). Images of enzyme structures were generated using VMD (*87*). The sequence alignment was generated initially by structurally aligning *C. perfringens, Z. mays* and *E. coli* enzymes. Then the archaeal sequences were aligned to this structural profile. All steps were performed using the MultiSeq tool from VMD.

Gel filtration was performed according to the same procedure as in (*68*). The concentration of the loaded sample was 0.9 mg/mL. Analytical ultracentrifugation was performed at 20 °C in 10 mM potassium phosphate buffer (pH 7.0) with 25 mM NaCl. The concentrations of protein used were 50, 150, and 200 μg per mL.

6.4. Results

Quaternary structure of *C. perfringens* PepcA (in the crystal)

The quaternary structure of the enzyme comprises of an octameric unit formed by the dimerization of two individual tetramers. Each monomer within the tetramers is inter-

connected by H-bonds and non-bonded interactions (Fig. 6.1). Each monomer is individually connected to a corresponding monomer in the tetramer by two interfaces on the protein surfaces, with average areas 650 A° and 1170 A°, as analyzed by PDBSum (*119*). Average interface areas for dimerization of the tetramers are around 350 A°. Interactions involved in this dimerization include H-bonding between Asp76 of chain C and Lys37 of chain F, Lys150 of chain C with Glu385 of chain G, Lys109 of chain A with Glu509 of chain G, Asp154 of chain C with Glu509 of chain G, Glu385 of chain D with Lys147 of chain F, Glu509 of chain D with Asp154 and Lys109 of chain F. Comparing the interfaces of tetramer formation in Pepcs and PepcAs, it is seen that both are distinct from each other.

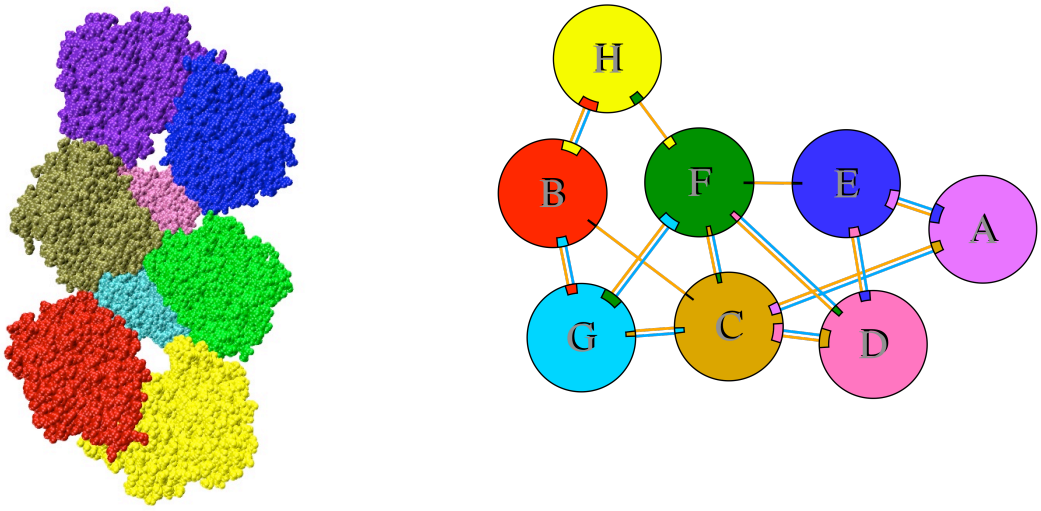

Fig. 6.1. Quaternary structure of *C. perfringens* PepcA. The tetramers are A-E-D-C and H-B-G-F. The interface between individual units is shown (on the left) and the connectivity is shown (on the right). The color coding for individual chains is the same in both figures. The connections indicate interactions between the chains, orange – non-bonded interactions, blue- H-bonds. The indicated area of each circle is proportional to the surface area of the corresponding protein chain. The extent of the interface region on each chain is represented by a coloured wedge whose colour corresponds to the colour of the other chain and whose size signifies the interface surface area. Figures generated by PDBSum (*119*).

Quaternary structure of the protein (in solution)

It was observed by both gel filtration and analytical ultracentrifugation (AUC) experiments that the predominant form of the enzyme at the specified concentrations is a dimer. Faint signals of other higher forms were also detected by AUC.

Overall structure of the protein

The overall structure of the protein conforms to the TIM-barrel family, with a $(\beta\alpha)_8$ barrel motif in the core, followed by an extensive α-helical domain (Fig. 6.2). The *C. perfringens* PepcA structure is however, smaller than that of the plant and bacterial enzymes (~520 residues compared to ~900 residues of the maize and ~870 residues of *E. coli* Pepc). The active site of *C. perfringens* PepcA seems fairly conserved with respect to its plant and bacterial counterparts (Fig. 6.3). The known X-ray structures of the *E. coli* enzyme all include aspartate and thus represent the T-state of the enzyme. An R-state structure of the *Z. mays* enzyme revealed an Arg residue moves 15 Å to form either part of the aspartate-binding site or the active-site.

In the R-state structure, Arg^{647} interacts with the C-terminal glycine's carboxylate group. In the T-state structures, the corresponding Arg^{587} is a partner in three interactions with aspartate, while Arg^{832} is involved in a second bidentate salt bridge to the aspartate, Asn^{881} provides two hydrogen bonds, and Lys^{773} provides one interaction.

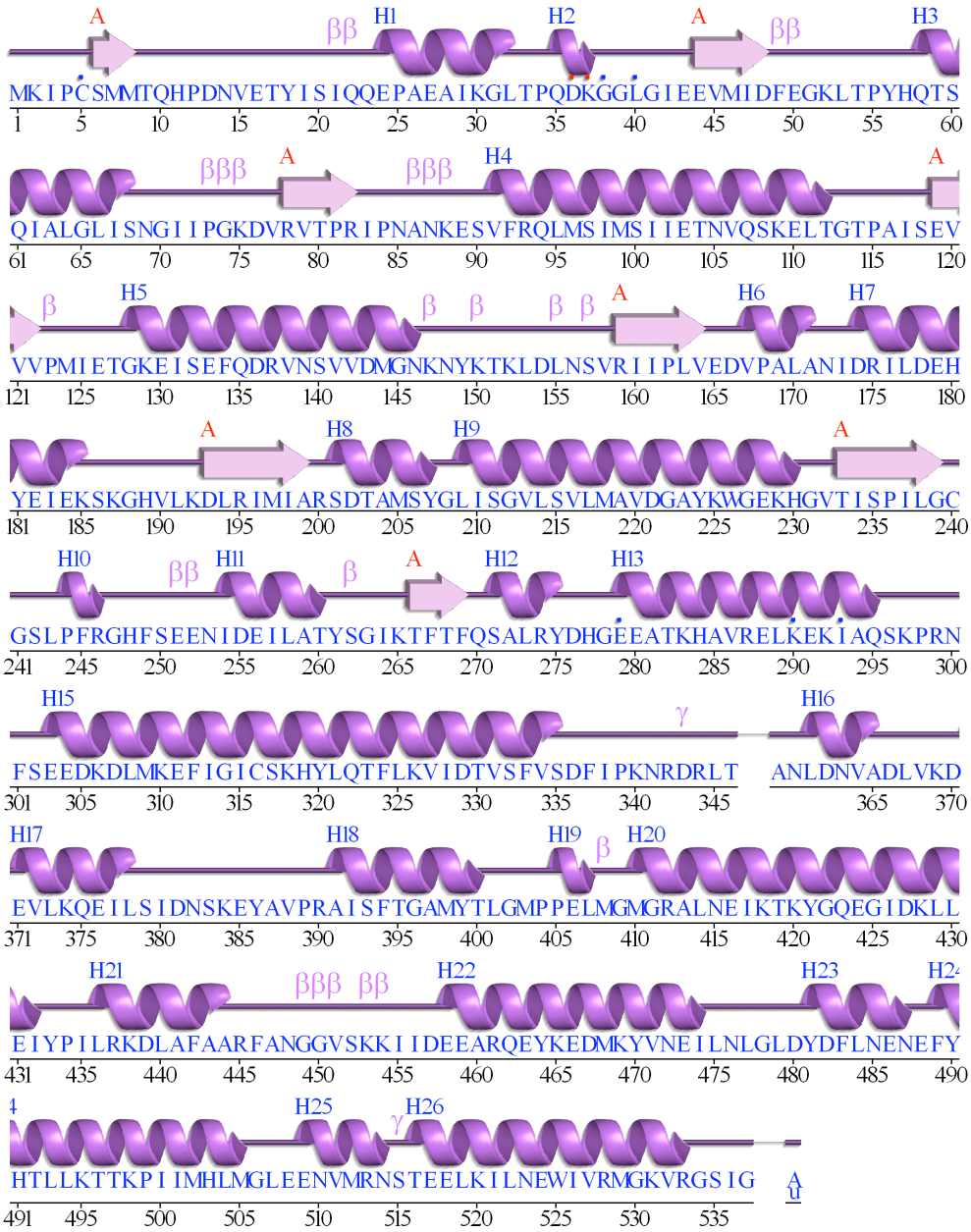

Fig. 6.2. Wiring diagram of *C. perfringens* PepcA. Distribution of the helices and strands, and the $(\beta\alpha)_8$ fold is displayed. Figures were generated by PDBSum (*119*).

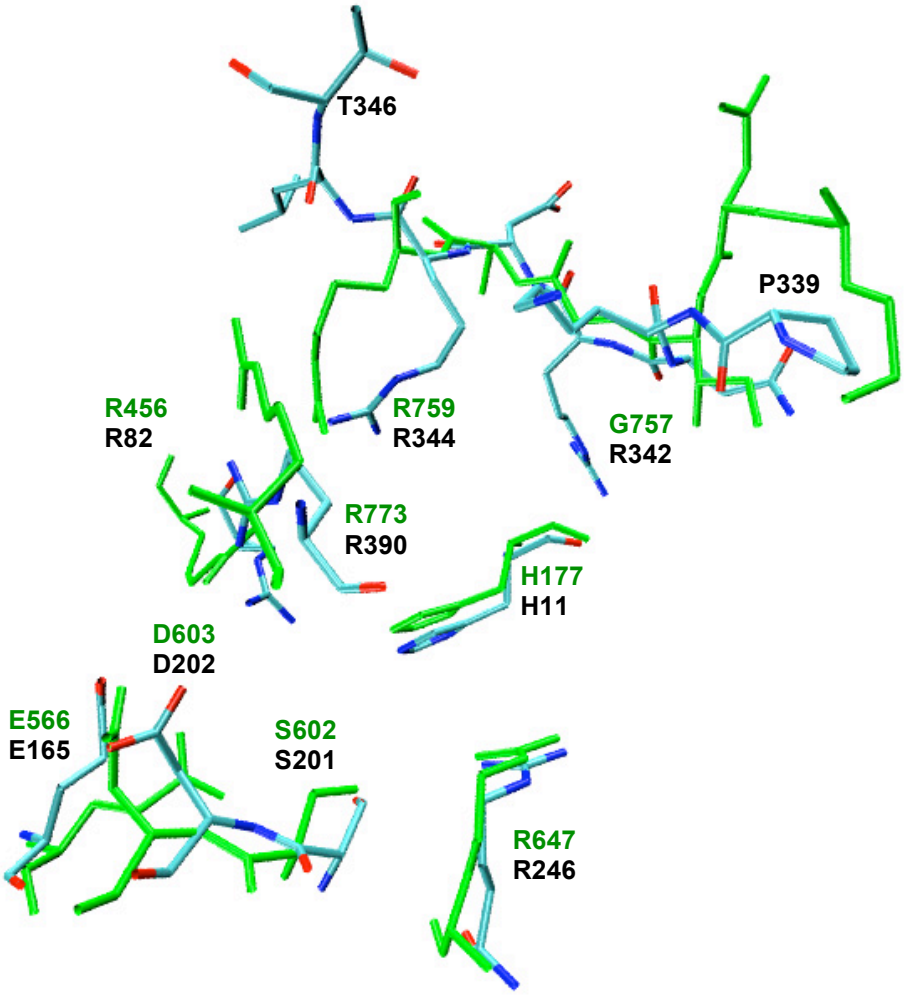

Fig. 6.3. Putative bicarbonate and aspartate binding residues of CpPepcA and comparison with equivalent residues in ZmPepc (in green). CpPepcA residues have been labeled in black and ZmPepc residues in green. The data are from reference (103), (PDB ID code 1JQO).

Movement of Arg^{587} to the aspartate-binding site is accompanied by shifts in the positions of residues 588 - 590 which extend the α-helix α21 between β-strands β7 and β8 by one residue at its N-terminal end. The *C. perfringens* enzyme lacks the equivalent of Arg^{832}, and neither Asn^{881} nor Lys^{773} is conserved.

The side-chain of Arg^{246} is located in the active site, as in the R-state *Z. mays* structure, and it interacts with the C-terminal carboxylate of Gly^{537}. The dramatic rearrangements seen in the *E. coli* versus *Z. mays* comparison seem unlikely to occur in PepcA. Phe^{249} packs well in a hydrophobic environment and would be energetically costly to move. The corresponding residues in the *E. coli* and *Z. mays* structures are Ala590 and Gly^{650}, respectively. Thus, the *C. perfringens* structure more closely resembles the R-state of Pepc, with both elements which are mobile in the Pepc structures positioned at the active-site. Neither of the allosteric regulatory sites seen in the bacterial and eukaryotic Pepcs is present in the PepcA structure (Fig. 6.4) [23].

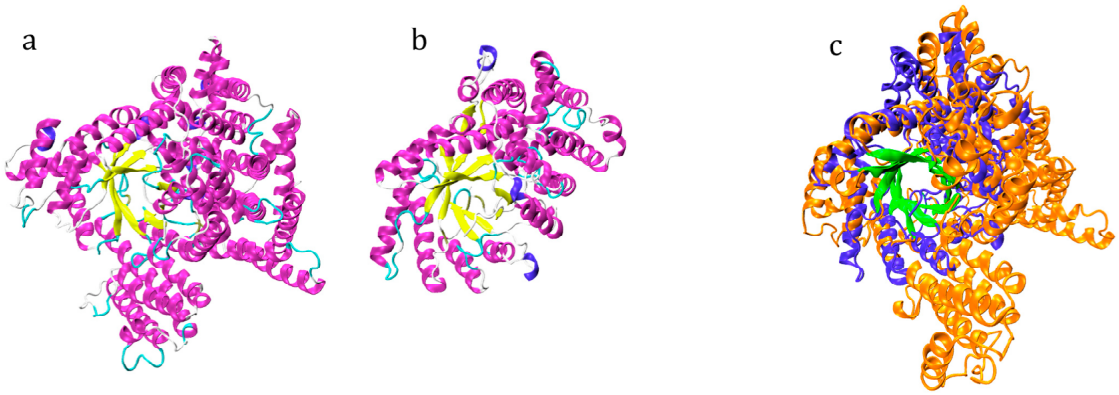

Fig. 6.4. a. *Z. mays* Pepc and b. *C. perfringens* PepcA. c. Superposition of *Z. mays* and *C. perfringens* Pepc structures, showing PepcA (in blue) lacks the extra helices involved in *Z. mays* (in orange) for allosteric activation. The common core beta barrel is shown in green. Figures were generated using VMD (*87*). PDB id used: 1JQO.

Malonate binding

Malonate was bound to the active site of the enzyme, interacting with His^{11}, Arg^{82}, Ser^{201} and Gln^{270} (Fig. 6.5). Since malonate is a weak inhibitor of Pepcs and mimics the

enol-pyruvate intermediate, this binding site could provide insights into oxaloacetate or aspartate binding (*44*) (Fig. 6.6).

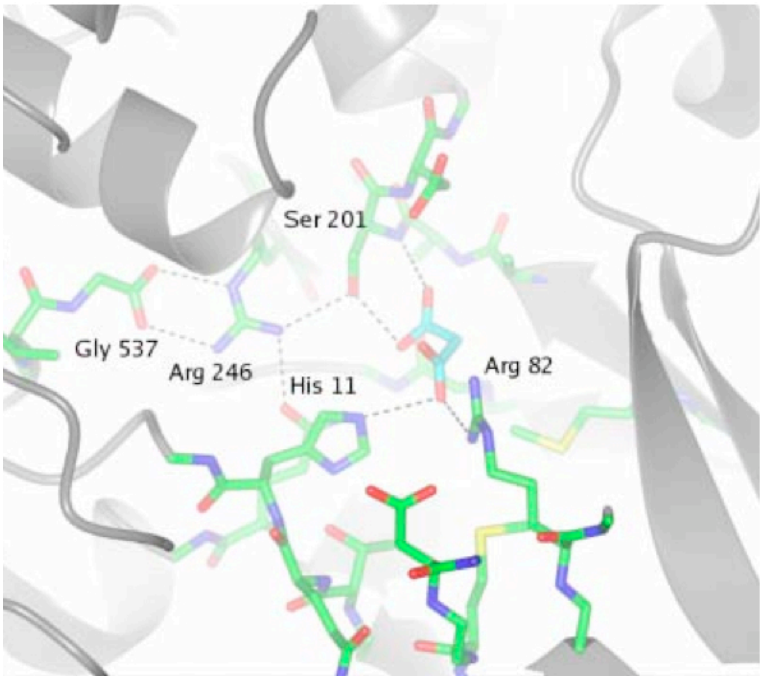

Fig. 6.5. Interactions of malonate (in blue) with active-site residues of *C. perfringens* PepcA.

Loop regions of *C. perfringens* PepcA

In *C. perfringens* PepcA structure, it is observed that four loop regions surround the active site. A comparison with *Z. mays* and *E. coli* enzymes suggest that the closure of Loop I (containing the catalytically essential Arg^{246}) and Loop $\beta1\alpha1$ (containing the catalytic His^{11}), would be essential for the enzyme to form its active site conformation. The third loop has the PEP-binding and fully invariant Arg^{344} and the fourth is the disordered active site lid (Loop II) (Fig. 6.7). The complete closed conformation is probably essential for catalysis and is reached upon binding of all the substrates. This suggests that the enzyme probably operates by the induced fit mechanism proposed by Koshland (*118*).

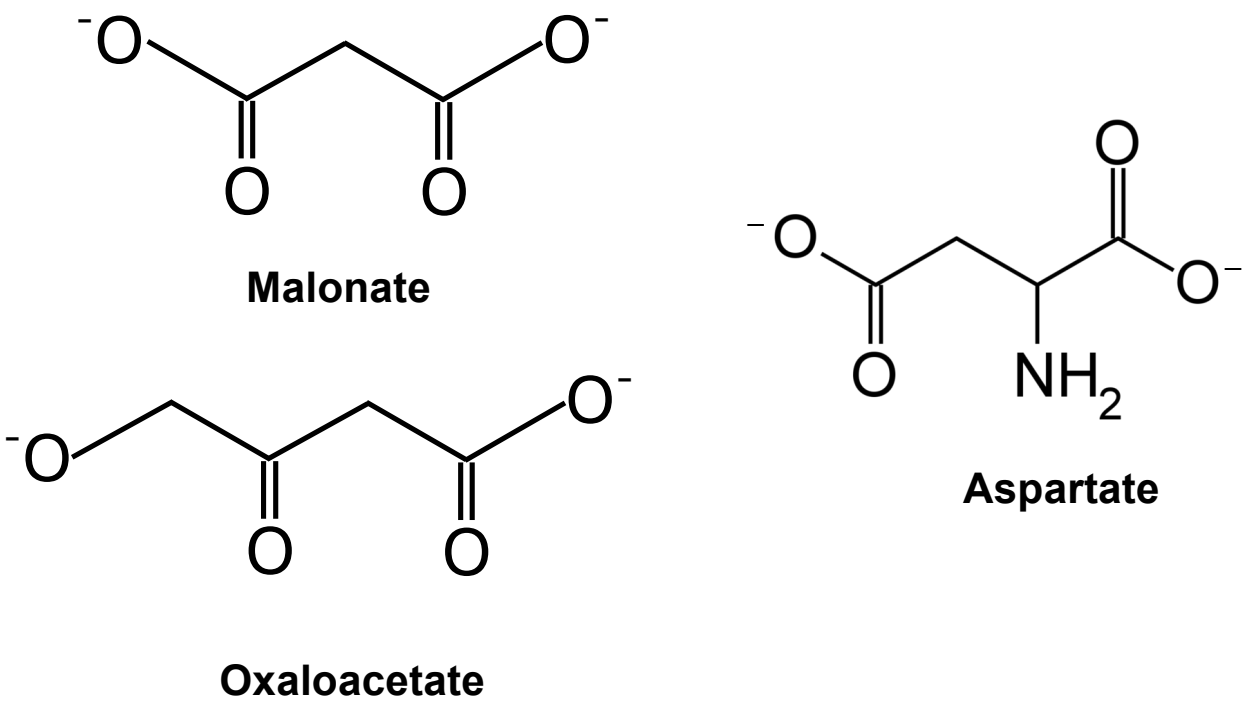

Figure 6.6. Structures of malonate, oxaloacetate and aspartate

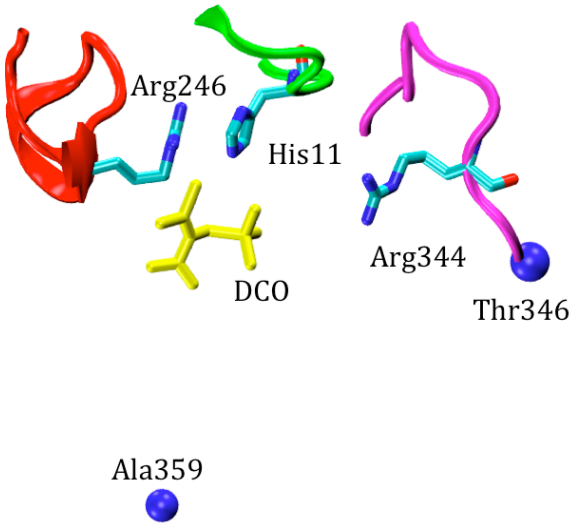

Fig. 6.7. Loop regions surrounding the active site of *C. perfringens* PepcA. Closure of the loops is probably essential for correct orientation of the substrate-binding residues. The terminal residues of the disordered active site loop (Loop II) are shown as blue beads. Figure generated by VMD (*87*) and coordinates of the PEP analog, DCO has been taken from PDB id 1JQN.

Upon performing a structural alignment of the *E. coli* Pepc, maize and clostridial enzymes, it is seen that Arg^{344} of *C. perfringens* PepcA is not at interacting distance (~ 6 Aº) to the PEP analog, DCO as in the *E. coli* enzyme (Fig. 6.8). The orientation of the equivalent residue Arg^{759} in *Z. mays* Pepc is similar. However, in *E. coli* Pepc, the residue Arg^{699} is closer to the analog (~ 3 Aº). This movement could have been induced by the conformational changes on aspartate binding, since this is an aspartate-bound structure. This suggests that upon PEP-binding, ligand-induced dynamic changes probably occur in the loop containing the residue, which cause the movement of the residue towards PEP. Further changes probably occur on bicarbonate binding, including lid closure, and positioning of the active site residues at optimal distance for catalysis.

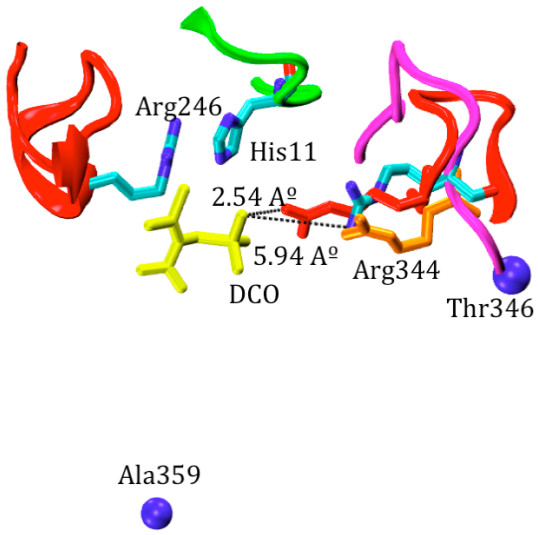

Fig. 6.8. Interaction of PEP analog, DCO with Arg^{344} of *C. perfringens* PepcA. *C. perfringens* residues are displayed in blue. Loops containing Arg^{246} and His^{11} are depicted in red and green, respectively. The corresponding residues to Arg^{344} from *Z. mays* (Arg^{759}) and *E. coli* (Arg^{699}) are shown in orange and red. The loop containing Arg^{344} is shown in pink and the corresponding loop in the *E. coli* enzyme in red. The terminal residues of the disordered active site loop (Loop II) are shown as dark blue beads. Figure generated by VMD (*87*) and coordinates of the PEP analog has been taken from PDB id 1JQN.

6.5. Summary

C. perfringens PepcA structure provides an interesting comparison with its plant and bacterial counterparts, especially in terms of regulation and allostery. The structure more closely resembles the active R-state of Pepc, and the allosteric regulatory sites seen in the bacterial and eukaryotic Pepcs is not present in the PepcA structure. The malonate-binding site could be indicative of hitherto unknown substrate binding or regulatory sites and future studies are required to provide further details.

Author contributions : Lakshmi Dharmarajan performed experiments and wrote this chapter, Jessica L. Kraszewski performed experiments, Pete W. Dunten performed experiments and prepared the final manuscript, Pete W. Dunten and Biswarup Mukhopadhyay supervised the work.

Chapter 7

Insights into the aspartate and bicarbonate binding sites of *Clostridium perfringens* PepcA

Authors : Lakshmi Dharmarajan, Jessica L. Kraszewski and Biswarup Mukhopadhyay

7.1. Abstract

Bacterial and plant Pepcs are homotetrameric and are allosterically regulated by metabolites such as aspartate and glucose-6-phosphate (*1*). However, PepcAs are not as strongly regulated by metabolites; in fact the corresponding binding sites are absent in these enzymes. Additionally, most of the substrate-binding sites of the plant and bacterial enzymes are conserved in their archaeal relatives, with the exception of the bicarbonate binding residues. In the absence of relevant crystal structure data of enzyme-inhibitor or enzyme-substrate complexes, we have employed a combination of structure-based modeling and enzyme kinetics experiments to provide hypotheses for the aspartate and bicarbonate sites. Our kinetic analysis indicated that aspartate is actually a competitive inhibitor of *C. perfringens* PepcA, with respect to the substrate Mg^{2+}-PEP. Based on sequence- and structure-based analyses, two possible modes for aspartate binding, one involving residues Arg^{82}, His^{11}, Arg^{390} and Ser^{201}, and the other, residues Lys^{340}, Arg^{344} and Arg^{390} are proposed. For the bicarbonate binding, a sequence element ^{339}PKNRDR^{344} and some basic residues downstream to it are probable binding sites.

7.2. Introduction

Plant and bacterial phosphoenolpyruvate carboxylases (Pepcs) are found in higher plants, green algae and many bacteria, but are absent in eukaryotes (*64*). The archaeal-type counterparts (PepcAs) are found mainly in archaea, and a few bacteria like *Lactobacillus*, *Leptospirillum* and *Leuconostoc* species and clostridial species (*17-20*). A

marked difference between these two classes of enzymes is their extent of regulation. Pepcs are highly regulated by metabolites and post-translational modifications, whereas PepcAs are not (*1*). Among the metabolites, Pepcs are strongly inhibited by the allosteric inhibitor, aspartate (*1, 65*). Residues interacting with aspartate are known in Pepcs from crystallographic data (*65*). However, these residues are not conserved in PepcAs. More interesting is the fact that among PepcAs, there is a difference in their sensitivity towards aspartate. Aspartate has been reported as an allosteric inhibitor of PepcA from *Sulfolobus acidocaldarius* and *Sulfolobus solfataricus*, while PepcA from *Methanothermobacter thermautotrophicus* and *Methanothermus sociabilis* is not sensitive to inhibition by aspartate (*1, 2*). A comparative analysis between the aspartate binding modes between the two classes of enzymes could provide an explanation for the different regulatory mechanisms of the enzymes.

Another important aspect that distinguishes these two Pepc groups is the difference in the K_m values for bicarbonate. PepcAs have a higher K_m for this substrate than their plant and bacterial counterparts (*1, 18*). It is also seen from sequence alignments that the bicabonate binding site of Pepc is not conserved in PepcAs. This could indicate a different mode of the substrate binding in the PepcAs, as compared to the Pepc family. We present here our hypotheses about a bicarbonate binding site for PepcAs.

7.3. Methods

Site–directed mutagenesis and protein purification

The plasmid pJLK15-19b (*68*) which carries the coding sequence for *C. perfringens*

Pepc and allows the expression of the protein under the control of a T7 promoter was used as a starting point. The coding sequence was mutagenized using an overlap PCR method. For each mutant, DNA sequencing of both strands of the coding region confirmed that the mutagenesis procedure altered only the targeted bases. Recombinant PepcA and variant enzymes were expressed and purified as described previously (*68*).

Gel filtration

Gel filtration was performed according to previous procedures (*68*). The concentration of the loaded sample was 0.9 mg/mL.

Kinetics and assays

Enzyme assays and kinetics were conducted as previously described (*68*). The concentration of PEP-Mg^{2+} in solution was calculated using a dissociation constant of 5.55 mM for the complex (*120*). IC50 for aspartate was determined at a PEP concentration of 1.5 mM.

Loop modeling

The unstructured loop region (residues 349 to 354) was modeled using Modeler9v7 (*121*). 200 loop conformations were generated and the one with the best Modeler score was chosen for further analysis.

Docking

Docking was performed using AutoDock Vina 1.1.1 (*122*). The aspartate structure was taken from the aspartate-bound *E. coli* Pepc structure (PDB i.d. 1JQN).

Modeling the surface area and cleft analysis

Cleft analysis was performed using the 3D-SURFER tool (*123*), and corresponding figures were generated using VMD.

Primary structure comparisons

A sequence alignment was generated initially by aligning crystal structures of *C. perfringens, Z. mays* and *E. coli* enzymes. Then other archaeal sequences were aligned to this structural profile. All steps in both alignments were performed using the MultiSeq tool from VMD.

7.4. Results and discussions

Gel filtration analysis

Gel filtration analysis in the presence of aspartate at a concentration ten-fold higher than the respective K_i value did not indicate any significant change in the hydrodynamic radius of the enzyme. This is in contrast to *E. coli* Pepc, where binding of aspartate shifts the equilibrium between dimers and tetramers towards the tetrameric form (*108*). Hence the binding mode of aspartate in PepcA is probably different than that in Pepc

and aspartate does not induce major structural changes as observed in the *E. coli* enzyme.

Aspartate inhibition kinetics

Previous kinetic analyses suggested PEP-Mg^{2+} is the substrate, rather than PEP, with a K_m value of 60 μM for the complex and V_{max} of 40 μmol min^{-1} mg^{-1} (*124*). PEP-Mg^{2+} has also been reported to be the substrate for several plant Pepcs (*67, 125, 126*). Our kinetic analyses indicate that aspartate is a competitive inhibitor of *C. perfringens* PepcA, and the K_i for aspartate is 0.2 mM, i.e. 3.5 times higher than the K_m for PEP-Mg^{2+} (Fig. 7.1).

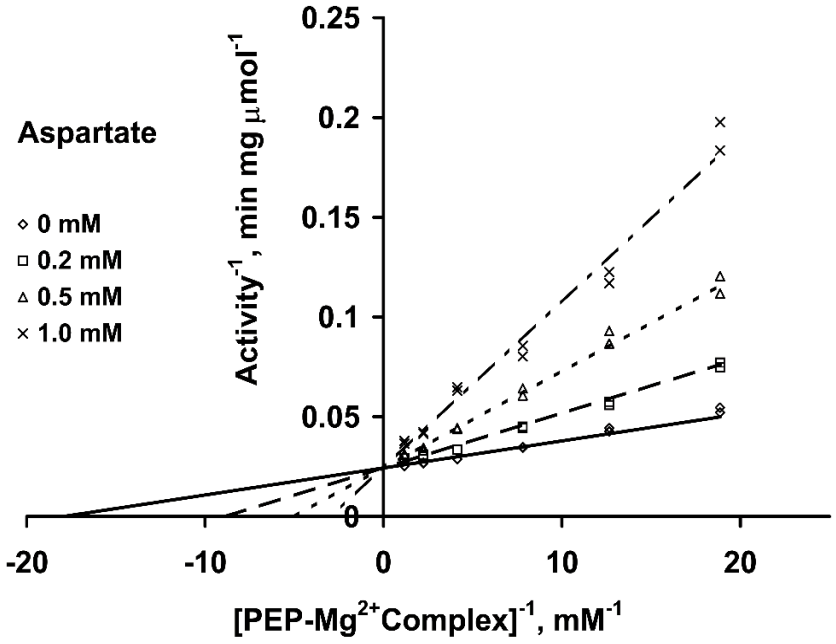

Fig. 7.1. Kinetics of aspartate inhibition in *C. perfringens* PepcA. Figure used from Kraszewski, J. Enzymology and Physiology of a New Type of Phosphoenolpyruvate Carboxylase and the Development of a Pyruvate Carboxylase Expression System, In *Biochemistry*, Virginia Tech (2007) (*124*), under fair use, 2011.

Docking studies of *C. perfringens* PepcA with aspartate

I. Using enzyme structure with disordered loop

First, docking was performed using our PepcA crystal structure with the disordered loop region. The studies indicated that aspartate bound at a site formed by residues, Asn^{253}, Lys^{438} and Arg^{445} (Fig. 7.2). The conservation of these residues within different PepcAs is also shown (Fig. 7.3). It is seen that the residues do not display any strict conservation among different PepcAs, thus questioning the feasibility of these residues forming the aspartate-binding site in PepcAs. Moreover, our kinetic data indicated that aspartate is a competitive inhibitor of *C. perfringens* PepcA with respect to the PEP-Mg^{2+} complex. This suggests that either aspartate would have a common binding site with PEP-Mg^{2+} complex or if it binds at a different site, some conformational change could occur which would ultimately cause interference with PEP-binding in the enzyme. The latter case is not supported by our gel filtration data. Since there is no crystal structure of Pepcs or PepcAs complexed with PEP until now, the binding site of a PEP analog (DCO) in *E. coli* enzyme has been thought to be analogous to the PEP-binding site. None of the residues equivalent to Asn^{253}, Lys^{438} or Arg^{445} of *C. perfringens* enzyme, which have been indicated by our docking results to be aspartate-binding residues, are common with the above-mentioned PEP-binding site of Pepcs. Thus, the results of this docking did not seem to support competitive inhibition of aspartate in PepcAs. We speculated whether we were getting inaccurate modeling results because of the absence of the structural data for the disordered loop region. This loop could potentially be an important structural element of the enzyme.

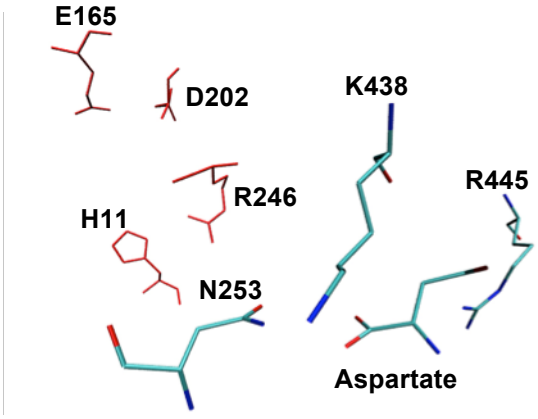

Fig. 7.2. Predicted aspartate-binding residues in *C. perfringens* PepcA. The structure used was with missing loop. Active site residues are shown in red.

Clostridium perfringens	252 ENI	437 RKD	444 ARF
Clostridium cellulovorans	253 ESL	438 KTD	445 WRY
Methanopyrus kandleri	253 GME	442 RED	449 VEY
Methanosarcina acetivorans	251 KNA	434 VSD	441 SRF
Ignicoccus hospitalis	251 WVI	403 PKD	410 YAF
Sulfolobus solfataricus	267 ENY	420 KHD	427 ARF
Sulfolobus islandicus	267 ENY	420 KHD	427 ARF
Sulfolobus tokodaii	267 MNF	420 KHD	427 ARF
Oenococcus oeni	268 KWI	423 RND	430 AHY
Metallosphaera sedula	266 ENY	419 KND	426 SEF
Lactobacillus brevis	274 LML	429 KAD	436 SHY
Pyrobaculum aerophilum	246 HLA	392 VEE	399 SRF
Methanothermobacter thermautotrophicus	305 DNV	451 GRD	458 ARY
Thermofilum pendens	245 RLV	396 EEE	403 AQF
Pyrococcus abyssi	262 DNV	406 YED	413 MRF
Halobacterium salinarum	270 ERA	418 FDH	425 ARY
Methanospirillum hungatei	274 DTV	421 TED	428 CRY
Archaeoglobus fulgidus	258 KNL	402 DGM	409 MSL

Fig. 7.3. Conservation of putative aspartate-binding residues in PepcAs. Identical residues are shaded in yellow and similar residues are shaded in green. Bacterial names are shaded in gray.

II. Using enzyme structure with modeled loop

In the next step, the disordered loop was modeled (Fig. 7.4), as described in the methods section and aspartate was docked to the enzyme structure. This time,

aspartate was observed to bind to a different site formed by residues His^{11}, Arg^{82}, Arg^{390} and Ser^{201} (Fig. 7.5). When the structure of *E. coli* Pepc with the PEP-analog DCO was superimposed upon the structure of the clostridial enzyme with modeled loop and bound aspartate, the positions of aspartate and DCO overlapped (Fig. 7.6). This is consistent with the kinetic analysis that indicates that aspartate probably competes with the PEP-Mg^{2+} binding. This is also in agreement with the malonate-binding site that we observed from our crystal structure data, and which is described in Chapter 6, Fig. 7.5. Site-directed mutagenesis studies and crystal structure with bound aspartate would provide the basis for this hypothesis.

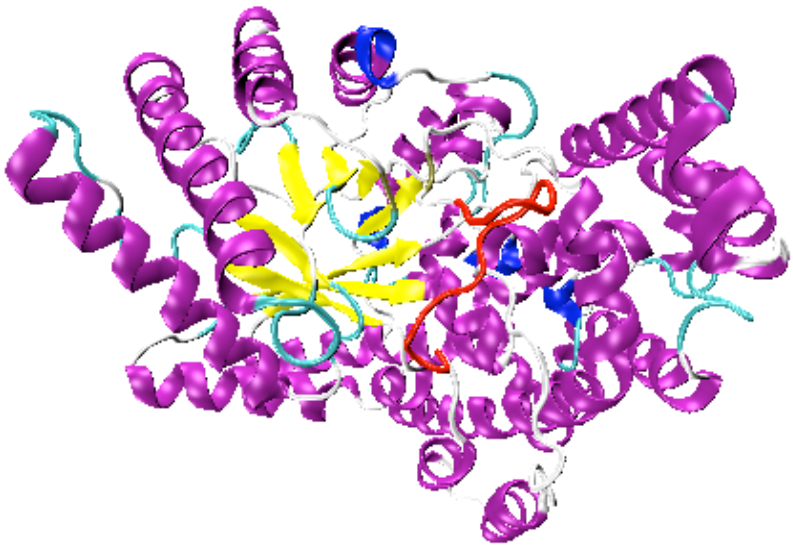

Fig. 7.4. *C. perfringens* PepcA with modeled loop. Residues - 349 to 354.

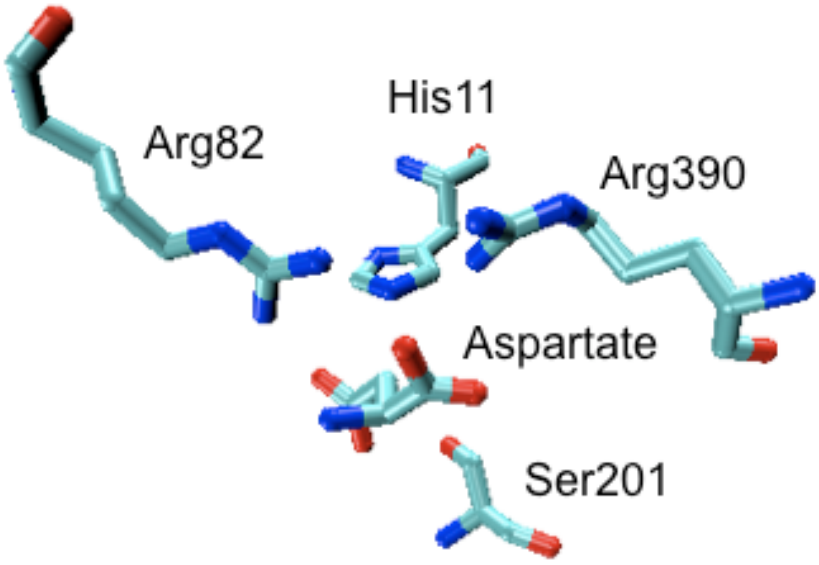

Fig. 7.5. Probable aspartate-binding site of *C. perfringens* PepcA indicated by docking analysis. (Performed with loop-modeled structure).

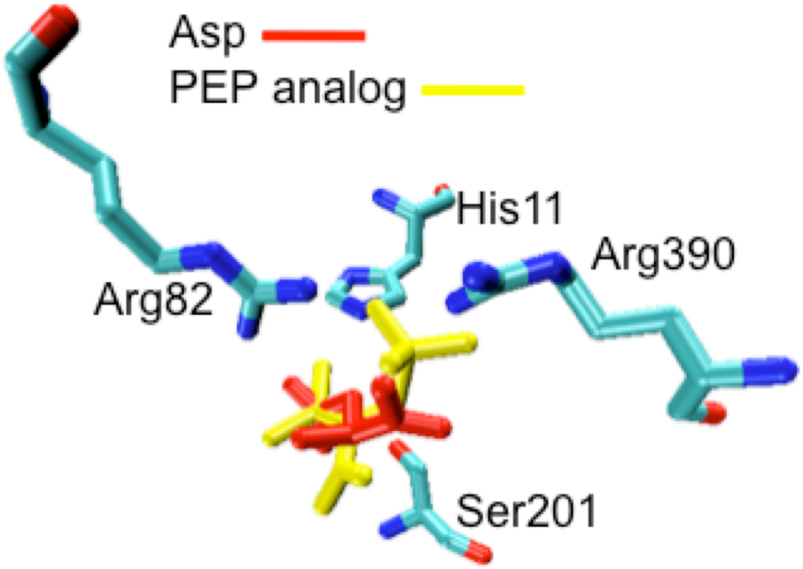

Fig.7.6. Superimposition of *C. perfringens* PepcA with docked aspartate and PEP-analog, DCO from *E. coli* Pepc structure.

Alternate hypothesis for aspartate-binding site and for differing sensitivities to this metabolite within PepcAs

Since we do not have a crystal structure of *C. perfringens* PepcA bound with aspartate, it is difficult to rationalize the structural basis for different sensitivities to aspartate within the PepcA family. However, from sequence comparisons, we can speculate that Lys^{340}, Arg^{344} and Arg^{390} could form a site for aspartate binding. Arg^{699} in the *E. coli* enzyme (corresponding to Arg^{344} of *C. perfringens*) is part of the binding site for the inhibitory PEP analog, DCO (*65*). Thus in PepcA inhibition by aspartate could be due to direct competition for a residue involved in PEP binding. Differing sensitivities to aspartate among PepcAs could be due to residue 340, which is Lys in the mildly-sensitive *C. perfringens* PepcA, Arg in the more-sensitive *S. solfataricus* PepcA and Gly in the almost-resistant *M. thermautotrophicus* enzyme (Fig. 7.7). Analysis of the structure of *C. perfringens* PepcA indicates a groove region lined by the basic residues K^{340}, R^{342}, R^{344} and R^{390} (Fig. 7.8). This further supports the theory that aspartate could bind at this site.

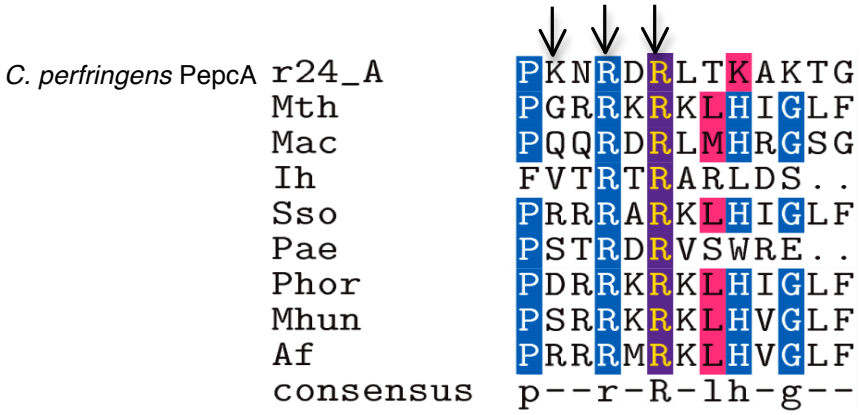

Fig. 7.7. Comparison of the hypothesized aspartate binding region within PepcAs. K^{340}, R^{342} and R^{344} of *C. perfringens* enzyme have been indicated by arrows. r24_A – *C. perfringens* PepcA (our structure). Organism names : Mac – *M. acetivorans*, Ih – I. *hospitalis*, Sso – *S. solfataricus*, Pae – *P. aerophilum*, Mth – *M. thermoautotrophicum*, Phor – *P. horikoshii*, Mhun – *M. hungatei*, Af – *A. fulgidus*.

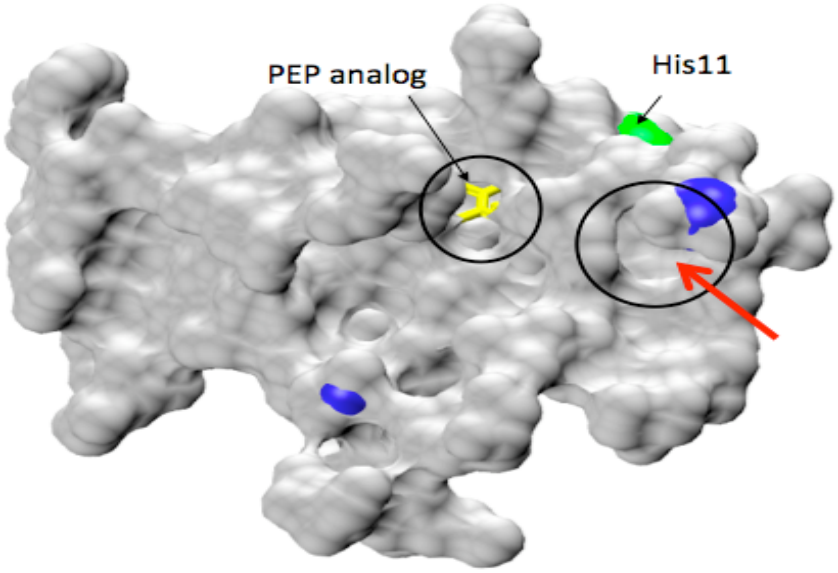

Fig. 7.8. Hypothesized aspartate binding site of *C. perfringens* lined by K340, R342, R344 and R390 residues. (Indicated by red arrow). Binding region of the PEP-analog (in yellow) is also indicated nearby.

Aspartate inhibition in K340 variants

The hypothesis for an aspartate binding mode in PepcAs was further tested by site-directed mutagenesis studies. Altering K^{340} of *C. perfringens* PepcA to D and S yielded variant enzymes with lowered specific activities (Table 7.1). Since the specific activities of the K340D and K340S variants were lower than that of the wild-type enzyme, K^{340} of *C. perfringens* PepcA could play some role in catalysis. Comparisons between the IC50 values for aspartate of the wild-type and variants revealed that a higher concentration of aspartate is needed for 50% inhibition of the variant enzymes (Table 7.2). This is consistent with our hypothesis that K^{340} is one of the residues binding aspartate or it influences the binding of aspartate. Further detailed studies will yield a better understanding of the role of this residue in aspartate binding and catalysis.

Table 7.1. Specific activities of wild-type PepcA and K340S and K340D variants

Enzyme	WT	K340D	K340S
Specific activity (U mg^{-1})	38-65	9-13	6-9

Table 7.2. IC50 values of aspartate inhibition for wild-type PepcA and K340S and K340D variants

Enzyme	WT	K340D	K340S
IC50 (Asp, mM)	6.7	11.6	11.8

Hypothesis for the bicarbonate binding site of *C. perfringens* PepcA

A sequence loop rich in basic residues, ^{339}PKNRDR^{344} (*C. perfringens* PepcA numbering) that seems conserved in all PepcAs, is a probable site for bicarbonate binding (Fig. 7.9). The corresponding regions in *E. coli* and *Z. mays* enzymes are "PAKRR" (EcPepc, ^{700}PAKRR^{704}; ZmPepc, ^{760}PAKRR^{764}), and they are part of a mobile disordered loop in both these enzymes (*64, 65*). From site-directed mutagenesis studies, this region has been indicated to be the bicarbonate-binding site in Pepcs (*65*). In case of *C. perfringens* PepcA, the corresponding binding residues could be part of the same loop rich in basic residues, ^{339}PKNRDRLTKAKTGLEYNREVANL^{361}. The element Arg^{342} - Arg^{344} is also part of an inverse gamma turn in *C. perfringens* PepcA. Gamma turns are tight turns, which can occur at ligand binding sites or active sites. An example is the loop where the catalytically important aspartate is located in serine proteases.

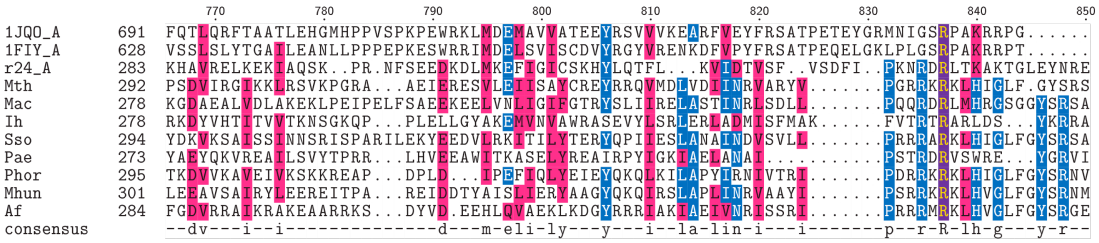

Fig. 7.9. Structure-based alignment of the putative aspartate binding region of *C. perfringens* PepcA. (Indicated by the blue bar). Color codes for the residues are: pink – similar; blue – mostly conserved and violet – fully conserved. 1JQO_A – PDB id of *Z. mays* Pepc, r24_A – *C. perfringens* (our structure), 1FIY_A – PDB id of *E. coli* Pepc. Organism names are: Mac – *Methanosarcina acetivorans*, Ih – Ignicoccus *hospitalis*, Sso – *Sulfolobus solfataricus*, Pae – *Pyrobaculum aerophilum*, Mth – *Methanothermobacter thermoautotrophicum*, Phor – *Pyrococcus horikoshii*, Mhun – *Methanospirillum hungatei*, Af – *Archaeoglobus fulgidus*.

A cleft analysis of the enzyme using 3D-SURFER (*123*) revealed three major cleft regions – the red being the largest (Fig. 7.10). Usually the active sites are part of the largest cleft in a protein. Superimposition of the structure of DCO, a PEP-analog from *E. coli* Pepc onto the PepcA structure showed that the molecule fits snugly into a groove in the above-mentioned major cleft region (Fig. 7.10). Further analysis reveals that ^{339}PKNRDR^{344} is also a part of the cleft region also and situated close to His^{11}, which could capture the proton from carboxyphosphate for CO_2 formation (*127*). Hence ^{339}PKNRDR^{344} could be involved in bicarbonate binding.

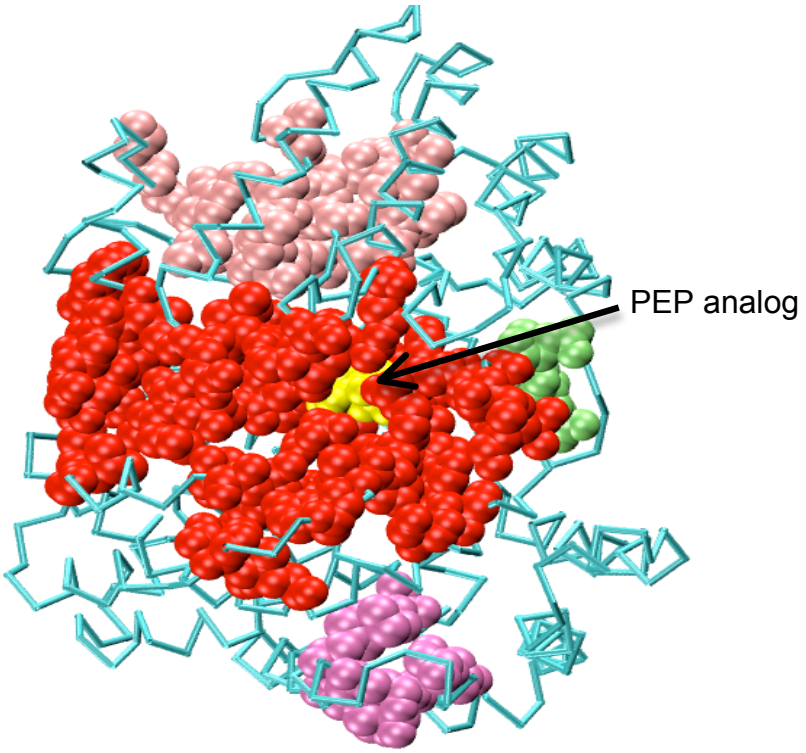

Fig. 7.10. Cleft analysis of *C. perfringens* PepcA. The 3 clefts are depicted in red, tan and pink, red being the major cleft. The ^{339}PKNRDR^{344} region is in green. PEP analog, DCO (from *E. coli* Pepc structure, 1FIY) has been indicated in yellow.

7.5. Conclusions

Our experimental data indicate that the inhibition mode of aspartate in *C. perfringens* PepcA is competitive compared to the allostery observed in plant and bacterial Pepcs. Due to the absence of an aspartate-bound structure for PepcA, we have used structure-based modeling to provide hypotheses for aspartate binding in the enzyme. Our docking studies have indicated that Arg^{82}, His^{11}, Arg^{390} and Ser^{201} form a binding site for this metabolite, while sequence comparisons suggested that Lys^{340}, Arg^{344} and Arg^{390} are involved in the binding. Preliminary kinetic data indicates that Lys^{340} influences

catalysis and plays a role directly or indirectly in aspartate binding. We have also used sequence comparisons to predict a bicarbonate-binding mode in PepcAs. These studies provided hypotheses for binding sites of these molecules in the absence of crystal structure data and further experimental approaches will be required to determine the validity of these hypotheses.

Author contributions : Lakshmi Dharmarajan designed and performed experiments and wrote this chapter, Jessica L. Kraszewski performed experiments and prepared Fig. 7.1. ; Biswarup Mukhopadhyay supervised the work.

Chapter 8

Appendix

The results summarized in this chapter do not fit into a “story” compared to the previous chapters and hence have been added as appendices. These studies can however, serve as a reference, or provide preliminary data for future studies in the same topics.

Appendix 8.1.

Is Pro^{82} of human PEPCK a catalytically influential residue?

Introduction

We are interested in modulating enzyme activity by influencing this PEP-Mn^{2+} distance in catalysis. Our approach involves perturbing this distance through long-range interactions with catalytically important residues. We have discovered an example of a catalytically influential residue, Asp^{75} of *Mycobacterium smegmatis* PEPCK (Asp^{81} in human PEPCK) (*11*) (Fig. 8.1). The kinetic data suggests that a substitution at Asp^{75} likely changes the positions of the active site residues, namely Asp^{78}, Val^{79}, Arg^{81} and Glu^{83} (Asp^{84}, Val^{85}, Arg^{87} and Glu^{89} in human PEPCK), and in the process alters the distance between the PEP-phosphate and the enzyme-bound Mn^{2+}.

Pro^{82} is distal to the active site in the human enzyme and lies on the same activity modulating sequence element that carries Asp^{81}. This residue forms a hinge by which one could subtly perturb PEP-Mn^{2+} distance and fine-tune the activity of the enzyme from a distance. To determine whether this is a catalytically influential residue, we developed three variants, P82A, P82G and P82GG and checked the respective specific activities. We discovered that the enzymes were active, although with slightly lowered specific activities, thus proving that Pro^{82} influences PEPCK catalysis.

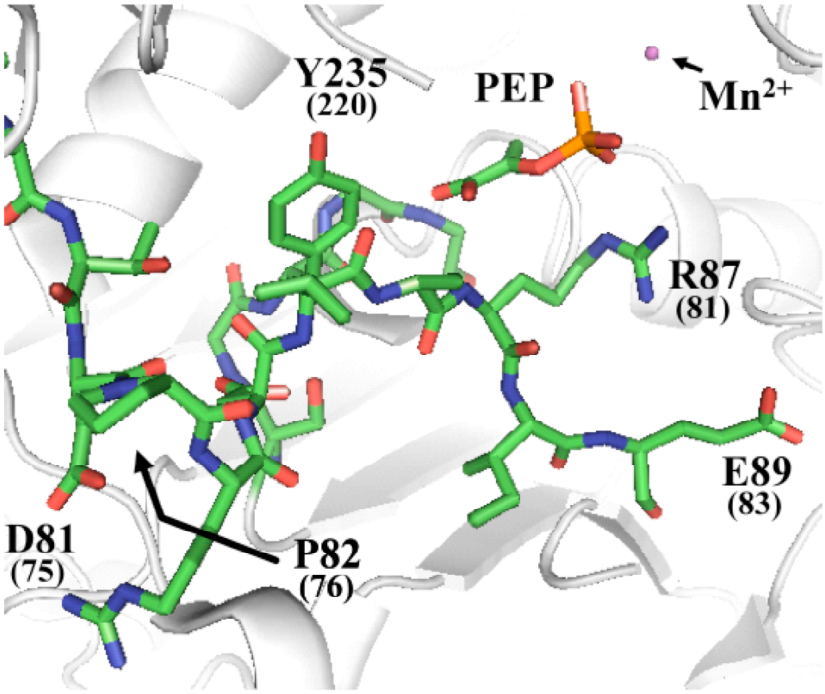

Fig. 8.1. An activity-modulating element of human PEPCK. Equivalent *M. smegmatis* residues are in parentheses. This research was originally published in Case, C. L., Concar, E. M., Boswell, K. L., and Mukhopadhyay, B. *J Biol Chem 281*, 39262-39272 (2006) (*11*) © the American Society for Biochemistry and Molecular Biology. Figure used with permission of ASBMB Journals, 2011.

Materials and methods

Cloning, protein expression and purification - The plasmid pCLC2-19b (*79*) which carries the coding sequence for human cytosolic PEPCK and allows the expression of the protein under the control of a T7 promoter was initially used to construct the mutants. The coding sequence was mutagenized using the QuikChange® kit from Stratagene (La Jolla, CA); details of the procedure have been described previously (*45*). In addition to creating the desired substitutions, each mutagenic primer introduced a BssHI site at nucleotide position 6096-7001 of the vector without changing the

corresponding amino acid sequence. The mutated plasmids were initially screened using this restriction site. Sequencing of both strands of the coding region confirmed that the mutagenesis procedure altered only the targeted bases. Recombinant human PEPCK and variant enzymes were expressed and purified as described previously (79). The His-tag was removed from homogenous rHumcPCK-His10 through treatment with enterokinase (Novagen, Inc.), leaving behind one non-native His residue at the N-terminus.

Enzyme and protein assays and data analysis – Protein was assayed as previously described (*45*). Enzyme activity was measured in the OAA-forming direction as described in (*45*).

Results and discussions

Activity assays of the purified variants showed that all three are active and have lower specific activities compared to the wild-type enzyme (Table 8.1).

Since mutagenesis of P82 caused a change in the specific activities of the variant enzymes, it agrees with our hypothesis that P82 is a catalytically influential residue. It is also surprising that even after introducing two glycines in place of proline in the P82GG variant, the enzyme was still active. Further detailed kinetic and structural studies are to be performed to determine the role of this residue in PEPCK catalysis.

Table 8.1. Specific activities of wild-type human PEPCK and P82 variants

Enzyme	*Activity*
	$\mu mol\ min^{-1}\ mg^{-1}$
WT	36.5
P82A	25.7
P82G	23.9
P82GG	18.5

Chapter 9

Conclusions and future work

During my Ph.D. studies my collaborators and I have made a number of useful observations, which will help in future studies in the PEPCK and Pepc fields, and also in the broader field of enzyme structure-function relationships.

PEPCK and Pepcs are two enzymes that have been extensively studied for more than half a century. The importance of both these enzymes is obvious, and while the focus of work on PEPCKs has been mainly on its regulation in animals, that of Pepcs has been the CO_2 fixation in plants. Although over the years, there have been numerous studies on the genetics and metabolic role of PEPCK, the structural basis of the enzyme mechanism has been elucidated only recently, by the aid of high resolution crystal structures of this enzyme from different organisms. Since PEPCK is an important enzyme at the junction of many metabolic processes, this structural knowledge will greatly benefit approaches to modulate the enzyme activity. In case of Pepc, such a structural revolution is awaited, and until now, there is no structure available of the enzyme with any of the substrates.

Work on PEPCK in our laboratory started in 2001 with the kinetic characterization of *Mycobacterium smegmatis* GTP-PEPCK, which was the first report of a vertebrate-type PEPCK in bacteria (*9*). We further identified an activity-modulating element in this PEPCK, which could influence the PEP-Mn^{2+} distance in catalysis in GTP-PEPCKS

(*11*). In the same study we also found examples of catalytically-influential residues in PEPCK, which could modulate the enzyme activity from a distance. We decided to focus on these two aspects to develop avenues for modulating PEPCK catalysis.

During my Ph.D. studies, we identified that Tyr^{235} plays a role in positioning PEP optimally with respect to Mn^{2+}, and is an important residue in PEPCK catalysis (*45*). We also analyzed the effect of the anion-quadrupole interaction between the aromatic ring of Tyr^{235} and the carboxylate of PEP by enzyme kinetics. Dr. Pete Dunten, who solved the structure of human PEPCK, previously proposed this phenomenon earlier (*26*). This interaction has been rarely studied in a biological system; PEPCK being the second enzyme, while the first was hemoglobin (*89*). Further, we also discovered from site-directed mutagenesis and kinetic assays that Pro^{82} is a catalytically influential residue of human cytosolic GTP-PEPCKs. Another avenue for the modulation of catalysis in GTP-PEPCKs is the conformation of the active-site lid, specifically because lid closure is essential for optimal PEPCK activity (*91*). It has been hypothesized that ligand binding induces lid closure (*34, 43*). Our simulation data are consistent with this hypothesis and we have shown that in the absence of ligands the lid adopts an open conformation. In the absence of crystal structure data for the open lid, our results provide the first observation of a lid-open configuration and intermediates of the lid opening process for GTP-PEPCKs. Our data also show the dynamic correlation between movements of the active-site lid, P-loop and nucleotide-binding regions, as hypothesized from existing crystal structure data (*34, 43*).

Our laboratory started work on Pepc in 2004, with the discovery of the enzyme in *Methanothermobacter thermautotrophicus,* which was the first primary structure characterization of an archaeal-type Pepc (*18*). This study highlighted the differences in the PepcA structure, compared to the Pepcs, which was followed by similar discoveries by another research group in the same year (*17*). No further structural analyses for PepcAs were available until 2006, when Matsumara and colleagues created a structural profile for PepcAs based on *E. coli* and *Z. mays* Pepc structures (*2*). Although their in-silico models were able to identify the gross features of PepcAs, there was still a need for a crystal structure of PepcA to look into subunit and substrate-protein interactions in depth.

During my Ph.D. research we determined the crystal structure of *Clostridium perfringens* PepcA, in collaboration with Dr. Pete Dunten. This is the first archaeal-type Pepc structure to be solved and it provided a platform for comparative structure-function studies with all types of Pepcs. Sequence and structure comparisons indicated a lack of allosteric regulatory sites in PepcAs and additional studies indicated differences in the oligomeric nature of the two classes of enzymes. Further, our kinetic data demonstrated that aspartate has a competitive inhibition mode in *C. perfringens* PepcA as compared to the allosteric mode in Pepcs. Sequence comparisons also showed that aspartate and bicarbonate binding sites of Pepcs are missing in PepcAs. Modeling on the structure data assisted us to develop hypotheses for the binding sites of both of these compounds. Two possible binding sites for aspartate were deduced, Arg^{82}, Ser^{201}, His^{11} and Arg^{390} forming the first site, while Lys^{340}, Arg^{344} and Arg^{390} formed the second site.

This was followed by a kinetic analysis that also indicated that Lys^{340} may play a direct or indirect role in aspartate binding in PepcAs. Additionally, sequence comparisons also suggested a sequence element lined with basic residues, and close to the active site as a putative site for bicarbonate binding.

Future work

The characterization of an enzyme activity modulating anion-quadrupole interaction in GTP-PEPCKs opens up the possibility of further studies of this type in other proteins. Detailed biophysical and quantum mechanical measurements are necessary to derive the basis of this interaction. In case of PEPCK, structural data of the Y235 variants may provide further information about this edge-on interaction. PEP-Mn^{2+} distance is a deciding factor in PEPCK catalysis and residues influencing this distance can provide sites for modulating enzyme activity. Another modulatory site in GTP-PEPCKs is the active-site lid. Although no electron density was observed for the open disordered loop in the crystal structures, molecular dynamics simulations provided information about the structure of this element. Detailed analysis of the intermediates of loop opening and the respective stabilizing interactions will provide a better understanding of the loop dynamics of GTP-PEPCKs.

The data from the first crystal structure of PepcA provided a platform for comparative studies about the mechanism of activity regulation in Pepcs and PepcAs. Structural modeling is a useful tool for enzymologists and has provided some indications of binding sites of aspartate and bicarbonate. Further experimental verification of these predictions is necessary. These also could provide future avenues of modulating Pepc

activities. Structural data is an important aspect of enzymology studies, and future work on PepcAs would greatly benefit from the structures of the enzyme complexed with aspartate and all the substrates.

References

1. Izui, K., Matsumura, H., Furumoto, T., and Kai, Y. (2004) Phosphoenolpyruvate carboxylase: a new era of structural biology, *Annu Rev Plant Biol 55*, 69-84.
2. Matsumura, H., Izui, K., and Mizuguchi, K. (2006) A novel mechanism of allosteric regulation of archaeal phosphoenolpyruvate carboxylase: a combined approach to structure-based alignment and model assessment, *Protein Eng Des Sel 19*, 409-419.
3. Hanson, R. W., and Patel, Y. M. (1994) Phosphoenolpyruvate carboxykinase (GTP): the gene and the enzyme, *Adv Enzymol Relat Areas Mol Biol 69*, 203-281.
4. Ashworth, J. M., and Kornberg, H. L. (1966) The anaplerotic fixation of carbon dioxide by *Escherichia coli*, *Proc R Soc Lond B Biol Sci 165*, 179-188.
5. Simpson, P. G., and W. B. Whitman. (1993) Anabolic pathways of methanogens, *In J. G. Ferry (ed.), Methanogenesis: Ecology, physioogy, biochemistry and genetics*, 445-472.
6. Matte, A., Tari, L. W., Goldie, H., and Delbaere, L. T. (1997) Structure and mechanism of phosphoenolpyruvate carboxykinase, *J Biol Chem 272*, 8105-8108.
7. Aich, S., Imabayashi, F., and Delbaere, L. T. (2003) Expression, purification, and characterization of a bacterial GTP-dependent PEP carboxykinase, *Protein Expr Purif 31*, 298-304.
8. Fukuda, W., Fukui, T., Atomi, H., and Imanaka, T. (2004) First characterization of an archaeal GTP-dependent phosphoenolpyruvate carboxykinase from the hyperthermophilic archaeon Thermococcus kodakaraensis KOD1, *J Bacteriol 186*, 4620-4627.
9. Mukhopadhyay, B., Concar, E. M., and Wolfe, R. S. (2001) A GTP-dependent vertebrate-type phosphoenolpyruvate carboxykinase from *Mycobacterium smegmatis*, *J Biol Chem 276*, 16137-16145.

10. Rohrer, S. P., Saz, H. J., and Nowak, T. (1986) Purification and characterization of phosphoenolpyruvate carboxykinase from the parasitic helminth *Ascaris suum*, *J Biol Chem 261*, 13049-13055.
11. Case, C. L., Concar, E. M., Boswell, K. L., and Mukhopadhyay, B. (2006) Roles of $Asp^{75,}$ Asp^{78}, and Glu^{83} of GTP-dependent phosphoenolpyruvate carboxykinase from *Mycobacterium smegmatis*, *J Biol Chem 281*, 39262-39272.
12. Matsumura, H., Xie, Y., Shirakata, S., Inoue, T., Yoshinaga, T., Ueno, Y., Izui, K., and Kai, Y. (2002) Crystal structures of C4 form maize and quaternary complex of *E. coli* phosphoenolpyruvate carboxylases, *Structure 10*, 1721-1730.
13. Miziorko, H. M., Nowak, T., and Mildvan, A. S. (1974) Spinach leaf phosphoenolpyruvate carboxylase: purification, properties, and kinetic studies, *Arch Biochem Biophys 163*, 378-389.
14. Smith, T. E. (1968) Escherichia coli phosphoenolpyruvate carboxylase: characterization and sedimentation behavior, *Arch Biochem Biophys 128*, 611-622.
15. Dong, L. Y., Hata, S., and Izui, K. (1997) High-level expression of maize C4-type phosphoenolpyruvate carboxylase in *Escherichia coli* and its rapid purification, *Biosci Biotechnol Biochem 61*, 545-546.
16. Dong, L. Y., Masuda, T., Kawamura, T., Hata, S., and Izui, K. (1998) Cloning, expression, and characterization of a root-form phosphoenolpyruvate carboxylase from *Zea mays*: comparison with the C4-form enzyme, *Plant Cell Physiol 39*, 865-873.
17. Ettema, T. J., Makarova, K. S., Jellema, G. L., Gierman, H. J., Koonin, E. V., Huynen, M. A., de Vos, W. M., and van der Oost, J. (2004) Identification and functional verification of archaeal-type phosphoenolpyruvate carboxylase, a missing link in archaeal central carbohydrate metabolism, *J Bacteriol 186*, 7754-7762.
18. Patel, H. M., Kraszewski, J. L., and Mukhopadhyay, B. (2004) The phosphoenolpyruvate carboxylase from *Methanothermobacter thermautotrophicus* has a novel structure, *J Bacteriol 186*, 5129-5137.

19. Sako, Y., Croocker, P. C., and Ishida, Y. (1997) An extremely heat-stable extracellular proteinase (aeropyrolysin) from the hyperthermophilic archaeon *Aeropyrum pernix K1*, *FEBS Lett 415*, 329-334.
20. Sako, Y., Takai, K., Uchida, A., and Ishida, Y. (1996) Purification and characterization of phosphoenolpyruvate carboxylase from the hyperthermophilic archaeon *Methanothermus sociabilis*, *FEBS Lett 392*, 148-152.
21. Yang, J., Kalhan, S. C., and Hanson, R. W. (2009) What is the metabolic role of phosphoenolpyruvate carboxykinase?, *J Biol Chem 284*, 27025-27029.
22. Tannen, R. L. (1978) *Am. J. Physiol. 235*, 265-277.
23. Burgess, S. C., Hausler, N., Merritt, M., Jeffrey, F. M., Storey, C., Milde, A., Koshy, S., Lindner, J., Magnuson, M. A., Malloy, C. R., and Sherry, A. D. (2004) *J Biol Chem 279*, 48941-48949.
24. She, P., Shiota, M., Shelton, K. D., Chalkley, R., Postic, C., and Magnuson, M. A. (2000) *Mol Cell Biol 20*, 6508-6517.
25. Soling, H. D., Kleineke, J. (1976) Species dependent regulation of hepatic gluconeogenesis in higher animals.
26. Dunten, P., Belunis, C., Crowther, R., Hollfelder, K., KammLott, U., Levin, W., Michel, H., Ramsey, G. B., Swain, A., Weber, D., and Wertheimer, S. J. (2002) Crystal structure of human cytosolic phosphoenolpyruvate carboxykinase reveals a new GTP-binding site, *J Mol Biol 316*, 257-264.
27. Chen, C. Y., Sato, Y., and Schramm, V. L. (1991) Isotope trapping and positional isotope exchange with rat and chicken liver phosphoenolpyruvate carboxykinases, *Biochemistry 30*, 4143-4151.
28. Delbaere, L. T., Sudom, A. M., Prasad, L., Leduc, Y., and Goldie, H. (2004) Structure/function studies of phosphoryl transfer by phosphoenolpyruvate carboxykinase, *Biochim Biophys Acta 1697*, 271-278.
29. Konopka, J. M., Lardy, H. A., and Frey, P. A. (1986) Stereochemical course of thiophosphoryl transfer catalyzed by cytosolic phosphoenolpyruvate carboxykinase, *Biochemistry 25*, 5571-5575.

30. Sheu, K. F., Ho, H. T., Nolan, L. D., Markovitz, P., Richard, J. P., Utter, M. F., and Frey, P. A. (1984) Stereochemical course of thiophosphoryl group transfer catalyzed by mitochondrial phosphoenolpyruvate carboxykinase, *Biochemistry 23*, 1779-1783.
31. Sudom, A. M., Prasad, L., Goldie, H., and Delbaere, L. T. (2001) The phosphoryl-transfer mechanism of *Escherichia coli* phosphoenolpyruvate carboxykinase from the use of AlF(3), *J Mol Biol 314*, 83-92.
32. Tari, L. W., Matte, A., Goldie, H., and Delbaere, L. T. (1997) Mg(2+)-Mn2+ clusters in enzyme-catalyzed phosphoryl-transfer reactions, *Nat Struct Biol 4*, 990-994.
33. Tari, L. W., Matte, A., Pugazhenthi, U., Goldie, H., and Delbaere, L. T. (1996) Snapshot of an enzyme reaction intermediate in the structure of the ATP-Mg2+-oxalate ternary complex of *Escherichia coli* PEP carboxykinase, *Nat Struct Biol 3*, 355-363.
34. Sullivan, S. M., and Holyoak, T. (2008) Enzymes with lid-gated active sites must operate by an induced fit mechanism instead of conformational selection, *Proc Natl Acad Sci U S A 105*, 13829-13834.
35. Carlson, G. M., and Holyoak, T. (2009) Structural insights into the mechanism of phosphoenolpyruvate carboxykinase catalysis, *J Biol Chem 284*, 27037-27041.
36. Dismukes, G. C. (1996) Manganese Enzymes with Binuclear Active Sites, *Chem Rev 96*, 2909-2926.
37. Goldie, A. H., and Sanwal, B. D. (1980) Allosteric control by calcium and mechanism of desensitization of phosphoenolpyruvate carboxykinase of Escherichia coli, *J Biol Chem 255*, 1399-1405.
38. Colombo, G., and Lardy, H. A. (1981) Phosphoenolpyruvate carboxykinase (guanosine 5'-triphosphate) from rat liver cytosol. Divalent cation involvement in the decarboxylation reactions, *Biochemistry 20*, 2758-2767.
39. Duffy, T. H., and Nowak, T. (1985) 1H and 31P relaxation rate studies of the interaction of phosphoenolpyruvate and its analogues with avian phosphoenolpyruvate carboxykinase, *Biochemistry 24*, 1152-1160.

40. Hebda, C. A., and Nowak, T. (1982) Phosphoenolpyruvate carboxykinase. Mn2+ and Mn2+ substrate complexes, *J Biol Chem 257*, 5515-5522.
41. Hlavaty, J. J., and Nowak, T. (2000) Characterization of the second metal site on avian phosphoenolpyruvate carboxykinase, *Biochemistry 39*, 1373-1388.
42. Lee, M. H., Hebda, C. A., and Nowak, T. (1981) The role of cations in avian liver phosphoenolpyruvate carboxykinase catalysis. Activation and regulation, *J Biol Chem 256*, 12793-12801.
43. Sullivan, S. M., and Holyoak, T. (2007) Structures of rat cytosolic PEPCK: insight into the mechanism of phosphorylation and decarboxylation of oxaloacetic acid, *Biochemistry 46*, 10078-10088.
44. Holyoak, T., Sullivan, S. M., and Nowak, T. (2006) Structural insights into the mechanism of PEPCK catalysis, *Biochemistry 45*, 8254-8263.
45. Dharmarajan, L., Case, C. L., Dunten, P., and Mukhopadhyay, B. (2008) Tyr^{235} of human cytosolic phosphoenolpyruvate carboxykinase influences catalysis through an anion-quadrupole interaction with phosphoenolpyruvate carboxylate, *FEBS J 275*, 5810-5819.
46. Wong, K. F., Selzer, T., Benkovic, S. J., and Hammes-Schiffer, S. (2005) Impact of distal mutations on the network of coupled motions correlated to hydride transfer in dihydrofolate reductase, *Proc Natl Acad Sci U S A 102*, 6807-6812.
47. Boden, D., and Markowitz, M. (1998) Resistance to human immunodeficiency virus type 1 protease inhibitors, *Antimicrob Agents Chemother 42*, 2775-2783.
48. Rod, T. H., Radkiewicz, J. L., and Brooks, C. L., 3rd. (2003) Correlated motion and the effect of distal mutations in dihydrofolate reductase, *Proc Natl Acad Sci U S A 100*, 6980-6985.
49. Knaggs, M. H., Salsbury, F. R., Jr., Edgell, M. H., and Fetrow, J. S. (2007) Insights into correlated motions and long-range interactions in CheY derived from molecular dynamics simulations, *Biophys J 92*, 2062-2079.
50. Jackson, M. R., Beahm, R., Duvvuru, S., Narasimhan, C., Wu, J., Wang, H. N., Philip, V. M., Hinde, R. J., and Howell, E. E. (2007) A preference for edgewise

interactions between aromatic rings and carboxylate anions: the biological relevance of anion-quadrupole interactions, *J Phys Chem B 111*, 8242-8249.

51. Mecozzi, S., West, A. P., Jr., and Dougherty, D. A. (1996) Cation-pi interactions in aromatics of biological and medicinal interest: electrostatic potential surfaces as a useful qualitative guide, *Proc Natl Acad Sci U S A 93*, 10566-10571.
52. Burley, S. K., and Petsko, G. A. (1988) Weakly polar interactions in proteins, *Adv Protein Chem 39*, 125-189.
53. Thomas, K. A., Smith, G. M., Thomas, T. B., and Feldmann, R. J. (1982) Electronic distributions within protein phenylalanine aromatic rings are reflected by the three-dimensional oxygen atom environments, *Proc Natl Acad Sci U S A 79*, 4843-4847.
54. Chollet, R., Vidal, J., and O'Leary, M. H. (1996) PHOSPHOENOLPYRUVATE CARBOXYLASE: A Ubiquitous, Highly Regulated Enzyme in Plants, *Annu Rev Plant Physiol Plant Mol Biol 47*, 273-298.
55. O'Leary, M. H. (1982) Phosphoenolpyruvate carboxylase : an enzymologist's view., *Annu. Rev. Plant Physiol. 33*, 297-315.
56. Utter, M. F., and Kolenbrander, H.M. (1972) Formation of oxaloacetate by CO2 fixation on phosphoenolpyruvate., In *The Enzymes*, pp 117-168, P.D. Boyer.
57. hatch, M. D. (1987) C4 photosynthesis : a unique blend of modified biochemistry, anatomy and ultrastructure., *Biochim. Biophys. Acta 895*, 81-106.
58. Raines, C. A. (2006) Transgenic approaches to manipulate the environmental responses of the C3 carbon fixation cycle, *Plant Cell Environ 29*, 331-339.
59. Leegood, R. C. (2002) C(4) photosynthesis: principles of CO(2) concentration and prospects for its introduction into C(3) plants, *J Exp Bot 53*, 581-590.
60. Jeanneau, M., Vidal, J., Gousset-Dupont, A., Lebouteiller, B., Hodges, M., Gerentes, D., and Perez, P. (2002) Manipulating PEPC levels in plants, *J Exp Bot 53*, 1837-1845.
61. Ku, M. S., Agarie, S., Nomura, M., Fukayama, H., Tsuchida, H., Ono, K., Hirose, S., Toki, S., Miyao, M., and Matsuoka, M. (1999) High-level expression of maize

phosphoenolpyruvate carboxylase in transgenic rice plants, *Nat Biotechnol 17*, 76-80.

62. Martinoia, E., and D. Rentsch. (1994) Malate compartmentation: responses to a complex metabolism., *Annu Rev Plant Physiol Plant Mol Biol 45*, 447-467.
63. Ting, I. P., and Osmond, C. B. (1973) Photosynthetic Phosphoenolpyruvate Carboxylases: Characteristics of Alloenzymes from Leaves of C(3) and C(1) Plants, *Plant Physiol 51*, 439-447.
64. Kai, Y., Matsumura, H., and Izui, K. (2003) Phosphoenolpyruvate carboxylase: three-dimensional structure and molecular mechanisms, *Arch Biochem Biophys 414*, 170-179.
65. Kai, Y., Matsumura, H., Inoue, T., Terada, K., Nagara, Y., Yoshinaga, T., Kihara, A., Tsumura, K., and Izui, K. (1999) Three-dimensional structure of phosphoenolpyruvate carboxylase: a proposed mechanism for allosteric inhibition, *Proc Natl Acad Sci U S A 96*, 823-828.
66. Izui, K., Taguchi, M., Morikawa, M., and Katsuki, H. (1981) Regulation of Escherichia coli phosphoenolpyruvate carboxylase by multiple effectors in vivo. II. Kinetic studies with a reaction system containing physiological concentrations of ligands, *J Biochem 90*, 1321-1331.
67. Tovar-Mendez, A., Rodriguez-Sotres, R., Lopez-Valentin, D. M., and Munoz-Clares, R. A. (1998) Re-examination of the roles of PEP and Mg2+ in the reaction catalysed by the phosphorylated and non-phosphorylated forms of phosphoenolpyruvate carboxylase from leaves of *Zea mays.* Effects of the activators glucose 6-phosphate and glycine, *Biochem J 332 (Pt 3)*, 633-642.
68. Dharmarajan, L., Kraszewski, J. L., Mukhopadhyay, B., and Dunten, P. W. (2009) Expression, purification and crystallization of an archaeal-type phosphoenolpyruvate carboxylase, *Acta Crystallogr Sect F Struct Biol Cryst Commun 65*, 1193-1196.
69. Rognstad, R. (1982) $^{14}CO_2$ fixation by phosphoenolpyruvate carboxykinase during gluconeogenesis in the intact rat liver cell, *J Biol Chem 257*, 11486-11488.

70. Valera, A., Pujol, A., Pelegrin, M., and Bosch, F. (1994) Transgenic mice overexpressing phosphoenolpyruvate carboxykinase develop non-insulin-dependent diabetes mellitus, *Proc Natl Acad Sci U S A 91*, 9151-9154.
71. Gomez-Valades, A. G., Vidal-Alabro, A., Molas, M., Boada, J., Bermudez, J., Bartrons, R., and Perales, J. C. (2006) Overcoming diabetes-induced hyperglycemia through inhibition of hepatic phosphoenolpyruvate carboxykinase (GTP) with RNAi, *Mol Ther 13*, 401-410.
72. Munoz, M. C., Barbera, A., Dominguez, J., Fernandez-Alvarez, J., Gomis, R., and Guinovart, J. J. (2001) Effects of tungstate, a new potential oral antidiabetic agent, in Zucker diabetic fatty rats, *Diabetes 50*, 131-138.
73. Barns, R. J., and Keech, D. B. (1972) Sheep kidney phosphoenolpyruvate carboxylase. Purification and properties, *Biochim Biophys Acta 276*, 284-296.
74. Ballard, F. J. (1970) Kinetic studies with cytosol and mitochondrial phosphoenolpyruvate carboxykinases, *Biochem J 120*, 809-814.
75. Chang, H. C., and Lane, M. D. (1966) The enzymatic carboxylation of phosphoenolpyruvate. II. Purification and properties of liver mitochondrial phosphoenolpyruvate carboxykinase, *J Biol Chem 241*, 2413-2420.
76. Goto, Y., Shimizu, J., Okazaki, T., and Shukuya, R. (1979) Purification and characterization of cytosol phosphoenolpyruvate carboxykinase from bullfrog (*Rana catesbeiana*) liver, *J Biochem 86*, 71-78.
77. Holten, D. D., and Nordlie, R. C. (1965) Comparative Studies of Catalytic Properties of Guinea Pig Liver Intra- and Extramitochondrial Phosphoenolpyruvate Carboxykinases, *Biochemistry 4*, 723-731.
78. Hebda, C. A., and Nowak, T. (1982) The purification, characterization, and activation of phosphoenolpyruvate carboxykinase from chicken liver mitochondria, *J Biol Chem 257*, 5503-5514.
79. Case, C. L., and Mukhopadhyay, B. (2007) Kinetic characterization of recombinant human cytosolic phosphoenolpyruvate carboxykinase with and without a His_{10}-tag, *Biochim Biophys Acta 1770*, 1576-1584.

80. Bradford, M. M. (1976) A rapid and sensitive method for the quantitation of microgram quantities of protein utilizing the principle of protein-dye binding, *Anal Biochem 72*, 248-254.
81. Noce, P. S., and Utter, M. F. (1975) Decarboxylation of oxalacetate to pyruvate by purified avian liver phosphoenolpyruvate carboxykinase, *J Biol Chem 250*, 9099-9105.
82. Nordlie, R. C., and Lardy, H. A. (1963) Mammalian liver phosphoneolpyruvate carboxykinase activities, *J Biol Chem 238*, 2259-2263.
83. Cleland, W. W. (1979) Statistical analysis of enzyme kinetic data, *Methods Enzymol 63*, 103-138.
84. Berman, H. M., Westbrook, J., Feng, Z., Gilliland, G., Bhat, T. N., Weissig, H., Shindyalov, I. N., and Bourne, P. E. (2000) The Protein Data Bank, *Nucleic Acids Res 28*, 235-242.
85. Compton, L. A., and Johnson, W. C., Jr. (1986) Analysis of protein circular dichroism spectra for secondary structure using a simple matrix multiplication, *Anal Biochem 155*, 155-167.
86. Sreerama, N., and Woody, R. W. (2000) Estimation of protein secondary structure from circular dichroism spectra: comparison of CONTIN, SELCON, and CDSSTR methods with an expanded reference set, *Anal Biochem 287*, 252-260.
87. Humphrey, W., Dalke, A., and Schulten, K. (1996) VMD: visual molecular dynamics, *J Mol Graph 14*, 33-38, 27-38.
88. Kosugi K, I. Y. N. N. (2001) Charge transfer interaction in the acetic acid–benzene cation complex, *J Chem Phys 114*, 4805-4816.
89. Perutz MF, F. G., Abraham DJ, Poyart C and Burseaux E. (1986) Hemoglobin as a receptor of drugs and peptides: x-ray studies of the stereochemistry of binding., *J Am Chem Soc 108*, 1064-1078.
90. Cotelesage, J. J., Puttick, J., Goldie, H., Rajabi, B., Novakovski, B., and Delbaere, L. T. (2007) How does an enzyme recognize CO_2?, *Int J Biochem Cell Biol 39*, 1204-1210.

91. Johnson, T. A., and Holyoak, T. (2010) Increasing the conformational entropy of the Omega-loop lid domain in phosphoenolpyruvate carboxykinase impairs catalysis and decreases catalytic fidelity, *Biochemistry 49*, 5176-5187.
92. DePaul, A. J., Thompson, E. J., Patel, S. S., Haldeman, K., and Sorin, E. J. (2010) Equilibrium conformational dynamics in an RNA tetraloop from massively parallel molecular dynamics, *Nucleic Acids Res 38*, 4856-4867.
93. Sorin, E. J., and Pande, V. S. (2005) Exploring the helix-coil transition via all-atom equilibrium ensemble simulations, *Biophys J 88*, 2472-2493.
94. Case, D. A., Cheatham, T. E., 3rd, Darden, T., Gohlke, H., Luo, R., Merz, K. M., Jr., Onufriev, A., Simmerling, C., Wang, B., and Woods, R. J. (2005) The Amber biomolecular simulation programs, *J Comput Chem 26*, 1668-1688.
95. Jorgensen, W. L., et al. (1983) Comparison of Simple Potential Functions for Simulating Liquid Water., *Journal of Chemical Physics 79*, 926-935.
96. van der Spoel, D. L., E.; Hess, B.; van Buuren, A. R.; Apol, E.; Meulenhobb, P. J.; Tieleman, D. P.; Sijbers, A. L. T. M.; Feenstra, K. A.; van Drunen, R.; Berendsen, H. J. C. (2005) http://www.gromacs.org/.
97. Berendsen, H. J. C. P., J. P. M.; van Gunsteren, W. F.; DiNola, A.; Haak, J. R. (1984) Molecular Dynamics with Coupling to an External Bath, *J. Chem. Phys. 81*, 3684– 3690.
98. Hess, B. B., H.; Berendsen, H. J. C.; Fraaije, J. G. E. M. (1997) LINCS: A Linear Constraint Solver for Molecular Simulations, *J. Comput. Chem. 18*, 1463– 1472.
99. Darden, T. Y., D.; Pedersen, L. G. (1993) Particle Mesh Ewald: An N-log(N) Method for Ewald Sums in Large Systems, *J. Chem. Phys. 98*, 10089– 10092.
100. Essmann, U. P., L.; Berkowitz, M. L.; Darden, T.; Lee, H.; Pedersen, L. G. A (1995) Smooth Particle Mesh Ewald Method, *J. Chem. Phys. 103*, 8577– 8593.
101. Nose, S. K., M. L. (1983) Constant Pressure Molecular Dynamics for Molecular Systems, *Mol. Phys. 50*, 1055– 1076.
102. Parrinello, M. R., A. (1981) Polymorphic Transitions in Single Crystals: A New Molecular Dynamics Method, *J. Appl. Phys. 52*, 7182– 7190.
103. http://www.arc.vt.edu/arc/SystemX/.

104. Turner, P. J. (2008) Grace, *Center for Coastal and Land-Margin Research Oregon Graduate Institute of Science and Technology: Beaverton, OR*.
105. Hausler, R. E., Hirsch, H. J., Kreuzaler, F., and Peterhansel, C. (2002) Overexpression of C(4)-cycle enzymes in transgenic C(3) plants: a biotechnological approach to improve C(3)-photosynthesis, *J Exp Bot 53*, 591-607.
106. Endo, T., Mihara, Y., Furumoto, T., Matsumura, H., Kai, Y., and Izui, K. (2008) Maize C4-form phosphoenolpyruvate carboxylase engineered to be functional in C3 plants: mutations for diminished sensitivity to feedback inhibitors and for increased substrate affinity, *J Exp Bot 59*, 1811-1818.
107. Fukayama, H., Hatch, M. D., Tamai, T., Tsuchida, H., Sudoh, S., Furbank, R. T., and Miyao, M. (2003) Activity regulation and physiological impacts of maize C(4)-specific phosphoenolpyruvate carboxylase overproduced in transgenic rice plants, *Photosynth Res 77*, 227-239.
108. Coomes, M. W., Mitchell, B. K., Beezley, A., and Smith, T. E. (1985) Properties of an Escherichia coli mutant deficient in phosphoenolpyruvate carboxylase catalytic activity, *J Bacteriol 164*, 646-652.
109. Kraszewski, J. L. M., B. (2005) In *Unpublished work*.
110. Gonzalez, A., Moorhead, P., McPhillips, S. E., Song, J., Sharp, K., Taylor, J. R., Adams, P. D., Sauter, N. K., and Soltis, S. M. (2008) Web-Ice: integrated data collection and analysis for macromolecular crystallography, *Journal of Applied Crystallography 41*, 176-184.
111. Leslie, A. G. W. (1992) *Jnt CCP4/ESF-EACBM Newsl. Protein Crystallogr. 26*.
112. Evans, P. R. (1997) *Joint CCP4/ESF-EACBM Newsl. Protein Crystallogr. 33*, 22-24.
113. Otwinowski, Z. M., W. (1997) *Methods Enzymol. 276*, 307-326.
114. Paithankar, K. S., Owen, R. L., and Garman, E. F. (2009) Absorbed dose calculations for macromolecular crystals: improvements to RADDOSE, *J Synchrotron Radiat 16*, 152-162.
115. Sheldrick, G. M. (2008) *Acta Cryst. A64*, 112-122.

116. Corwin, L. M., and Fanning, G. R. (1968) Studies of parameters affecting the allosteric nature of phosphoenolpyruvate carboxylase of Escherichia coli, *J Biol Chem 243*, 3517-3525.
117. Dharmarajan, L., Kraszewski, J, Mukhopadhyay, B and Dunten, P (2011) Structure of an archaeal-type phosphoenolpyruvate carboxylase sensitive to inhibition by aspartate.
118. Koshland, D. E., Jr., Ray, W. J., Jr., and Erwin, M. J. (1958) Protein structure and enzyme action, *Fed Proc 17*, 1145-1150.
119. Laskowski, R. A. (2009) PDBsum new things, *Nucleic Acids Res 37*, D355-359.
120. Dawson RMC, E. D., Elliot WH & Jones KM. (1986), Vol. 3rd edition.
121. Sali, A., and Blundell, T. L. (1993) Comparative protein modelling by satisfaction of spatial restraints, *J Mol Biol 234*, 779-815.
122. Trott, O., and Olson, A. J. (2010) AutoDock Vina: improving the speed and accuracy of docking with a new scoring function, efficient optimization, and multithreading, *J Comput Chem 31*, 455-461.
123. La, D., Esquivel-Rodriguez, J., Venkatraman, V., Li, B., Sael, L., Ueng, S., Ahrendt, S., and Kihara, D. (2009) 3D-SURFER: software for high-throughput protein surface comparison and analysis, *Bioinformatics 25*, 2843-2844.
124. Kraszewski, J. (2007) Enzymology and Physiology of a New Type of Phosphoenolpyruvate Carboxylase and the Development of a Pyruvate Carboxylase Expression System, In *Biochemistry*, Virginia Tech.
125. Meyer, C. R., Rustin, P., Black, M. K., and Wedding, R. T. (1990) The influence of pH on substrate form specificity of phosphoenolpyruvate carboxylase purified from Crassula argentea, *Arch Biochem Biophys 278*, 365-372.
126. Wedding, R. T., Rustin, P., Meyer, C. R., and Black, M. K. (1988) Kinetic studies of the form of substrate bound by phosphoenolpyruvate carboxylase, *Plant Physiol 88*, 976-979.
127. Terada, K., and Izui, K. (1991) Site-directed mutagenesis of the conserved histidine residue of phosphoenolpyruvate carboxylase. His^{138} is essential for the second partial reaction, *Eur J Biochem 202*, 797-803.